INVESTIGATION OF CORRUGATED CARDBOARD FOR VIBRATION ISOLATION

A Thesis
Submitted to the College of Graduate Studies and Research
in Partial Fulfillment of the Requirements
for the Degree of
Master of Science
in the
Department of Mechanical Engineering
University of Saskatchewan
Saskatoon, Saskatchewan
Canada

By

Jialei Huang

PERMISSION TO USE

In presenting this thesis in partial fulfilment of the requirements for a Master of Science degree from the University of Saskatchewan, the author agrees that the Libraries of this University may make it freely available for inspection. The author further agrees that permission for copying of this thesis in any manner, in whole or in part, for scholarly purposes may be granted by the professor or professors who supervised the thesis work or, in their absence, by the Head of the Department or the Dean of the College in which the thesis work was done. It is understood that any copying or publication or use of this thesis or parts thereof for financial gain shall not be allowed without the author's written permission. It is also understood that due recognition shall be given to the author and to the University of Saskatchewan in any scholarly use which may be made of any material in this thesis.

Requests for permission to copy or to make other use of material in this thesis in whole or part should be addressed to:

Head of the Department of Mechanical Engineering

University of Saskatchewan

Saskatoon, Saskatchewan S7N 5A9 CANADA

ABSTRACT

Vibration isolation is a common approach to reduce the undesired vibration of a dynamic system from its surrounding. The common material used for the vibration isolator is rubber (for example) which is known to be environmentally unfriendly. This thesis presents a study on the use of corrugated cardboard for the vibration isolator, which is known to be a highly environment-friendly material. The focus of the study is on understanding and modeling of stiffness and damping of cardboard when it or its system (several cardboards) is used for isolating the vibration coming from the vertical direction of cardboard.

In this thesis, a study is presented of finite element modeling of stiffness of corrugated cardboard in its vertical direction with the aim of overcoming two major shortcomings in modeling in the current literature: (1) the width effect is neglected even for cardboard with its width greater than length and (2) the non-linear constitutive relation is not accurately determined. Indeed, it is likely that these shortcomings are responsible for inaccuracy with the models in the current literature to predict the stiffness and peak load. Further, a test bed was set up for the measurement of damping of cardboards in this study. This thesis also presents an application of the theoretic development in the stiffness and damping of corrugated cardboard to design an isolator for the vacuum pump at Canadian Light Source.

Several conclusions are drawn from this study: (1) modeling with consideration of the width effect and non-linear constitutive relation is necessary to improve the accuracy of prediction of stiffness of cardboard; (2) set up for the measurement of damping of cardboard is accurate; and (3) cardboard systems are feasible for vibration isolation in terms of the reduction of amplitude of vibration.

The contribution of this thesis includes: (1) providing a finite element method for modeling of corrugated cardboards which have a complex non-linear constitutive relation, variable contact configuration, and 3D geometrical effect and (2) providing the feasibility of proving that corrugated cardboard can be used for vibration isolation.

ACKNOWLEDGEMENTS

I would like to express my sincere gratitude to my supervisor Professor W.J. (Chris) Zhang, who provided me with dedicated guidance, broad knowledge, and continuous encouragement through my master study. His enthusiasm and dedication on his work has impressed and influenced me greatly. I would also like to acknowledge his moral and financial support. I appreciate all what he has provided me during my whole life.

I would also like to acknowledge the Department of Mechanical Engineering through the graduate scholarship for my second year, from which I have got an opportunity to gain more financial support, which is always good to graduate students.

I would like to thank the members of my Advisory committee (Professor Allan Dolovich and Professor Akindele Odeshi, Professor Lal Kushwaha) for their advices and examination during the process. I would like to thank J.W. (Mark) Li for initiating this project. I would like to thank Hans-Jurgen Steinmetz and Louis Roth for helping me set up the measurement test-bed for measuring the stiffness of corrugated cardboard and fulfilling the measurement described in Chapter 3. I would like to thank Doug Bitner, who helped me set up the measurement test-bed for measuring the damping and vibration and fulfilling the measurement described in Chapter 4. I would like to thank Tim May from the Canadian Light Source for providing me the vacuum pump to fulfill the measurement described in Chapter 4. I would like to thank the cleaning staff of the University for providing me cardboards for my research, which does give a lovely example of how wasted materials can be recycled without any penny.

Many thanks also go to my peers and friends in the AEDL. Thanks to Xiaohua Hu, Zhiming Zhang, Yu Zhao, Fan Zhang, Sampath Mudduda, and Fang He to support my research and to care my life during the study. I would also like to thank Wubin Cheng, Paul Miao, Bin Zhang

and Lin Cao, for sharing their experience on using the ANSYS software. Special thanks to Tan Zhang and Zhengzhou Yang, who provide me the room for keeping the stuff related to my research.

The last but definitely not the least, I would like to thank my family for their love and support, in particular, Yiwen Lu (mom), and Yihong Lu (auntie).

DEDICATION

To my parents:

Yiwen Lu and Hua Huang

TABLE OF CONTENTS

LIST OF FIGURES

Figure .....Page

LIST OF TABLES

Table Page

LIST OF ABBREVIATIONS

AEDL	Advanced Engineering Design Laboratory
FE	Finite element
MD	Machine direction
CD	Cross direction
ZD	Vertical direction
VS	versus
BCT	Box compression test
ECT	Edge crush test
FCT	Flat crush test
MCT	Concorra Medium Test

CHAPTER 1 INTRODUCTION

1.1 Research Background and Motivation

There are numerous unwanted vibration sources in our living and work places, such as rotating or reciprocating machinery, earthquake, and so on. The presence of these vibrations could lead to system failures, extra costs of the maintenance of machine, and threats to human health (Rao, 2003). Therefore, how to reduce these undesired vibrations has been a common engineering problem.

One of the common means to reduce unwanted vibration is the use of vibration isolator. The vibration isolator system or isolator is a device to hinder transmission of vibrations from vibration sources to the ground or protected machines, in which an isolator is placed between the vibration source and the protected device (Housner and Bergman, 1997). Fig. 1.1 illustrates an example of the vibration isolator or isolation system. In this figure, vibration isolators are placed between the large operating machine and the ground to stop transmission of the vibration from the machine to the ground.

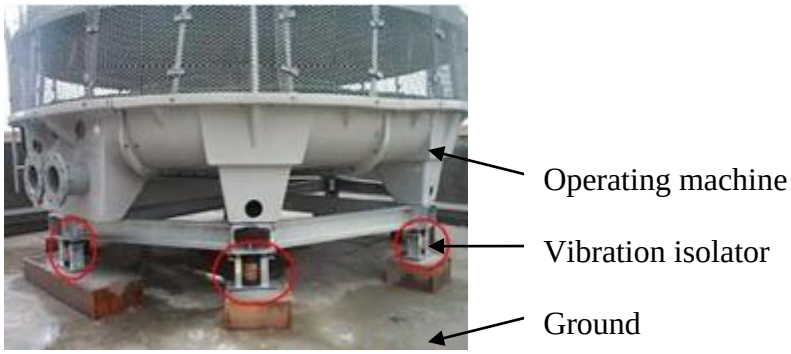

Fig. 1.1 Example of vibration isolator system (http://files.b2b.cn/product/ProductImages /2010_05/07/07101602230_b.jpg)

Several well-known concepts regarding vibration isolation are adapted from Rao (2003). A

vibration isolation system can be active or passive depending on whether or not an external power and/or resource is required for the isolator to perform its function. A passive vibration isolator consists of an elastic or deformable member (related to stiffness) and energy dissipater (related to damping). An active vibration isolator also includes an actuator which may affect an elastic member, energy dissipater, a machine, and/or the ground. An active isolator may operate with a servomechanism, for which the isolator also includes sensors and computing processors.

It is noted that the terms such as resilient member, energy damper, machine and ground all make sense at the logical level, which implies that physically they (or parts of them) may be integrated into one object. This is true especially for an elastic member and an energy dissipater with a piece of rubber (for example), commonly the former referring to the stiffness property and the latter to the damping property.

For whatever passive or active isolators are, the common things in all isolation systems are such that there is a body of materials, e.g., rubber, iron, etc., to serve as a physical entity of the isolator. In the existing isolator system, the issue of using environment-friendly materials has never been addressed to the best of author's knowledge. In this thesis, a material system of "corrugated cardboard" was studied for vibration isolation in particular as an isolator. The focus of this thesis was on understanding and modeling of the material properties of corrugated cardboard, which are stiffness and damping in this case.

1.2 Research Question

Corrugated cardboard has been widely used for packaging in industry due to its numerous advantages, notably its environment-friendliness (Talbi et al., 2009). Once the package is opened, corrugated cardboard is reused or recycled for purposes other than the one that just now ended. A typical corrugated cardboard as an isolator under a dynamic system (e.g. pump) is illustrated in Fig. 1.2 (a) and (b). Fig. 1.2 (c) shows the structure of corrugated cardboard, which consists of a corrugated core and two liners.

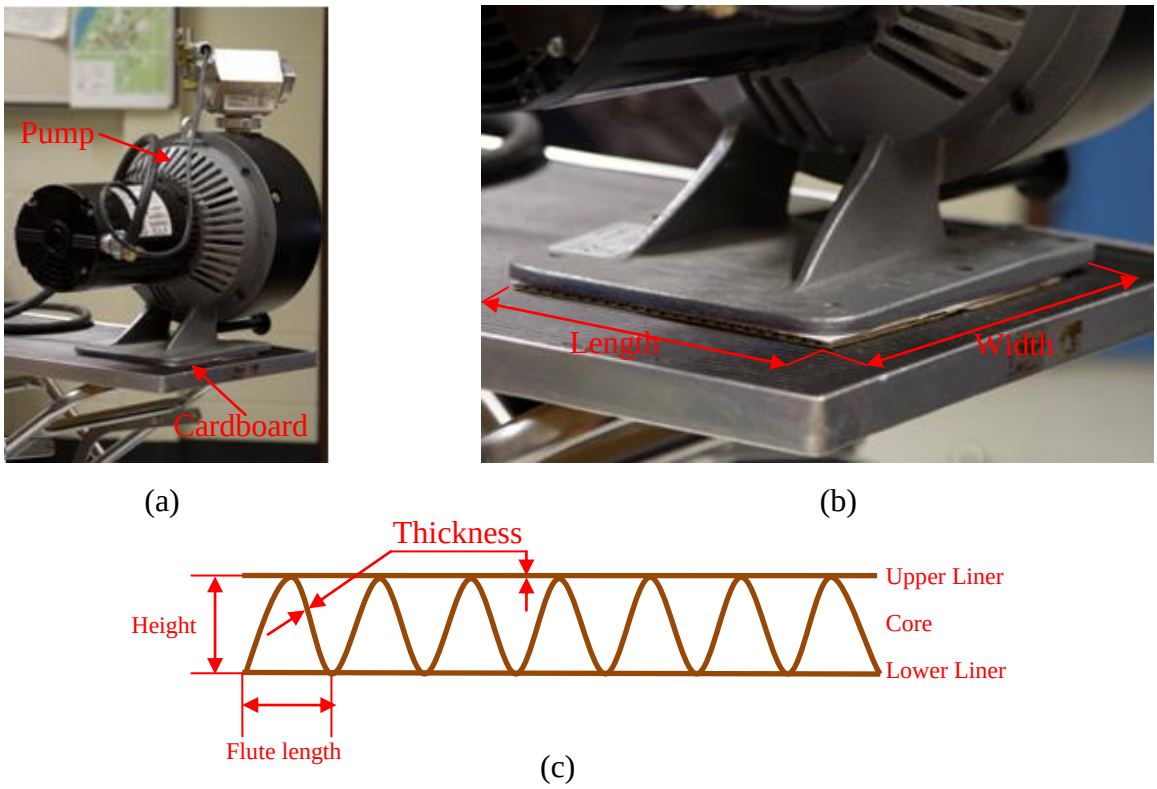

Fig. 1.2 A corrugated cardboard as an isolator under dynamic system: (a) far view; (b) near view; (c) Structure

The geometry of corrugated cardboard can be found in Fig. 1.2 (b) and (c). From Fig. 1.2 (b), it can be seen that the length and width of cardboard is defined referring to its location under the pump. Specifically, the length is along the direction of the core of cardboard while the width is perpendicular to the direction of the core. From Fig. 1.2 (c), it can be seen that the thickness is the thickness of the core and liner; the height is the distance between the upper liner and the lower liner; and the Flute length is the distance between two peaks of the corrugated core. Further, Flute length is the parameter that characterizes corrugated cardboard commercially available (Fig. 1.3). The common flute lengths are the standard A-flute (4.67 mm), B-Flute (2.46 mm), C-flute (3.6 mm), E-flute (1.19 mm); as shown in Fig. 1.3.

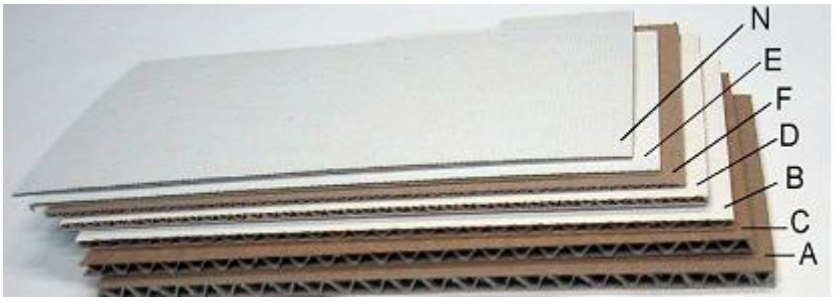

Fig. 1.3 Different flutes of corrugated cardboard (http://commons.wikimedia.org/wiki/File: Cardboard_Main_Flutes_Labeled.jpg)

It is well known that the effectiveness of vibration isolation is related to the mass (or inertia), stiffness, and damping of a vibration isolator. In a vibration isolation system, mass is an inherent property. Stiffness and damping are behavioural properties of the system (Zhang, 2012), which describe the relationship between the excitation and response. Particularly, stiffness represents a system's ability to resist by deformation in response to an external force applied along a direction of the displacement in space (Huang et al., 2012). It is known that in space, there are six directions of displacements (three translations and three rotations); Fig. 1.4. Therefore, the stiffness of a system can be represented in general as a 6×6 matrix to any point on the system. In this thesis, the author only considered the stiffness along the vertical direction of cardboard system because the vibration in this direction is a concern (Fig. 1.5). Damping represents the resistance to motion (velocity) that the body exhibits subject to an external force applied along a direction of motion in space, and it thus plays a major role as dissipation of energy. Damping follows the same structure; i.e., it is in general a 6×6 matrix. However, this thesis only considered the damping in the vertical direction.

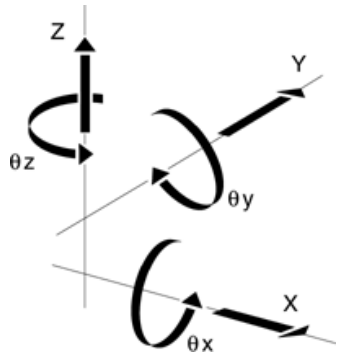

Fig. 1.4 Six degrees of freedom in the generalized coordinate system (http://www.newport.com/ servicesupport/Tutorials/default.aspx?id=143)

The effectiveness of corrugated cardboard as an isolator depends on its stiffness and damping properties. Furthermore, to "optimize" the design of a corrugated cardboard isolator, there is a need to understand the relationship between its stiffness and damping properties and the parameters. Finally, to facilitate the design of a system that consists of several corrugated cardboards, a so-called lumped schematic model of corrugated cardboard is very helpful. This thesis took a vacuum pump in the synchrotron facility of Canada as a case to facilitate the research. Further, corrugated cardboards were assumed to be installed under the compressive loading in its vertical direction only (Fig. 1.5).

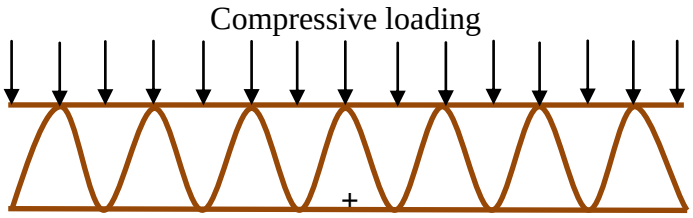

Fig. 1.5 Corrugated cardboard under the compressive loading in its vertical direction

The research questions of this thesis are described as follows:

Question (1): What are the stiffness and damping of cardboard in the vertical direction? The answer to this question is important to evaluate the suitability of cardboard for the purpose of vibration isolation.

Question (2): How can the stiffness of cardboard in the vertical direction be actually modelled? The answer to this question is important to design a cardboard isolator which may contain several cardboards in different assembly configurations. The answer to this question is also useful to optimize the structure of cardboard for the purpose of vibration isolation.

This thesis research was motivated to generate the answers to the above questions.

1.3 A Brief Review of the Related Studies

There have been several studies on the above research questions. In the literature, the finite element method is usually used for corrugated cardboard for the sake of its accuracy. Lu et al. (2001) and Krusper et al. (2007) performed a finite element (FE) analysis for the stiffness of cardboard in the vertical direction. The result of Lu's work differs from the experiment results significantly, while the results of Krusper's work match the experimental results well. However, both Lu's model and Krusper's model are found to have two disadvantages: (1) The model cannot be applied to cardboard with different widths; (2) The peak load cannot be predicted accurately. It should be noted that the width parameter and peak load are important for the application of cardboard for vibration isolation. Difference in the width parameter could give rise to significantly different stiffnesses of cardboard. The peak load gives information of how much load cardboard can sustain. If the load from the vibrating machine is larger than the load cardboard can sustain, cardboard cannot provide the stiffness and is useless for vibration isolation. The disadvantage (1) is because the beam element used in their work is not suitable to modeling different widths of cardboard, and the disadvantage (2) is because no accurate nonlinear material property of cardboard is considered in their work.

1.4 Research Objective and Scope

Based on the research questions and brief review above, specific research objectives were proposed as follows:

Objective 1: Develop an accurate finite element model for the stiffness of corrugated cardboard under loading in its vertical direction with special attention to capturing the information of the width parameter and peak load.

Objective 2: Set up a test-bed for measuring the stiffness of corrugated cardboard. The measured stiffness will be used to validate the finite element model as developed in Objective 1.

Objective 3: Set up a test-bed for measuring the damping of corrugated cardboard.

Objective 4: Demonstrate the effectiveness of the model of stiffness and measurement of damping by designing a vibration isolation system using corrugated cardboard for reduction of the vibration of a vacuum pump system.

This research was focused on the vibration in the vertical direction only and with no consideration of the humidity and thermal effects on cardboard from the environment.

1.5 Outline of the Thesis

This thesis consists of five chapters. The remaining four chapters are outlined as follows:

Chapter 2 provides a literature review to further confirm the need and significance of the research objectives as described before. The literature review is focused on the finite element modelling and measurement of stiffness and damping of corrugated cardboard.

Chapter 3 presents a finite element model for the stiffness of corrugated cardboard and a test-bed for the measurement of stiffness of corrugated cardboard under the loading in its vertical direction. The validation of the finite element model through the test-bed will be described.

Chapter 4 presents the application of the developments in stiffness and damping of corrugated board to design an isolator for the vacuum pump. This includes both the design and experimental validation.

Chapter 5 concludes the thesis with discussion of the research results, contributions, and future wor

CHAPTER 2 LITERATURE REVIEW

2.1 Introduction

This chapter provides a literature review necessary to facilitate understanding of this thesis, in particular its proposed research objectives and scope discussed in Chapter 1. Section 2.2 introduces corrugated cardboard and its application. Section 2.3 presents the relevant research to finite element analysis of corrugated cardboard. Section 2.4 discusses the relevant research on measurement methods for stiffness. Section 2.5 discusses the measurement of damping. Section 2.6 gives a summary of the literature and revisits the proposed research objectives.

2.2 Corrugated Cardboard and its Application

Corrugated cardboard was first patented by Albert Jones (Jones, 1971) and was used for protecting fragile products such as bottles and glass. Later, Oliver Long (Long, 1974) improved Jones' design by strengthening corrugated board with liner sheets added on both sides, thereby inventing corrugated cardboard as it is known now; as shown in Fig 1.2(a). It is known that the initial use of corrugated cardboard was for the purpose of the packaging of fruits in the farm. Nowadays, corrugated cardboard is widely used in the packaging industry to protect and transport goods due to its lightness, recyclability and low cost (Talbi et al., 2009). The use of this material continuously increases every year. The common structure of corrugated cardboard has been illustrated in Fig. 1.2(a) and (b) before, which consists of a corrugated core and two liners. The liner boards provide a high bending stiffness of the composite board, while the corrugated core provides shear stiffness to prevent cardboard from sliding relative to each other and prohibiting the localized buckling (Gilchrist et al., 1999). As shown in Fig. 2.1, there are three

main directions that characterise the cardboard, where MD is the machine direction, CD is the cross direction, and ZD is the vertical direction (Fig. 2.1). Further, throughout this thesis, it is noted that (1) MD: x-axis, CD: y-axis, and ZD: z-axis; (2) the length of cardboard is along the x-axis or MD, the width is along the y-axis or CD, and the height is long the z-axis or ZD; (3) the vertical direction corresponds to the z-axis or ZD; (4) the whole piece of cardboard is called plate.

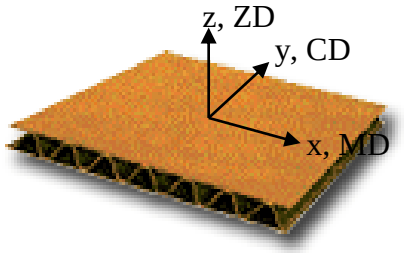

Fig. 2.1 Three main directions that characterize cardboard **(**http://www.kitepackaging.co.uk/images/singlewall.jpg**)**

2.3 Finite Element Modeling of Corrugated Cardboard

Finite element (FE) modeling of corrugated cardboard has been studied, including the top-to-bottom compression strength, edge-compression strength, bending stiffness, creasing behavior, and flat-compression stiffness, and they are briefly discussed in the following.

2.3.1 Top-to-bottom compression strength

One of the common applications for corrugated cardboard is cardboard box for storing and transporting goods. A cardboard box is box made of corrugated cardboards, as shown in Fig. 2.2(a) and (b). The most important loading case for cardboard box is top-to-bottom compressive loading from stacking; as shown in Fig. 2.3. Thus, the strength of cardboard under top-to-bottom compressive loading needs to be known. The standard method to determine the strength is the box compression test (BCT), in which buckling behavior can be observed; (Fig. 2.4). In the BCT test, compression loading is applied on the top surface of a box and the bottom surface is fixed. The vertical deformation of the box is recorded, and the compressive strength is then calculated based on the load VS deformation plot from the measurements.

(a) (b)

Fig. 2.2 Cardboard box from (a) front view **(**http://filmenglish.files.wordpress.com/2011/10/cardboard-box.jpg); (b) top view (http://www.alliedpackaginguk.co.uk/images/1.jpg)

Fig. 2.3 Box stacking (http://image.shutterstock.com/display_pic_with_logo/739267/105698087/stock-photo-stacking-cardboard-boxes-in-a-tidy-stack-on-a-white-background-105698087.jpg)

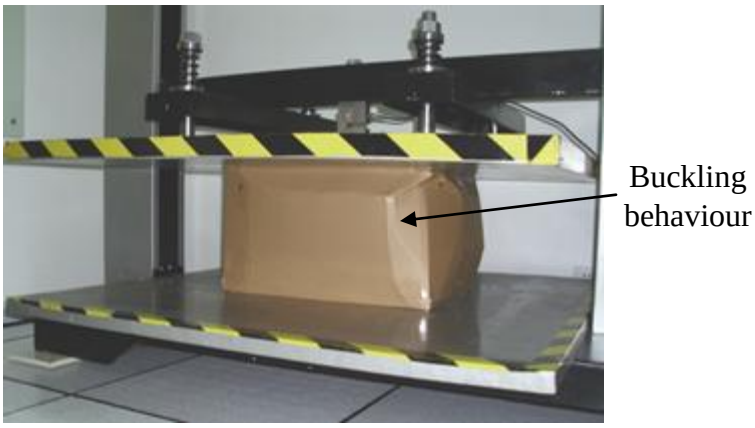

Fig. 2.4 BCT test set-up (http://upload.wikimedia.org/wikipedia/commons/6/6b/Packaging_ Compression_tester.jpeg)

The experimental study was first conducted on the cardboard box under top-to-bottom compression loading by McKee et al. (1963), in which the compression strength of the cardboard box was derived. McKee et al. (1963) developed a critical compression load equation for the cardboard box. McKee et al. (1963) proposed a semi-empirical equation to predict strength of the cardboard box under compression. The strength from the box compression test (BCT) is given by McKee's equation as follows (McKee, 1963):

$$BCT = a \times ECT^{b} \times \sqrt{D_{MD} D_{CD}}^{1-b} Z^{2b-1} \qquad (2.1)$$

where

a, b : constants determined experimentally,

ECT : strength from Edge Crush Test,

Z : perimeter of the cardboard box, and

D : bending stiffness of corrugated cardboard.

From Eqn. (2.1), it can be found that the strength is related to the strength of corrugated cardboard from the edge crush test (ECT), the MD and CD flexural stiffness, cardboard box perimeter, and cardboard box depth. The ECT is a test to derive the stiffness of corrugated cardboard under compressive loading on its edge. Further, Eqn. (2.1) is simplified as a product of the board ECT, board thickness, and box perimeter and it is as follows (http://en.wikipedia.org/ wiki/Edge_crush_test):

$$BCT = 5.876 \times ECT \times \sqrt{Z \times d} \qquad (2.2)$$

where Z is the box perimeter, and d is the thickness of corrugated board.

The compression strength is mainly determined by the ECT strength of cardboard. In other words, the buckling behavior of the cardboard box can be predicted by the ECT strength of corrugated cardboard. Urbanik (1996) stated: "the accuracy of the McKee formula (McKee, 1963) was found within 6.1% on average. The McKee formula is limited to regular slotted-style cardboard boxes. Regular slotted-style cardboard box is the box with the length does not exceed three times the width and the perimeter does not exceed seven times the depth. Thus, the relevance of the McKee formula to the cardboard boxes other than the regular ones needs to be studied." Urbanik (1996) further stated: "Statistical formulas (Maltenfort, 1956) demonstrated a greater sensitivity to the cardboard box length and width effects than predicted by the McKee formula. Elastic boundary conditions examined by Bulson (1969) introduced a more significant length sensitivity for the buckled plates than that allowed by the McKee formula."

Finite element methods have also been studied to analyze the cardboard box other than the regular slotted-style cardboard boxes. A finite element model (Pommier and Poustis, 1989) was proposed as an alternative to the McKee formula to predict the top-to-bottom strength of the cardboard box. In their model, the linear material property was considered, including bending stiffness and shear stiffness of corrugated cardboard, which were measured through an anticlastic bending test. According to Gilchrist et al. (1999), the free rotational boundary of the folding ridges of the cardboard sleeve was modeled since all four sides the corrugated board expands outward under the top-to-bottom compression. The finite element methods provided results in agreement with their experimental results. Pommier et al. (1991) further refined the finite element model to optimize the components of the cardboard box under top-to-bottom compression loading. The linear material property was first determined from the bending stiffness experiment. Each corrugated cardboard was then taken as an effective homogeneous plate and its structure was obtained by assembling four vertical plates. The equivalent material properties of each plate were calculated by means of a homogenization process. The shell quadratic interpolation rectangular element was used to discretize the structure as these can model the membrane and bending stiffness of the board. Only the quarter of the structure was analyzed, which is shown in Fig. 2.5. Four different boundary conditions were imposed on the

model as shown in Fig. 2.6, according to Pommier et al. (1991): (a) the side edge can rotate freely around z-axis and can move freely in the x-y plane; (b) the side edge cannot rotate freely around z-axis but can move freely in the x-y plane ; (c) the side edge can rotate freely around z-axis but cannot move freely in the x-y plane; (d) the side edge can neither rotate freely around z-axis nor move freely in the x-y plane. In Fig. 2.6, the solid curve is the shape of the plate before deformation, while the dashed curve is the shape of the plate after deformation. The results have shown that the first boundary condition (Fig. 2.6a) most fit the real tested condition and the BCT results of the finite element model are consistent with the experimental results.

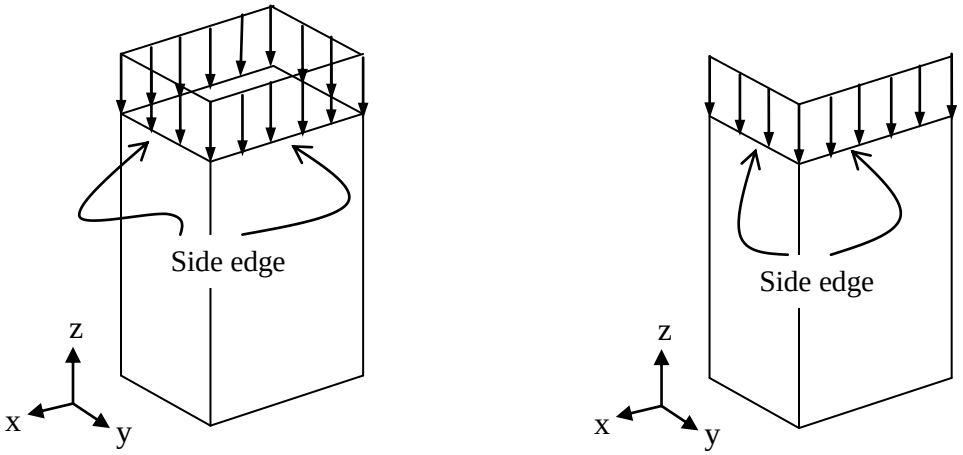

(a) (b)

Fig. 2.5 (a) Full size (b) one quarter size (Adapted from Pommier et al., 1991)

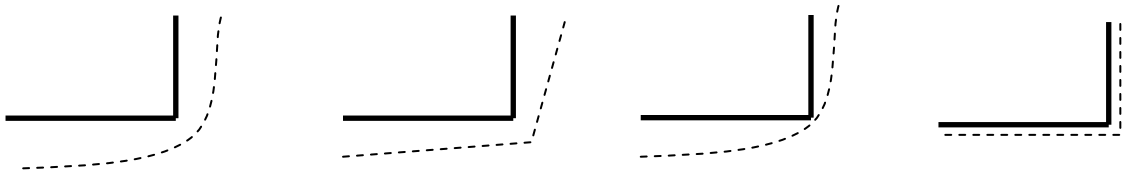

(a) (b) (c) (d)

Fig. 2.6 Boundary conditions on cardboard subject to the vertical loading from top view (Adapted from Pommier et al., 1991)

Biancolini and Brutti (2003) also used FE models for the buckling analysis of cardboard boxes. Linear elastic material properties were first derived from the experimental results. Further, each corrugated cardboard of the cardboard box was taken as an effective homogeneous plate and its equivalent material properties were calculated by means of a dedicated homogenization process,

as described by Biancolini and Brutti (2003). Shell elements were used to discretize corrugated cardboard. Further according to Biancolini and Brutti (2003), for the boundary conditions, the nodes on the bottom edges were constrained in the vertical displacement, and the node on the vertical displacements of the node on upper edges were connected to a master node, loaded with the compression load. The reliability of the proposed model was checked by comparing the finite element results with the experimental ones. The results have shown that the proposed model can accurately predict the strength and buckling behavior of the cardboard box under a compression test. However, the above studies were not able to predict the inelastic buckling response of the cardboard box as a nonlinear material model was not considered.

The nonlinear material finite element model was further implemented to predict both elastic and inelastic behaviors of the cardboard box subjected to top-to-bottom compressive loads. Beldie et al. (2001) used Hill's orthotropic yield criterion to characterize the nonlinear material property. The same boundary condition was used, where the nodes on the bottom edges were constrained in vertical displacement, and loaded on the top edge. The study represented three sets of experiments and analysis models: compression of corrugated cardboard, cardboard box segments, and a cardboard box. Their experimental results showed that the middle segment of the cardboard box exhibits a higher stiffness than that of corrugated cardboard and that of the cardboard box, which led to the conclusion that the low initial stiffness of the cardboard box was caused by the low stiffness of the upper and lower corners. Besides, the stiffness of the cardboard box from the FE model was found to be inconsistent with the experimental results This was because the FE model did not consider the behavior of creases of the cardboard box. Urbanik and Saliklis (2002) conducted a parametric study of the material characteristics that affect the critical buckling stress of cardboard box based on finite element model with the consideration of both the material nonlinearities and initial geometric imperfections. Their finite element model was subjected to a uniform displacement on the top edge and the other edges were taken as simply supported. The results from the proposed model were consistent with the experimental results and a simplified failure formula for the corrugated box was developed based on the parameter study.

2.3.2 Edge compression strength

According to Nordstrand (2004), analysis of the top-to-bottom compression loading of cardboard was often associated with uncertainties; for example, the creases between flaps and side panels introduced eccentricities along the loaded edges. The buckling behavior is of primary interest and it is mainly determined by the ECT strength of corrugated cardboard; see Eqn. (2.2). Many studies were conducted on the ECT strength of corrugated cardboard. Fig. 2.7 shows the schematics of the experiment test set-up for an edge crush test. In the ECT test, compression loading is applied on the edge of cardboard in the MD or CD direction, while the bottom edge is fixed. The deformation is recorded and the ECT compression strength is then calculated based on the load VS deformation plot from the experiments.

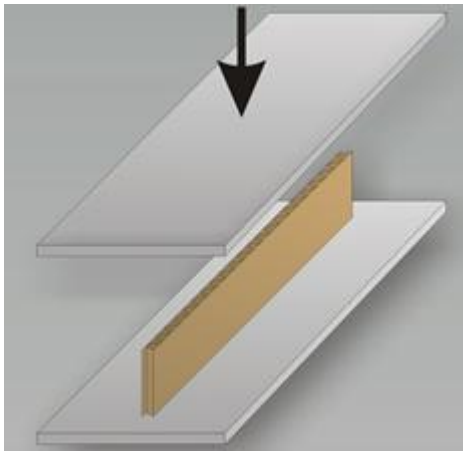

Fig. 2.7 Schematics of the edge crush test (http://www.klingele.com/uploads/pics/ect_labor_01.jpg)

The strength of the simply supported corrugated cardboard subjected to edge compressive loading was studied experimentally using a specially developed test fixture by Hahn et al. (1992). The load VS in-plane displacement response was recorded to calculate the strength. It was found by Hahn et al. (1992) that the presence of initial imperfections in corrugated cardboards was very sensitive to the response; however, the collapse loads did not change very much. This was further attributed to the stable post-buckling behavior of cardboards. In their work, a simplified design analysis was also derived from the approximate post-buckling analysis and compared with an existing design formula for corrugated cardboard. Local buckling of the liner on the concave side of the buckled cardboard was observed at load levels close to the collapse load.

Cardboard collapse was triggered by a compressive failure of the liners initiated at the unloaded edges. According to Hahn et al. (1992), the non-linear property was very important to render an accurate model for corrugated cardboard as cardboard may undergo large out-of-plane displacement, i.e. deflections many times the thickness of corrugated cardboard.

Analysis of the strength and buckling behavior of corrugated cardboard under edge compressive load requires consideration of geometrical non-linearity due to large deflection. Several analytical studies that considered large deflection (Coan, 1951; Yamaki, 1959) were conducted on the edge compression strength of corrugated cardboard. According to Folie (1971), there were few analytical solutions available due to the complexity of the structure of corrugated cardboard.

In order to solve this difficulty, the finite element method was used. Finite element analysis (Johnson and Urbanik, 1989) was employed to analyze the elastic buckling and strength of the corrugated board under the edge compressive loading. Geometrical nonlinearity was considered and the nonlinear material model was applied by using an orthotropic elastic-plastic stress-strain relation. The model considered the actual structure of corrugated cardboard, and the plate element was used to model the structure in a two dimensional (2D) domain. Fig. 2.8 is an illustration of the finite element model with plate elements. Good agreements were shown between the model predicted and experimental results on the strength and buckling load of corrugated cardboard and the model was applied to optimal design of a wide variety of structures. Biancolini and Brutti (2003) also studied the strength of corrugated cardboard under the edge compressive load by means of experimental and finite element analysis with commercial code MSC/Natran. Linear material properties were used and derived from experiments. Shell elements were used, which were properly orientated to reproduce the actual structure of corrugated cardboards of liners and flutings in a three dimensional (3D) domain. Fig. 2.9 is an illustration of the finite element model with shell elements. In the model of Bianolini and Brutti (2003), the upper side node was subjected to load and shared with the lower side node. The lower side node was constrained to have the vertical displacement only. The linearized eigenvalue buckling analysis in the finite element method was used to evaluate the model with the experimental results on the strength and buckling load of corrugated cardboard, in which good agreement was achieved. However, the collapse load of corrugated cardboard was not considered in their studies.

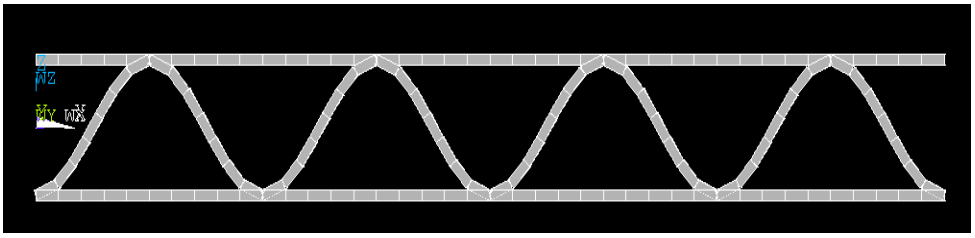

Fig. 2.8 Illustration of the finite element model with plate element

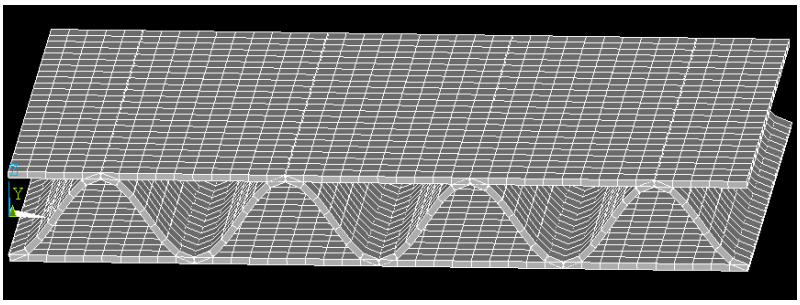

Fig. 2.9 Illustration of the finite element model structure with shell element

Nordstrand (1995) refined the model and performed parametric studies on the strength of corrugated cardboard subjected to edge compressive loading based on the geometrically nonlinear finite element analysis. The corrugated core was simplified as a homogeneous linear-elastic layer in the finite element model. A shell element based on an iso-parametric approach was selected, which accounts for the bending and shear deformation. Loading and boundary conditions for the model are shown in Fig. 2.10 (Nordstrand, 1995), where w: the lateral displacement in the Z-direction; P_x: load applied on both edges, and a and b: the length and width of cardboard, respectively. All the edges can only deform only in the x-y plane and can rotate freely. Both buckling load and collapse load of corrugated cardboard were analyzed. The collapse load was calculated based on material failure of the facings predicted from the Tsai-Wu failure theory. The model was validated with the analytical solution of a previous work (Reddy, 1994). Parametric studies were then performed to investigate the sensitivity of the collapse load with respect to changes in the transverse shear stiffnesses of the core, initial out-of plane imperfections, asymmetry in board construction, slenderness ratio and eccentric loading of the plate. Nordstrand (1995) found that a reduction of the transverse shear stiffnesses of the core below a certain limit produced a significant reduction in the collapse load, and the collapse load was insensitive to small imperfections but sensitive to large imperfections.

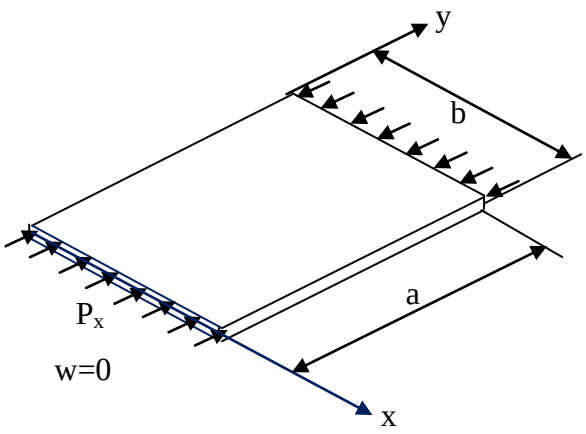

Fig. 2.10 Edge loading of corrugated cardboard (Adapted from Nordstrand, 1995)

Allansson and Svard (2001) performed a finite element analysis on corrugated cardboard with both detailed model and simplified model. Allansson and Svard (2001) only considered the anisotropic linear material behavior. Only the quarter of the structure were considered due to the symmetrical structure as well as loading; Fig. 2.11. The boundary conditions are as follows: u_1, u_5 and u_6 were set to zero (Fig. 2.12), u_2, u_4 and u_6 were set to zero, u3 and u4 were set to zero (Fig. 2.12). A load was introduced on a master node on the upper side, slaving the vertical displacements of the nodes on the upper face. A good agreement of the load–displacement curves between experiments and finite element simulation was achieved. However, the above models cannot predict the accurate inelastic buckling behavior of corrugated cardboard, as nonlinear material properties were not considered.

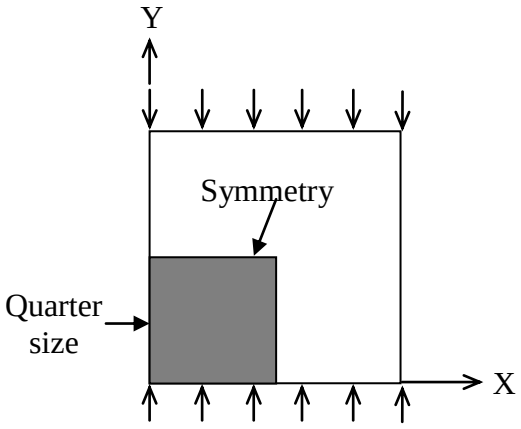

Fig. 2.11 Quarter of cardboard with symmetry lines (Adapted from Allansson and Svard, 2001)

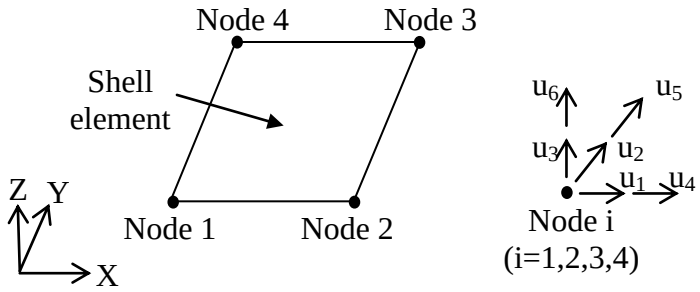

Fig. 2.12 Degrees of freedom of the shell element (Adapted from Allansson and Svard, 2001)

Urbanik and Saliklis (2002) proposed a finite element analysis to predict both elastic and inelastic buckling behavior of corrugated cardboard under edge-compression loading, and further parameter study was performed to find the formula for predicting the failure of corrugated cardboard. The commercial ANSYS_ FE code was used to calculate the buckling load. Material nonlinearities and initial geometric imperfections were taken into account. A uniform displacement on the top edge were considered, while the other edges are simply supported. Results led to a finite element model to fit the experiments and a simplified formula to predict the failure of corrugated cardboard was formulated. Rami Haj-Ali et al. (2008) improved the nonlinear finite element model for analysis of corrugated cardboard under edge-compressive loading. Rami Haj-Ali et al. (2008) considered the anisotropic nonlinear material relation between stress and strain. The connection between the tips of the core and the liners was assumed to be a fully bonded contact. This was achieved by making the tips of the core connected to the liner by letting them share the same node as shown in Fig. 2.13. The model was simulated subject to two kinds of edge compressive loading test: non-standard test and Tappi-type edge crush test. For both tests, the fixed boundary degree of freedom conditions were used for bottom edge nodes. The boundary conditions were the same as those at the top edge except for the axial DOFs where all the edge nodes were made to be of the same displacement in compression. The result has shown that the proposed model is accurate for predicting the strength and ultimate failure of the corrugated board.

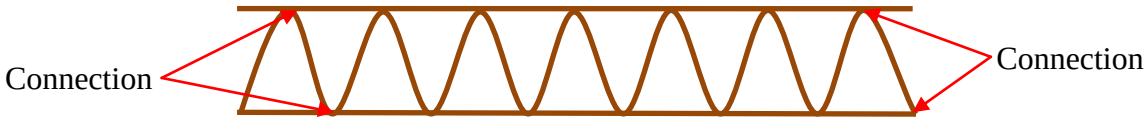

Fig. 2.13 Connection between the tips of core and the liner (Adapted from Haj-Ali et al., 2009)

2.3.3 Bending stiffness

Bending stiffness is another important factor for designing the strength of corrugated cardboard box under the top-to-bottom compression loading. Numerous studies have been conducted on the bending stiffness of corrugated cardboard using analytical and experimental approaches. In these studies, the bending stiffness was determined based on beam formulations. Specifically, the bending stiffness is equivalent to the product of elastic modulus and a moment of the inertia. Review of previous analytical and experimental work on bending stiffness of corrugated cardboard can be found in the work of Luo et al. (1995). There are two typical tests for measuring the bending stiffness of corrugated cardboard: (1) three point bending test; (2) four point bending test. Fig. 2.14(a) shows the principle of the three-point bending test. Cardboard is subjected to bending by the lateral force F on the top surface, while the two ends of the bottom surface is fixed. Fig. 2.14(b) shows the principle of the four point bending test. Cardboard is subjected to bending by the lateral forces on both end of the top surface, while the bottom is fixed.

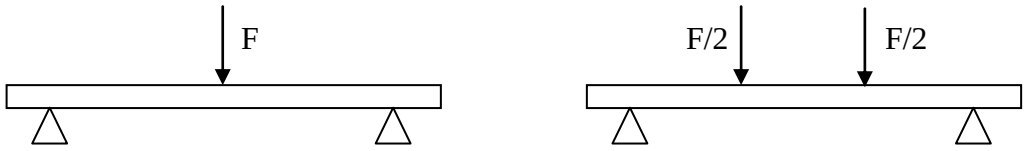

(a) (b)

Fig. 2.14 (a) three point bending test (b) four point bending test

Finite element modeling (Peterson, 1983) was first applied to study the stress fields in corrugated cardboard under the three-point bending load. The linear-elastic and symmetrical material properties were used. The liner and the core were discretized into beam elements, and the core was treated as a sine geometry. Loading was applied on the middle of the top surface of corrugated cardboard, while the two ends of the lower surface were fixed. Stress was predicted from the model and validated with the experiment results. The result indicated that the critical location in terms of the stress was at the core.

Further, Pommier and Poustis (1990) performed finite element analysis on the bending stiffness

of corrugated cardboard under a three-point loading. Linear material property was used and the corrugated core was treated as a trapezoidal mesh structure. Assumption were that the bonding between the fluting and liners was permanent. Similarly, loading was applied on the middle of the top surface of corrugated cardboard, while the two ends of the lower surface were fixed. The results were compared with the measured results for the bending stiffness, and it was found that the model was insufficient to predict the bending stiffness. Nordstrand and Carlsson (1997) investigated both the bending and transverse shear stiffness of corrugated cardboard under three-point bend test using a finite element approach. Linear material properties were used and the finite element model was discretized as a sine meshed structure using the shell element. The model included the following features: (1) the connection between the liner and core was constrained; (2) only a part of cardboard was considered; and (3) loading was uniform lateral displacements over the nodes on the cross-section at the left end of the bottom surface. The calculated bending stiffness from the finite element model was found to be consistent with the measured result, while the calculated shear stiffness was found to be significantly larger than the measured result. The explanation for this was that the finite element model was based on the material properties measured before corrugation, which is inconsistent with the measurement set-up.

Investigation on the bending stiffness of corrugated cardboard has also been performed using a finite element approach under the four-point bending test (Gilchrist et al., 1999). Both geometric and material nonlinearities were included in the model. The parameters in the model were determined through tests. The shell elements were used to model cardboard. In the model, the connection between the linear and core was modeled in two different ways: (1) the extreme position of the core was connected to the liner by sharing the same node; (2) the multi-point constraint (MPC) was utilized using a beam element. The results from both ways were found approximately the same. The load vs deformation relation from the finite element model was plotted and the model result was compared with the experimental result. The result underestimated the bending stiffness of cardboard; the explanation for this error was that this was due to neglecting the stiffness added by the glue which bonds the liners to the core.

The finite element model for bending was also studied by homogenizing corrugated cardboard as

an equivalent orthotropic plate for the purpose of computational efficiency (Aboura et al., 2004). In this model, two situations were considered: thin shell element and the plate elements. For the 3D model, linear orthotropic material property was considered and obtained through their experiments. The connection between the liner and core was modeled as a perfect bonding. The tips of the core were connected directly to the liner by letting them share the same nodes. For the 2D model, the linear elastic property was used and calculated from a homogenized analytical model proposed in their paper. A good correlation between the experimental result and the two FE results was achieved. The results have shown that the simplified homogenized procedure is adequately accurate and 10 times faster than the 3D approach. Talbi et al. (2008) refined the homogenized analytical model by considering the behaviors under the transversal shear efforts and torsion moments. The model is discretized by the shell element. Different loadings were applied to the model including tensile loading, shear loading, and bending loading. The results obtained by the present model were compared with those given by the 3D shell simulations and experiments. The comparison had shown a satisfactory efficiency and accuracy with the homogenization model.

2.3.4 Creasing behavior

According to Gooren (2006), creasing of corrugated cardboard is an important technique to reduce the necessary moment in the fold . The creasing behavior of corrugated cardboard has been studied by a combined experimental-numerical approach (Gooren, 2006). An experiment set-up was designed to perform creasing on small samples of cardboard (Fig. 2.15), where cardboard was put on an anvil and a creaser applies a force on a certain point of the top surface of cardboard. Only the case in which the creasing force was applied in the cross direction was considered, as this orientation is the most critical.

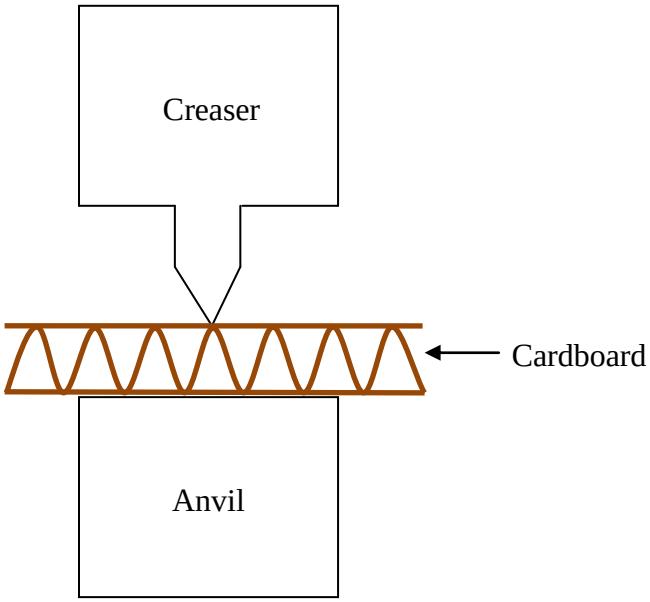

Fig. 2.15 Creasing experiment set-up (Adapted from Gooren, 2006)

A numerical approach was used to provide insight into the stress and strain distribution (Gooren, 2006). In this work, an orthotropic elastic-plastic material model was employed. The elastic model was determined by the orthotropic Hooke's Law, while the plastic model was based on the Hill yield criterion. The material properties were partially determined by a tensile test and partially determined by empirical estimation due to some measurement difficulty. The core of corrugated cardboard was assumed to be a sine shape. The so called washboard effect, i.e. non-flatness of the inner liner, was included in the model. For the boundary and loading condition (Fig. 2.16), the creaser tip is modeled as a rigid circular body and undergoes a negative linear displacement: w. Three positions of the creaser in the experiments were analyzed in the FE model. The FE result was compared with the experimental result, but no good agreement wass achieved. The author's explanation was that the disagreement was caused by the limitation of the experiment set-up. The anvil cannot constrain cardboard fully, which causes cardboard to bend during the crease test (Fig. 2.17). This is not expected in the crease test.

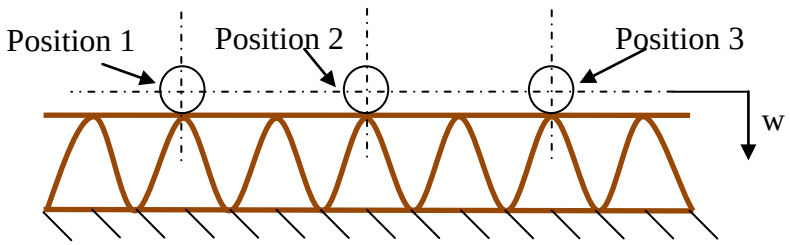

Fig. 2.16 Loading and boundary condition imposed on the FE model (Adapted from Gooren, 2006)

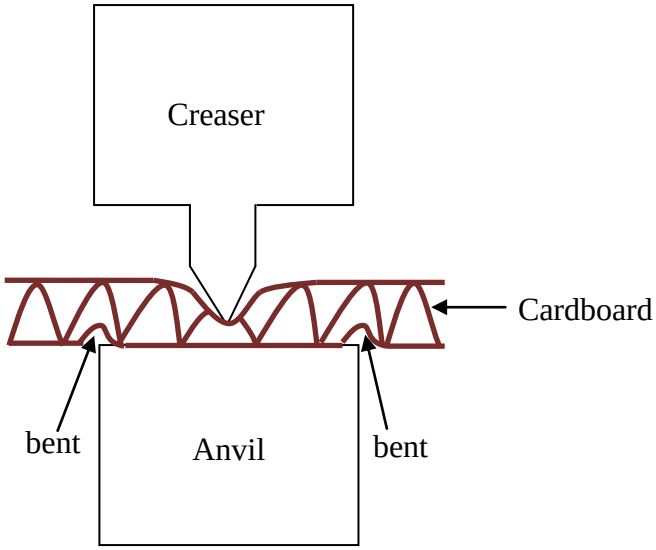

Fig. 2.17 Bending of cardboard during the crease test (Adapted from Gooren, 2006)

Limits found in the work (Gooren, 2006) were solved by proposing a refined experiment set-up (Romans 2008). In Fig 2.18, a refined creasing experiment set-up is shown, in which the specimen is attached between four rubber clamps to constrain the board ends, and loaded by the creaser. The FE model followed the same approach of Gooren (2006) except that the so called washboard effect was not considered as it was marginal for the creasing behavior. A good agreement was achieved between the finite element results and experiment results.

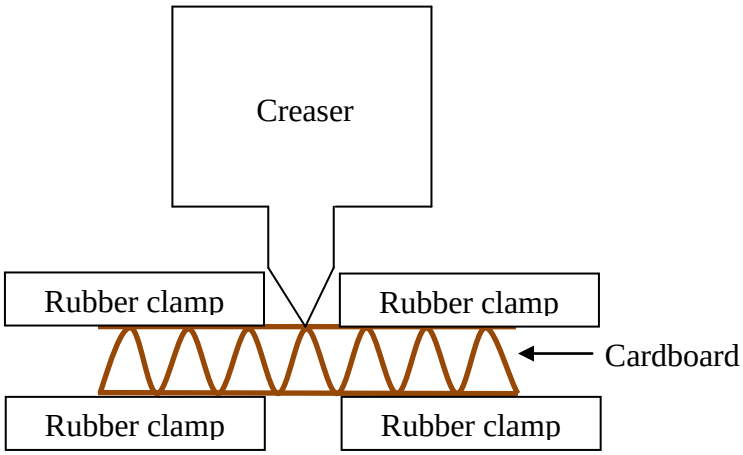

Fig. 2.18 Refined creasing experiment set-up (Adapted from Romans 2008)

Finite element methods have been discussed above on corrugated cardboard under a top-to-bottom compressive loading, edge-compressive loading, bend loading, creasing loading. However, these methods are not found adequate to modeling the behavior of corrugated cardboard under vertical compressive loading due to no consideration of the contact behavior, which will be discussed in detail in Section 2.3.5.

2.3.5 Flat compression stiffness

The stiffness of corrugated cardboard under compressive loading in its vertical direction is essential to know for both manufacturing process and vibration isolation. For the vibration isolation, as mentioned previously, it is governed by the stiffness of the corrugated board in its vertical direction. The standard test for measuring the stiffness is called the flat crush test (FCT). Thus, the stiffness in its vertical direction can be called the flat compression stiffness. Fig. 2.19 is an illustration of the FCT test, in which the corrugated board is placed between two plane-parallel plates and is subjected to a compressive loading, and during the test, the load vs displacement relation is recorded. The stiffness is then calculated based on the load vs displacement relation plot.

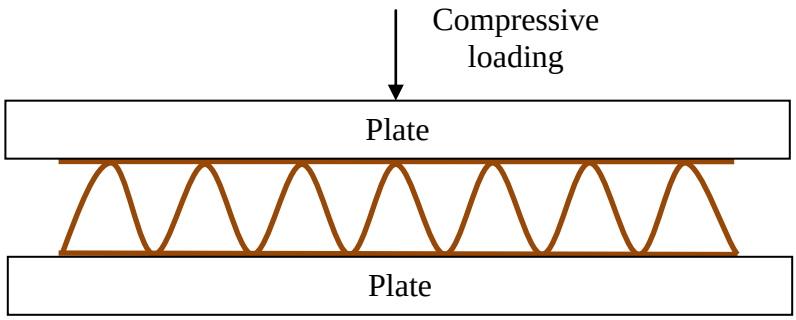

Fig. 2.19 Illustration of the FCT test

There have been studies on the stiffness of corrugated cardboard under compressive loading in its vertical direction. Lu et al. (2000) proposed a finite element model to predict the compressive behaviour of corrugated cardboard under uniform flat compressive loading. Lu et al. (2000) used 2D curved beam elements and the elasto-plastic material which were represented by a bi-linear constitutive model satisfying the J2-flow theory (Lu et al., 2000). Surface contact elements were employed to model the change in the contact behaviour of corrugated cardboard during the compression as shown in Fig. 2.20 shown. This is because the area of the contact between the core and the liner is changing significantly in different phases of the compression (A,B,C,D,E in Fig. 2.20).

The C flute cardboard with the same length and width was analyzed It can be found that their FEM result differs from the experimental results quite significantly, with an error of about 30% estimated by the author of this thesis. This is due to two factors: (1) the model used an approximate sine shape; (2) the nonlinear material property was not accurately given.

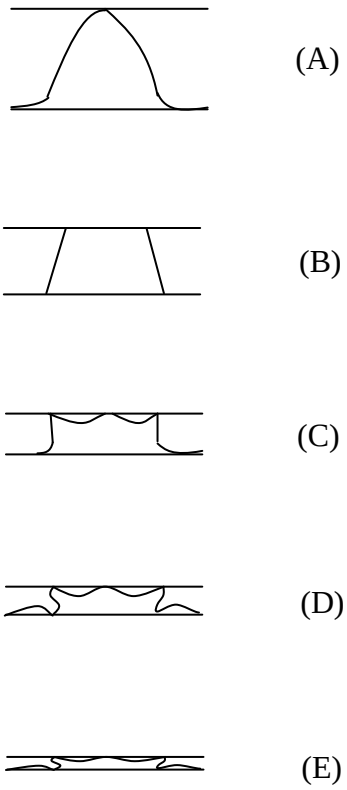

Fig. 2.20 Contact change during compression (Adapted from Lu et al., 2001)

Krusper et al. (2007) has refined the finite element model of Lu's work with a more accurate core shape. In this model, corrugated cardboard was modelled by 2D beam elements, and linear elastic material property was considered. Cardboard was analyzed with the same length and width as the one studied by Lu et al. (2001). The FEM result and experimental result matched until the peak load (where displacement is 0.2 mm) was reached. It was found that the peak load was caused by the buckling behaviour, which was determined by the nonlinear material properties of corrugated board (Krusper et al., 2007). However, the first peak of the load-displacement relation could not be predicted by their model because the model has not considered nonlinear material properties.

Overall, both Lu's model and Krusper's model are found to have two disadvantages: (1) The model cannot be applied to cardboard with different widths; (2) The peak load and the its

subsequent response cannot be predicted accurately. It should be noted that the width parameter and peak load are two important variables for the application of cardboard for vibration isolation. Difference in the width parameter could give rise to significantly different stiffnesses of cardboard. The peak load gives information of how much load cardboard can sustain. If the load from the vibrating machine is larger than the load cardboard can sustain, cardboard is useless for vibration isolation. The disadvantage (1) is because the element used in their work was a beam element. The beam element models the geometry such that the length is considerably longer than the width and the vertical. The beam element is not suitable to modeling cardboard with the width longer than the length. The disadvantage (2) is because no accurate nonlinear material property of cardboard is included in their models. Thus, a refined model with consideration of the width parameter and accurate nonlinear material property should be developed.

2.4 Measurement of Stiffness

By definition, stiffness represents the resistance of an elastic body to deform in response to a force applied along a direction of displacement in space. Stiffness can be identified as static and dynamic due to the imposed forces. Specifically, static stiffness is the property of a structure under loads including no inertia effects, while dynamic stiffness is the property of a structure subjected to forces including inertia and damping effects (Chen, 2009). Usually, the dynamic stiffness was found to be different from that measured from static tests (Dekker, 1999).

For a vibration isolator, stiffness under flat-compressive loading is the main concern. There have been many studies on the measurement of both the static and dynamic stiffness under flat-compressive loading. Mallik et al. (1999) studied the static stiffness of rubber isolators by conducting a compression test in a Universal Testing Machine. A load was applied by the machine and corresponding deformation was recorded. The static stiffness was then calculated as the slope of the load VS deformation relation. Richards and Singh (2001) also performed a test to measure the static stiffness of a rubber isolator. Fig. 2.21 shows the apparatus of the test, where static loads can be applied by adding mass block. The static deformation of the isolator was recorded from the displacement dial indicator. The static stiffness was then calculated based on

the load VS deformation relation. From the perspective of accuracy of measurement, the approach (Mallik et al., 1999) is more accurate than the one of (Richards and Singh, 2001). This is because there are more errors in the latter work (e.g. reading errors due to some misalignment in the dial indicator; the misalignment between the weights and the rubber isolator, etc).

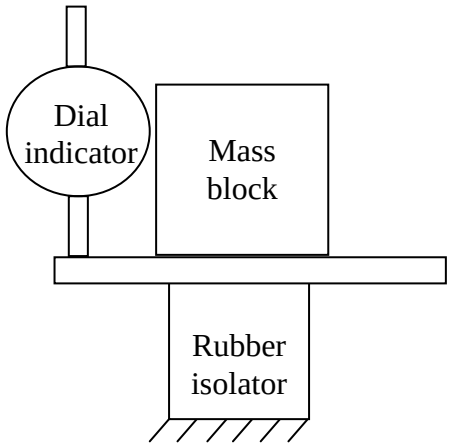

Fig. 2.21 Apparatus of the static stiffness test (Adapted from Richards and Singh, 2001)

Many different techniques have been developed to estimate dynamic stiffness experimentally, in which damping is also estimated. Estimation of damping will be further illustrated in Section 2.5. The direct method was used to measure dynamic stiffness of engine mounts (Nadeau and Champoux, 2000). Fig. 2.22 shows the schematics of the measurement set-up. The mount was fixed at one end, while the other end was subject to a sinusoidal excitation produced by a shaker. The force resulting from the imposed displacement was recorded by the force transducer. The dynamic stiffness was then defined as (Nadeau and Champoux, 2000)

$$K = \frac{F}{X} e^{j\theta} \tag{2.3}$$

where F: the amplitude of the reaction force on the blocked terminal of the rubber; X: the amplitude of displacement on the rubber free end; θ: the phase angle between the displacement and force.

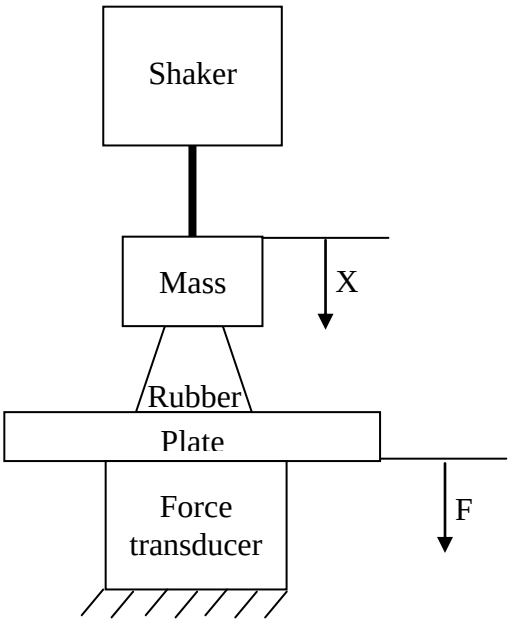

Fig. 2.22 Schematics of the measurement set-up for dynamic stiffness (Adapted from Nadeau and Champoux, 2000)

A direct stiffness method was also applied to study dynamic stiffness of rubber at discrete frequencies (Lapcik et al., 2001), in which servo-hydraulic systems were used. Fig. 2.23 shows the schematic diagram of the experiment set-up, in which the hydraulic actuator was used to apply the dynamic loading. The test specimen was subjected to both a static pre-load and a dynamic load with controlled displacement amplitude. The displacement sensor and force transducer were used to measure the displacement and reaction force, respectively. In this work, the dynamic stiffness was defined as (Lapcik et al., 2001):

$$K = \frac{F}{X} \tag{2.4}$$

where the phase shift in the work (Nadeau and Champoux, 2000) was not considered. F here is the amplitude of the dynamic force applied to the specimen, and X is the displacement amplitude.

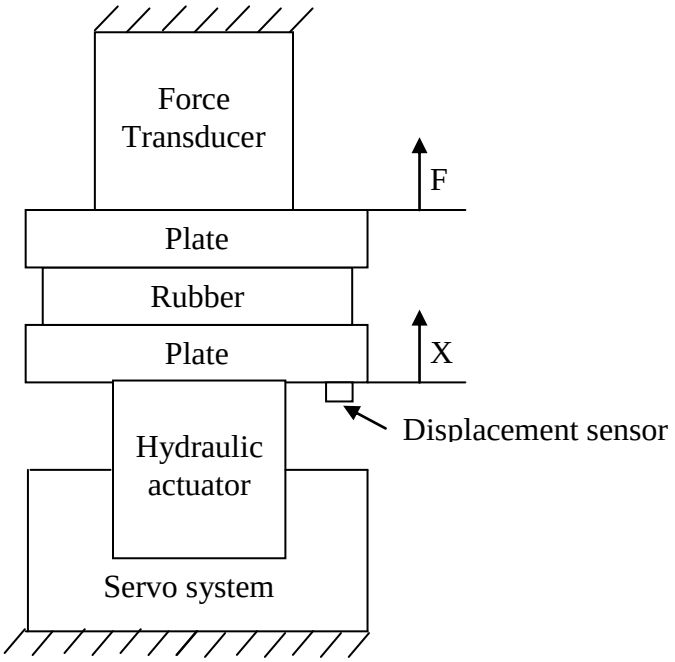

Fig. 2.23 Schematics of the measurement set-up for dynamic stiffness (Adapted from Lapcik et al., 2001)

However, both works on the direct method are limited to a low frequency range due to sensitivity of the shaker/actuator to the excitation signal. The other limitation is that the direct method is often limited to the axial direction, whereas other directions are also important. An indirect method (Thompson et al., 1998) has been developed an indirect method as an alternative, which extends the possibility of measuring at higher frequency or other degrees of freedom. The measurement apparatus is shown schematically in Fig. 2.24(a). It consisted of two blocks of known mass and the specimen was mounted between the two blocks. Here, the reaction force was the product of acceleration of the lower block and mass of the lower block. Governing equations of the system were established based on the model of the system in Fig. 2.24(b), and dynamic stiffness can be derived. The measurement method was applied to a resilient rail pad for use in railway track and good accuracy was achieved. However, the disadvantage of the method is that bulky seismic masses and elaborate laboratory setting are required.

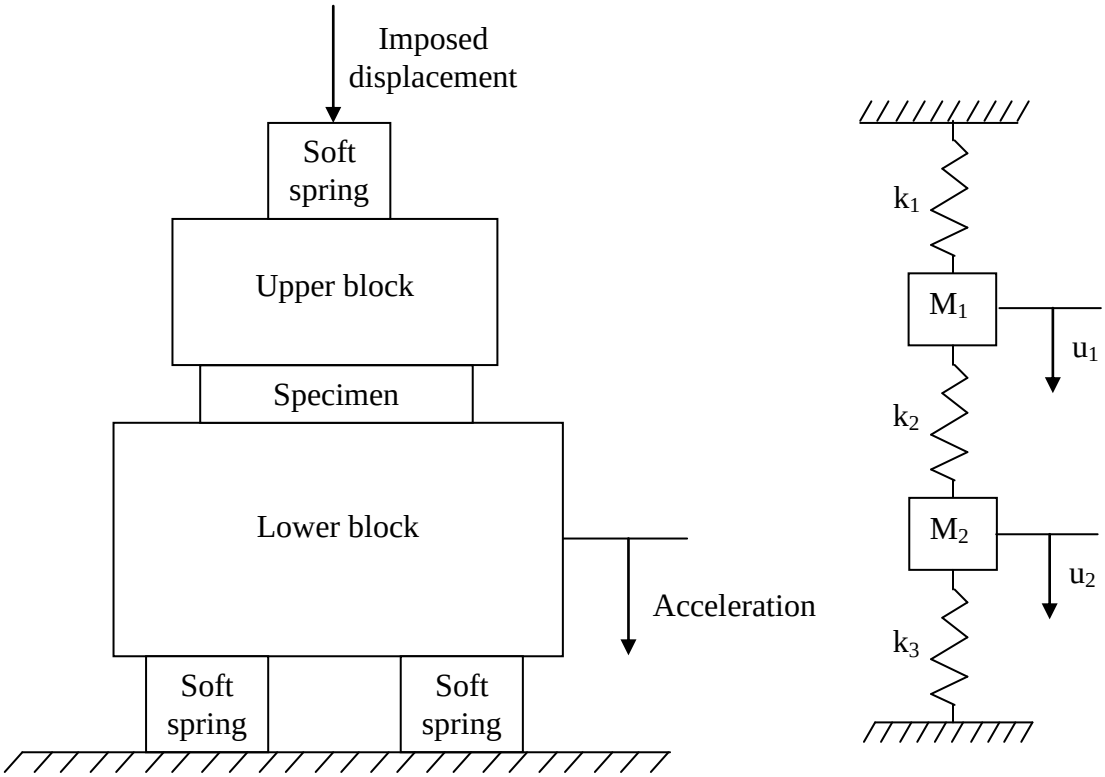

Fig. 2.24 (a) Schematics of the measurement set-up using indirect method (Adapted from Thompson et al., 1998); (b) Model of the measurement system (Adapted from Thompson et al., 1998)

Lin et al. (2005) further proposed a simple experimental method to measure the dynamic rubber mount stiffness characteristics; (Fig. 2.25). A rubber was mounted with an end steel cap. The loading was added by steel mass. An impact hammer was used to apply force along the center of the mass while the displacement of the mass was measured by two accelerometers attached to the mass. The impact force and displacement were recorded and dynamic stiffness was calculated based on the equation derived by Lin et al. (2005):

$$K = \frac{\mathrm{Re}(R)}{|R|^2 (1 - r^2)} \tag{2.5}$$

$$R = \frac{X}{F} = \frac{1}{K[(1 - r^2) + j\eta]} \tag{2.6}$$

where the variable $r = \frac{w}{w_n}$ is the frequency ratio, $w_n = \sqrt{\frac{K}{m}}$ is the natural frequency of the system, η is the loss factor and R is ratio of displacement to force, which were all determined by measured impact force and displacement response. The proposed method was validated by comparing its results with those obtained by using mechanical shaker excitations and those of a conventional direct stiffness method (Nadeau and Champoux, 2000) using blocked transfer frequency response functions.

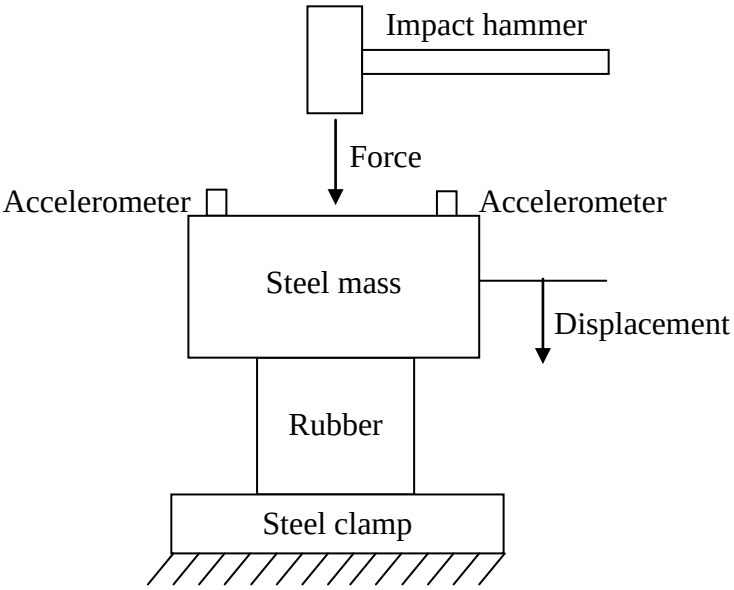

Fig. 2.25 Schematics of the measurement set-up of impact test (Adapted from Lin et al., 2005)

An alternative experiment test bed (Mallik, 1999) was established to obtain the dynamic stiffness of a rubber isolator. Fig. 2.26 shows the experiment apparatus, in which the specimen is fixed at one end in a base, and loaded under a mass in the other end. Two accelerometers are attached to measure the acceleration and displacement of the base and the mass. When the shaker moved, the excitation force and deformation of the specimen can be derived. The excitation force is the product of the acceleration of the mass times mass, and the deformation is the displacement at the mass minus the displacement at the vibration shaker. The resulting force and the deformation can be plotted and the dynamic stiffness can be calculated

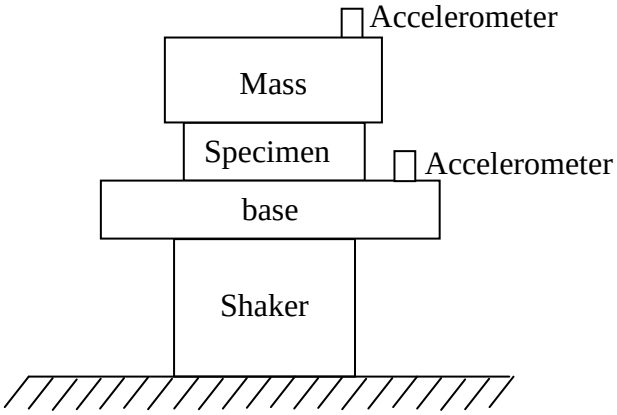

Fig. 2.26 Schematics of the measurement set-up for dynamic stiffness (Adapted from Mallik, 1999)

It is well known that the effectiveness of a vibration isolator is related to its inertia, stiffness, and damping. Here this stiffness refers to static stiffness, but not dynamic stiffness. Thus, knowing the static stiffness is enough for the design of a vibration isolator.

2.5 Measurement of Damping

By definition, damping is the dissipation of energy from different elements of a vibrating structure (Zhang, 2012). In spite of many studies, understanding of damping mechanisms is quite primitive. A commonly used mechanism regarding the damping is the so-called "viscous damping" and it is expressed by the damping force F_d assumed to be proportional to the instantaneous velocity $\dot{x}$, (Rao, 2003):

$$F_d = c\dot{x} \tag{2.7}$$

where F_d: the damping force; $\dot{x}$: velocity; c: the viscous damping constant. Further, damping ratio is widely accepted as a basic measure of the damping, which is related to the viscous damping constant. The damping ratio ξ is defined as the ratio of viscous damping constant c to the critical damping constant c_c, which is given by (Rao, 2003);

$$\xi = c / c_c \tag{2.8}$$

The critical damping constant c_c is defined as the damping constant c when the vibration system converges to zero as fast as possible without oscillating, and it is defined as (Rao, 2003)

$$c_c = 2\sqrt{km} \tag{2.9}$$

There are three typical ways to estimate the viscous damping (Nashif, 1985, Rao, 2003): Logarithmic decrement method, bandwidth method, and transmissibility ratio method. Logarithmic decrement method (Rao, 2003) is used to measure the damping in time domain as Fig 2.27 shown. In this method, the history of vibration decay (Fig. 2.27) is recorded. The following equation (Rao, 2003) is applied:

$$\delta = \log_e(\frac{x_i}{x_{i+1}}) = 2\pi\xi \tag{2.10}$$

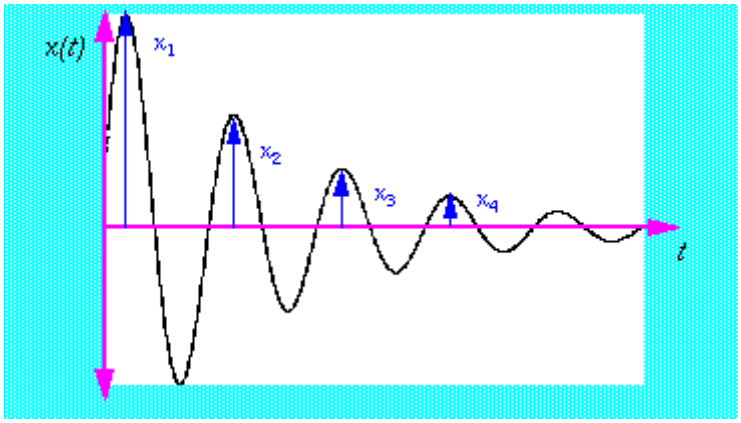

Fig. 2.27 Response of Logarithmic decrement method (http://www.mfg.mtu.edu/cyberman/machtool/machtool/vibration/damping.html)

The half-power bandwidth method was developed to estimate damping from frequency domain (Rao, 2003). In this method, the frequency response function (FRF) amplitude of the system under forced vibration (Fig. 2.28) was obtained. Corresponding to each natural frequency, there is a peak in FRF amplitude, and there are two points corresponding to half power point, 3 dB down from the peak. It is well-known that half-power bandwidth BD is defined as the ratio of the frequency range between the two half power points to the natural frequency at this mode. Based on the observed bandwidth, the damping ratio is calculated (Rao, 2003):

$$\frac{\omega_2 - \omega_1}{\omega_n} = 2\xi \tag{2.11}$$

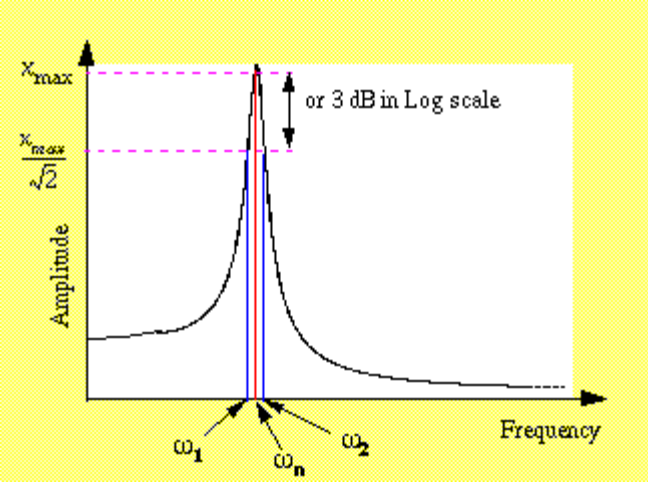

Fig. 2.28 Response of Half-power bandwidth method (http://www.mfg.mtu.edu/cyberman/machtool/machtool/vibration/damping.html)

The transmissibility ratio method was proposed to estimate damping from the transmissibility ratio VS frequency plots. The displacement ratio (T_r) is ratio of the vibration force or motion from the vibration source to the vibration force or source transmitted, which describes the percentage of reduction of vibration by means of the isolator. T_r can be found by (Rao, 2003)

$$T_r = \frac{F_{source}}{F_{transmitted}} = \frac{X_{source}}{X_{transmitted}} = \left\{ \frac{k^2 + \omega^2 c^2}{(k - m\omega^2)^2 + \omega^2 c^2} \right\}^{1/2} \qquad (2.12)$$

where

F_{force} : vibration force from vibration source,

$F_{transmitted}$: vibration force transmitted,

X_{source} : vibration displacement from vibration source,

$X_{transmitted}$: vibration displacement transmitted,

k : the stiffness of corrugated cardboard,

m : the mass of the steel block,

ω : the frequency from the vibration exciter (unit: rad/s), and

c : the damping of corrugated cardboard.

When the resonance ($\omega = \omega_n = \sqrt{\frac{k}{m}}$, where the ω_n is the natural frequency of the whole system) takes place, the damping can be found by (Rao, 2003)

$$c = \sqrt{\frac{km}{T_r^2 - 1}} \tag{2.13}$$

Viscous damping models are not the only damping models. Coulomb damping and hysteretic damping are other typical damping models. Coulomb damping is used to represent dry friction present in sliding surfaces, such as structural joints.

When a material is deformed, energy is absorbed or dissipated by the material and is called material damping. This effect is caused by friction between the internal planes within the material, which slip or slide as deformations take place (Crandall, 1970). The material damping is responsible for the so-called hysteresis phenomenon, as shown in Fig. 2.29. The energy loss in loading and unloading cycle of vibration is equal to the area enclosed by the hysteresis loop. The energy loss per cycle is approximately proportional to the square of the amplitude (Rao, 2003), in which the material damping constant can be derived by

$$\Delta W = \pi h X^2 \tag{2.14}$$

where ΔW is the energy loss per cycle, X is the amplitude, and h is the material damping constant. An experiment test bed (Mallik, 1999) was established to obtain the damping of a rubber isolator. The test bed was also used to measure the dynamic stiffness. Through the experiment, the resulting excitation force and the deformation can be plotted and a hysteresis loop was exhibited. From the loop, the material damping was then calculated according to Eqn. (2.15). The material damping is found convertible with the viscous damping, which is given by (Rao, 2003)

$$c = \frac{h}{\omega} \tag{2.15}$$

where ω is the frequency of the vibration.

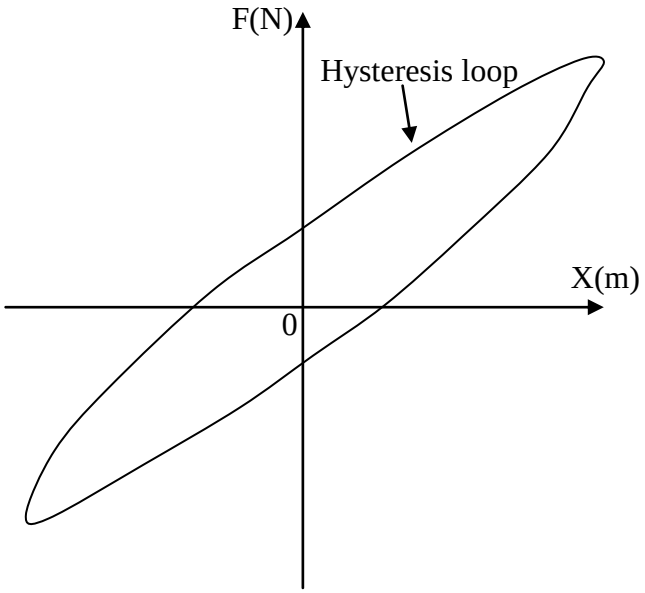

Fig. 2.29 Hysteresis phenomenon

For the vibration isolator, the methods for both material damping and viscous damping can be readily applied. However, it is noted that for cardboard, no test bed for measuring cardboard damping is available in the literature.

2.6 Conclusions

A literature review on the vibration-related properties of cardboard along with how to acquire them was presented in this chapter. These properties are stiffness and damping. Acquisition methods for them include both modeling and experiment or measurement. It has been found that there was no accurate model available in the literature for predicting the stiffness and buckling behaviour of corrugated cardboard with the width longer than length under compressive loading in its vertical direction, to the best knowledge of the author. This is further attributed to no consideration of its nonlinear material property and width parameter in modelling. Further, no test bed for measuring damping of cardboard is available in the literature. Thus, an improved finite element model for stiffness of cardboard and a test bed for measuring damping of cardboard needs to be developed to design and construct a better cardboard system for the purpose of vibration isolation. Revisiting Section 1.4, the proposed objectives 1-3 were defined

for meeting the aformentioned need. Finally, objective 4 provide a proof of the significance of the research developed.

CHAPTER 3 FE MODELING FOR STIFFNESS OF CARDBOARD

3.1 Introduction

This chapter presents a study of finite element modeling and analysis for stiffness of corrugated cardboard under a compressive loading in its vertical direction in the context of using the commercial software ANSYS. Lu et al. (2001) and Krusper et al. (2007) previously performed finite element analysis for cardboard with some limitations. The work presented here is expected to overcome these limitations. The organization of this chapter is as follows: Section 3.2 will describe details of cardboard that is considered for this study. Section 3.3 will present the finite element model. Section 3.4 will present the result and discussion. Section 3.5 will present the conclusions.

3.2 Cardboard System

Cardboard is a real-world system to be modeled. Further, cardboard will be used in the situation where it is put underneath a dynamic system (e.g., vacuum pump); shown in Fig. 3.1. The dynamic system will generate inertial force while it is in operation. The inertial force changes periodically and creates force to the ground. This force is usually called shaking force. The effect of shaking force is vibrations of the ground. The role of cardboard is then to reduce vibrations of the ground in particular in the vertical direction. Cardboard is much like an "isolator", namely making isolation of the dynamic system and the ground.

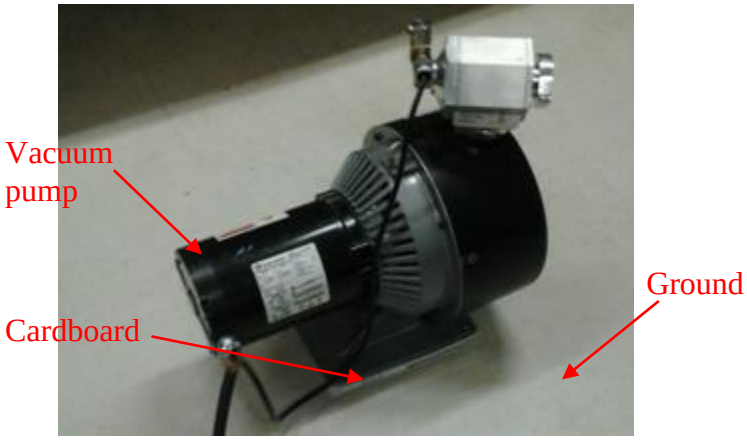

Fig. 3.1 The cardboard system

Fig. 3.2 is a schematic diagram of cardboard and its application situation. In this figure, the information of cardboard (as an example) is given as follows: the thickness of the liner and core is 0.23 mm; the height is 3.6 mm; the length is 32 mm; the width is 38 mm. The FE model is supposed to represent the stiffness of cardboard in the vertical direction (Fig. 3.2).

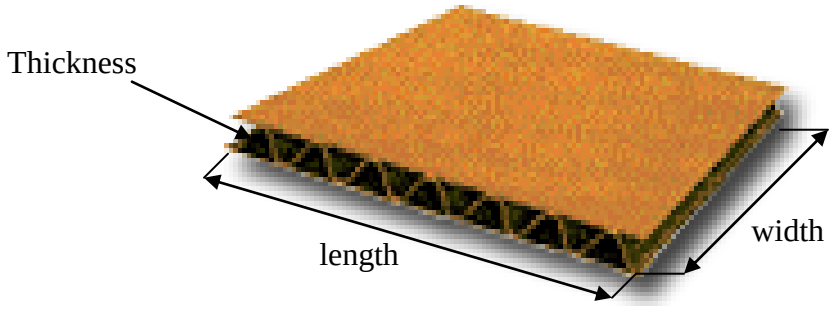

Fig. 3.2 Schematic diagram of cardboard (http://www.kitepackaging.co.uk/images/singlewall.jpg)

3.3 FE Modeling for Stiffness of Cardboard

In this section, a finite element modeling and analysis for stiffness of corrugated cardboard under a compression loading in its vertical direction is performed. Based on the well known general procedure of FE analysis in particular recommended by ANSYS (ANSYS, 2004), the finite element model which describes stiffness of cardboard system is described in the following sections.

3.3.1 Element assignment

The shell element is used to represent corrugated cardboard. By definition, a shell is a geometric form where the thickness of the element is much smaller than the length and the width of the element. Apparently, the shell element has an excellent fit to both the liner and core of corrugated cardboard as shown in Fig. 3.1. Specifically, the shell 181 element (see Fig. 3.3) in ANSYS software is selected, as it includes reduced integration schemes and thus more computationally efficient.

The shell 181 element has 4 nodes (I, J, K, L in Fig. 3.3) and six degrees of freedom at each node (translations in the nodal x, y, and z directions and rotations about the nodal x, y, and z axes). The element enables to model plasticity, stress stiffening, large deflection, and large strain.

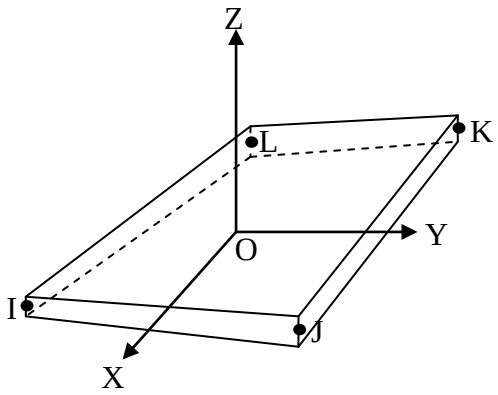

Fig. 3.3 Shell 181 4-Node Structure Shell Element (Adapted from ANSYS, 2004)

3.3.2 Element real constants

There are three real number constants available for the shell 181 element, and they are (1) thickness, (2) element coordinate system orientation, and (3) mass per unit area. According to ANSYS (2004), the shell 181 element assumes that the thickness changes (if not constant) smoothly over the area of the element. The element allows for description of varying thickness in the region which is covered by the element, and this is achieved by having different thickness at each of the four corner nodes I, J, K, L (in Fig. 3.3), respectively. If the element has a constant thickness, only the thickness of the corner node I is specified; otherwise, the thicknesses at all

four nodes need to be specified. For cardboard as shown in Fig. 3.2, the thickness is a constant, 0.28 mm in particular.

The orientation of the element coordinate system is named as THETA in ANSYS software. Unless otherwise stated, the orientation of the element coordinate system is the default orientation for that element type, that is, 0 degrees. It is noted that the origin of the element coordinate system is at the node I (see Fig. 3.3). The element coordinate system is called local coordinate system. The mass per unit area is named as ADMSUA in ANSYS software, and it is 0 as default for cardboard system, as shown in Fig. 3.2.

3.3.3 Material property

Corrugated cardboard is made of oriented wood fibers, and its material properties are thus anisotropic. Commonly, the fiber orientation is approximately symmetric. This means that the material property can be assumed to be orthotropic. Generally, the material property is described by the material constitutive relationship or model. In this thesis, an orthotropic material constitutive model was employed for the two liners and core of corrugated cardboard. The orthotropic constitutive model consists of two parts: the linear elastic and the nonlinear plastic portion. The linear elastic portion is governed by orthotropic Hooke's Law, while the plastic portion is governed by a quadratic Hill yield criterion. The linear elastic orthotropic constitutive model, in terms of relation between stresses and strains for the paper, is assumed to be one as follows (Allasson and Svard, 2001):

$$\begin{bmatrix} \varepsilon_x \\ \varepsilon_y \\ \varepsilon_z \\ \gamma_{xy} \\ \gamma_{xz} \\ \gamma_{yz} \end{bmatrix} = \begin{bmatrix} \frac{1}{E_x} & \frac{-\nu_{yx}}{E_y} & \frac{-\nu_{zx}}{E_z} & 0 & 0 & 0 \\ \frac{-\nu_{xy}}{E_x} & \frac{1}{E_y} & \frac{-\nu_{zy}}{E_z} & 0 & 0 & 0 \\ \frac{-\nu_{xz}}{E_x} & \frac{-\nu_{yz}}{E_y} & \frac{1}{E_z} & 0 & 0 & 0 \\ 0 & 0 & 0 & \frac{1}{G_{xy}} & 0 & 0 \\ 0 & 0 & 0 & 0 & \frac{1}{G_{xz}} & 0 \\ 0 & 0 & 0 & 0 & 0 & \frac{1}{G_{yz}} \end{bmatrix} \begin{bmatrix} \sigma_x \\ \sigma_y \\ \sigma_z \\ \tau_{xy} \\ \tau_{xz} \\ \tau_{yz} \end{bmatrix} \tag{3.1}$$

where

ε_x, ε_y, ε_z : Strain in x, y, z direction,

γ_{xy}, γ_{xz}, γ_{yz} : Strain in xy, xz, yz plane,

E_x, E_y, E_z : Young's modulus in x, y, z direction,

ν_{xy}, ν_{xz}, ν_{yz} : Poisson ratio in xy, xz, yz plane, and

G_{xy}, G_{xz}, G_{yz} : Shear modulus in xy, xz, yz plane.

The symmetrical geometry of cardboard leads to (Allasson and Svard, 2001):

$$\frac{\nu_{xy}}{E_x} = \frac{\nu_{yx}}{E_y}, \ \frac{\nu_{xz}}{E_x} = \frac{\nu_{zx}}{E_z}, \ \frac{\nu_{yz}}{E_y} = \frac{\nu_{zy}}{E_z} \tag{3.2}$$

Thus, there are nine unknown parameters to be determined, and they are: E_x, E_y, E_z, ν_{xy}, ν_{xz}, ν_{yz}, G_{xy}, G_{xz}, G_{yz}. Generally, all these parameters have to be measured. However, it is impossible to measure some of the parameters due to the small dimension in the vertical direction of the liner and core. For cardboard system as shown in Fig. 3.2, the in-plane material parameters (E_x and E_y) are measured by the standard tensile test (see Appendix A). While the other parameters are derived empirically as follows.

For the Young's modulus in the vertical direction, it is approximated according to Persson (1997), which is given by

$$E_z = E_x / 200 \tag{3.3}$$

The shear modulus are approximated according to (Mann et al., 1980; Baum et al., 1981) with

$$G_{xy} = 0.387\sqrt{E_x E_y} \tag{3.4}$$

$$G_{xz} = E_x / 55 \tag{3.5}$$

$$G_{yz} = E_y / 35 \tag{3.6}$$

The value of ν_{xy}, ν_{xz} and ν_{yz} are set according to (Nordstand, 1995). A trial and error procedure has also been performed, in which different values of the material parameters have been tested in order to get the results as close as possible to that of the experiments. Based on the trial and error, the elastic material parameters used for the model are listed in Table 3.1. The detailed identification of these material parameters can be found in Appendix A.

Table 3.1 Elastic material parameters of the liner and core of corrugated cardboard

Elastic material property	liner	Core
E_x (GPa)	3.2	5
E_y (GPa)	2	1.3
E_z (GPa)	0.016	0.025
ν_{xy}	0.34	0.34
ν_{yz}	0.01	0.01
ν_{xz}	0.01	0.01
G_{xy} (GPa)	1	1
G_{yz} (GPa)	0.058	0.05
G_{xz} (GPa)	0.057	0.005

The nonlinear plastic orthotropic constitutive model is governed by the Quadratic Hill yield criterion (Hill, 1983). Yield criterions have been developed for orthotropic plastic deformations. The most widely used version was the Quadratic Hill yield criterion (Hill, 1983), and it is commonly applied in sheet metal applications. However, this yield criterion has not considered different in yield strength in tension and compression, which was however considered by Shin and Lee (1978) and known as generalized Hill potential theory. Both yield criterions above were designed for material that do not have pressure-dependent yield surfaces to model foams and polymers. An extension that allows for pressure dependence was proposed in (Caddell et al.,

1973; Deshpande et al., 2001). In this thesis, Quadratic Hill yield criterion in ANSYS is used, as the model is simplified by assuming there is no difference in yield strength in tension and compression. The yield criterion is used with the isotropic hardening option, which is given by (ANSYS, 2004)

$$f\{\sigma\} = \sqrt{\{\sigma\}^T [P]\{\sigma\}} - \sigma_0(\varepsilon^p) = 0 \tag{3.7}$$

Where

σ_0 : yield stress in x direction,

ε_p : equivalent plastic strain,

$\{\sigma\}$: yield stress matrix, and

$[P]$: Plastic compliance matrix.

The plastic compliance matrix $[P]$ (ANSYS, 2004) can be written as:

$$P = \begin{bmatrix} G+H & -H & -G & 0 & 0 & 0 \\ -H & F+H & -F & 0 & 0 & 0 \\ -G & -F & F+G & 0 & 0 & 0 \\ 0 & 0 & 0 & 2N & 0 & 0 \\ 0 & 0 & 0 & 0 & 2L & 0 \\ 0 & 0 & 0 & 0 & 0 & 2M \end{bmatrix} \tag{3.8}$$

F, G, H, L, M and N are material constants that can be determined experimentally. They (ANSYS, 2004) are defined as:

$$F = \frac{1}{2}\left(\frac{1}{R_{yy}^2} + \frac{1}{R_{zz}^2} - \frac{1}{R_{xx}^2}\right) \tag{3.9}$$

$$G = \frac{1}{2}\left(\frac{1}{R_{zz}^2} + \frac{1}{R_{xx}^2} - \frac{1}{R_{yy}^2}\right) \tag{3.10}$$

$$H = \frac{1}{2}\left(\frac{1}{R_{xx}^2} + \frac{1}{R_{yy}^2} - \frac{1}{R_{zz}^2}\right) \tag{3.11}$$

$$L = \frac{3}{2}\left(\frac{1}{R_{yz}^2}\right) \tag{3.12}$$

$$M = \frac{3}{2}\left(\frac{1}{R_{xz}^2}\right) \tag{3.13}$$

$$N = \frac{3}{2}\left(\frac{1}{R_{xy}^2}\right) \tag{3.14}$$

Here, the yield stress ratios $R_{xx}, R_{yy}, R_{zz}, R_{xy}, R_{yz}$ and R_{xz} (ANSYS, 2004) are calculated as:

$$R_{xx} = \frac{\sigma_{xx}^{y}}{\sigma_0} \tag{3.15}$$

$$R_{yy} = \frac{\sigma_{yy}^{y}}{\sigma_0} \tag{3.16}$$

$$R_{zz} = \frac{\sigma_{zz}^{y}}{\sigma_0} \tag{3.17}$$

$$R_{xy} = \sqrt{3}\frac{\sigma_{xy}^{y}}{\sigma_0} \tag{3.18}$$

$$R_{yz} = \sqrt{3}\frac{\sigma_{yz}^{y}}{\sigma_0} \tag{3.19}$$

$$R_{xz} = \sqrt{3}\frac{\sigma_{xz}^{y}}{\sigma_0} \tag{3.20}$$

where σ_{ij}^{y} is the yield stress in x, y, z direction and xy, yz and xz plane.

Further, the plastic slope of the material after yield point (ANSYS, 2004) is:

$$E^{pl} = \frac{E_x E_t}{E_x - E_t} \tag{3.21}$$

where

E_x : Elastic modulus in x direction

E_t : Tangent modulus after the yield point

Thus, in order to fulfill the yield criterion, σ_0, E_t, R_{xx}, R_{yy}, R_{zz}, R_{xy}, R_{yz} and R_{xz} need to be determined. Specifically, the in-plane material parameters σ_0, E_t, R_{xx}, R_{yy} were derived from the results of tensile test mentioned above, while the other parameters were set according to Gooren (2006). A trial and error procedure has also been performed, in which different values of the material parameters have been tested in order to get the results as close as possible to that of the experiments. Based on the trial and error, the plastic material parameters used for the model

are listed in Table 3.1. The detail identification of these material parameters can be found in Appendix A.

Table 3.2 Plastic material parameters of the liner and core of corrugated cardboard

Plastic material property	Liner	Core
σ_0 (GPa)	0.03	0.011
E_t (GPa)	2.5	0.01
R_{xx}	1	1
R_{yy}	0.35	0.3
R_{zz}	0.23	0.3
R_{xy}	0.635	0.63
R_{yz}	0.635	0.63
R_{xz}	0.635	0.63

3.3.4 Element mesh

The indirect generation approach is applied to create the finite element model, as it is more effective for the complicated geometry of model, e.g., the core of corrugated cardboard. In this approach, the geometric shape of the model is first created, and then the ANSYS program is instructed to automatically mesh the geometry with nodes and elements. Thus, the modeling procedure has two steps as below: (a) Geometrical model; (b) Finite element mesh.

a. Geometrical model

The geometry of cardboard is modeled for a C flute corrugated cardboard. The geometry of the core is usually approximately as a sine shape. Fig. 3.4 shows a diagram comparing the actual shape and the sine shape (Biancolini and Brurri, 2003). The actual shape is preferred for the sake of accuracy. In this FE model, the actual shape is estimated according to Fig. 3.4 (Biancolini and Brurri, 2003) and it is shown in Fig. 3.5. Referring to Fig. 3.5, the dimensions of cardboard for a single core are: the thickness of the liner and core is 0.23 mm; the height is 3.6 mm; the flute length is 7.6 mm; the width is 7.6 mm.

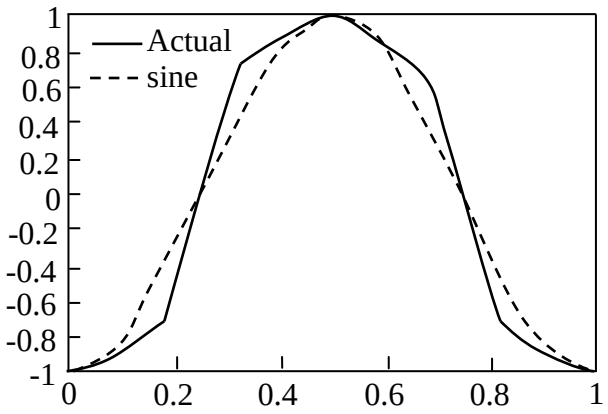

Fig. 3.4 Actual shape and sine shape (Adapted from Biancolini and Brurri, 2003)

In the finite element model, it is noted that the connected nodes between the tip of the core and the liner are modeled (Fig. 3.5) by making them share the same node.

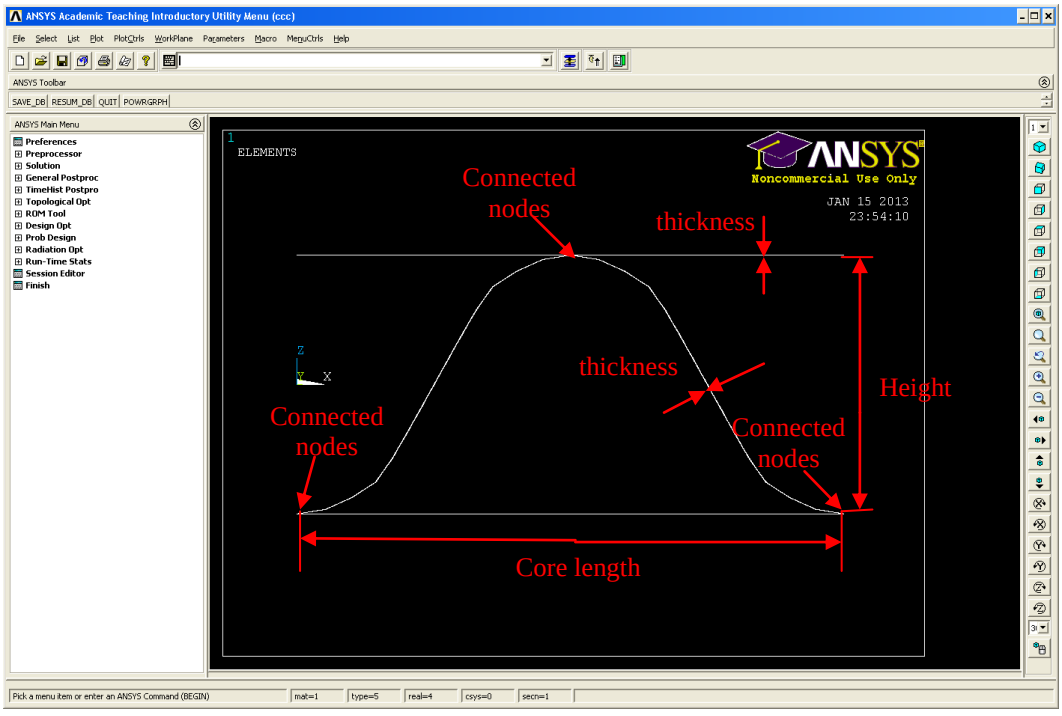

Fig. 3.5 Geometry of corrugated cardboard with the actual shape in FE model

b. Finite element mesh

Shell 181 elements were used to mesh the structure of cardboard. To identify the number of elements that are needed for a mesh in the finite element model to give satisfactory prediction, a mesh sensitivity study was performed for the stiffness of a corrugated cardboard under a compressive loading in its vertical direction. The specimen studied is a cardboard with a single core with the same geometry parameters as described above. Fig. 3.6 shows several mesh schemes for the same corrugated cardboard. It is noted that the core has more elements than the liner with the same mesh density due to the difference in their geometry. This work investigated ten meshing densities. The results indicated that the stiffness derived from 20 elements for the liner and 30 elements for core has no difference from the system with more elements. Thus, 20 elements for the liner and 30 elements for a cardboard with a single core are adequate to model the compressive stiffness of the corrugated board.

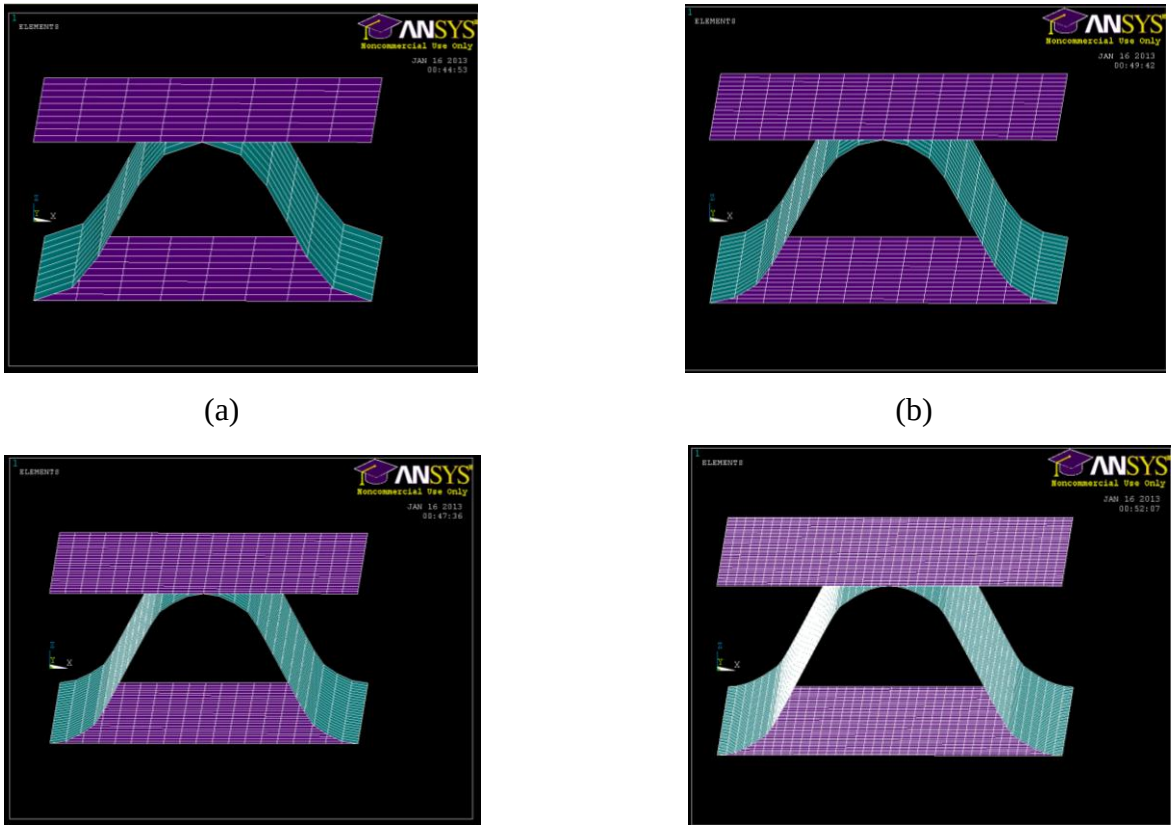

Fig. 3.6 Meshing schemes with (a) 8 elements for liner and 12 elements for core; (b) 13 elements for liner and 20 elements for core; (c) 20 elements for liner and 30 elements for core; (4) 40 elements for liner and 60 elements for core.

3.3.5 Contact behavior

It has been observed that during the loading process, the contact between the core and liners changes (Lu et al., 2001). There are 5 phases of contact as shown in Fig. 3.7 (A, B, C, D, E). The common phenomenon in all these phases is that during a compressive loading, the core and two liners share the same force and deformation in the vertical direction while have slipping between them in the contact tangential direction or horizontal direction if the perfect motion is assumed; as shown in Fig. 3.7.

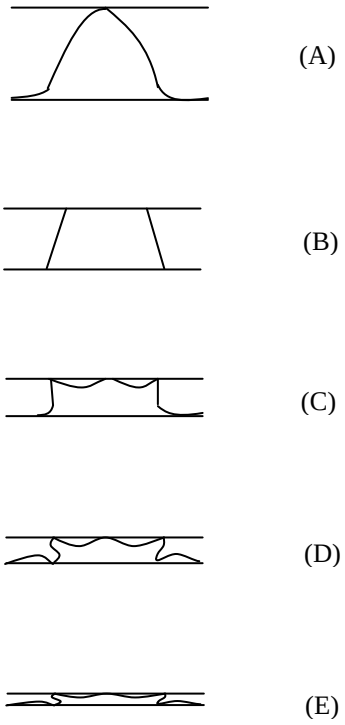

Fig. 3.7 Contact behavior during different phase of compression (A, B, C, D, E) (Adapted from Lu et al., 2001)

The contact was then modeled by the surface to surface contact elements. In ANSYS, for such problems involving contact between two surfaces, one of the surfaces is conventionally taken as the "target" surface, and the other as the "contact" surface (ANSYS 2004). For the rigid-to-flexible contact, the target surface is always the rigid surface, and the contact surface is the

deformable surface. For the flexible to flexible contact, it follows the rules below (ANSYS, 2004):

a) If a convex surface is expected to come into contact with a flat or concave surface, the flat/concave surface should be taken as the target surface.
b) If one surface has a fine mesh, while the other has a coarse mesh, the fine meshed surface is taken as the contact surface and the coarse mesh as the target surface.
c) If one surface is stiffer than the other, the softer surface is taken as the contact surface and the stiffer surface as the target surface.
d) If a high-order element underlies one of the two surfaces and a lower order element underlies the other surface, the former is taken as the contact surface and the latter as the target surface.
e) If one surface is marked larger than the other surface, where particularly in one surface surrounds the other surface, the larger surface is taken as the target surface.

For cardboard, a flexible-to-flexible situation was considered, because both the core and the liners are deformable. Following the rule (c), the liner is taken as the target surface, while the core is as the contact surface.

Further one needs to examine the sliding behaviour between two contact surfaces. In ANSYS, several sliding behaviours can be modeled (ANSYS, 2004):

i. Standard contact. Once in contact, the surfaces slide.
ii. Rough contact. Once in contact, the surfaces are not able to slide.
iii. No separation contact. Once in contact, the surfaces slide but permanently tie together
iv. Bonded contact. Once in contact, the surfaces are not able to slide but permanently tie together.
v. No separation always contact. Once in contact, the surfaces slide but permanently tie together. It differs from (iii) as contact only happens in the contacted area where designated.
vi. Bonded always contact. Once in contact, the surfaces are not able to slide but permanently tie together. It differs from (iv) as contact only happens in the contacted area where designated.

vii. Bonded initial contact. Once in contact, the surfaces are not able to slide but permanently tie together. It differs from (iv), (vi) as contact only happens in the initial contacted area.

For corrugated cardboard, the (i) standard sliding behaviour is most appropriate based on the observation of the real operation of cardboard. Fig. 3.8 illustrates the contact model of corrugated cardboard, where two pairs of the target element and contact element are set for the top liner and core, and the bottom liner and core, respectively. The contact behaviour was performed by ANSYS and recorded for different phases of loading (see Fig. 3.9), which is the same as what was observed in the experiment.

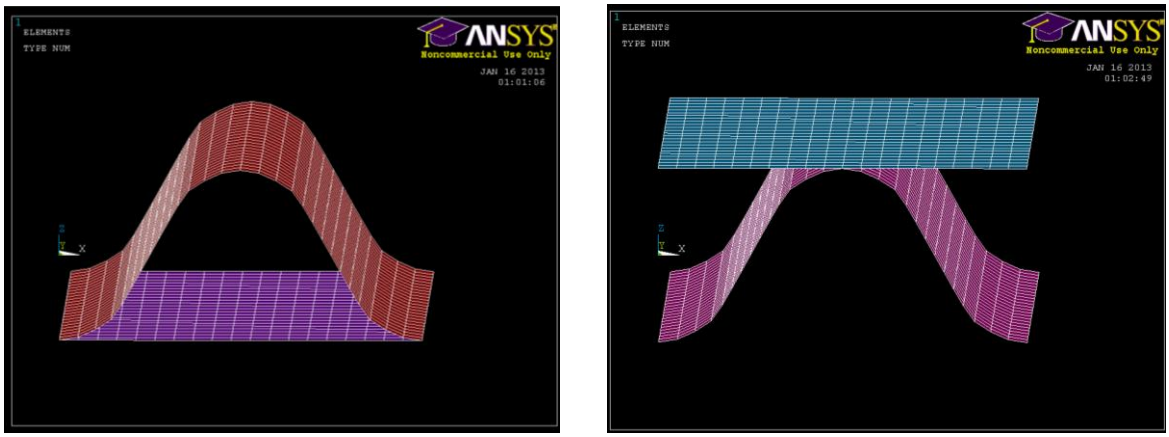

(a) (b)

Fig. 3.8 Contact model of (a) the top liner and core; (b) the bottom liner and core

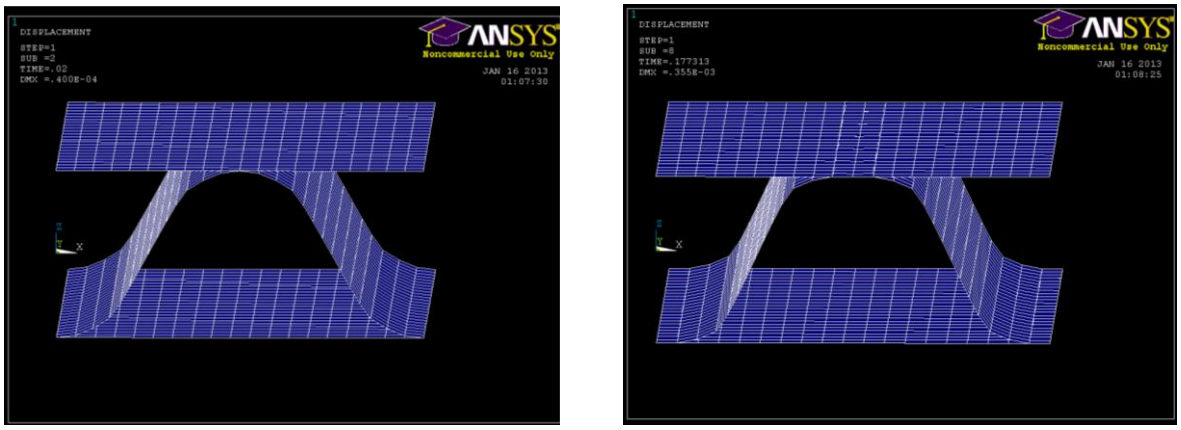

(a) (b)

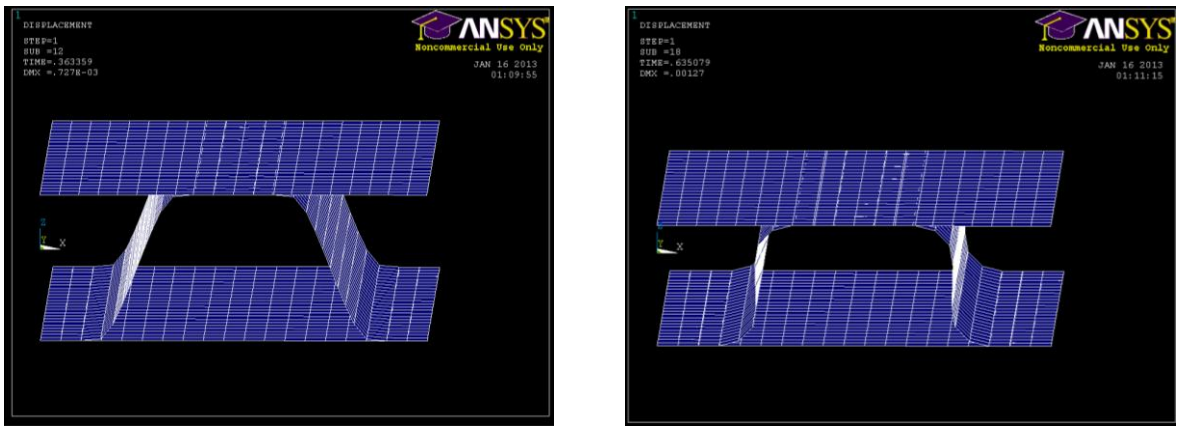

(c) (d)

Fig. 3.9 Contact behavior of corrugated cardboard at displacement level of (a) 0.1mm; (b) 0.3mm; (d) 0.7mm; (e) 1.1mm

3.3.6 Boundary condition and loads

The boundary condition and loads were defined for the FE model above. To make the model as simple as possible, the following assumption of the boundary condition and loads is made: the friction between the machine and cardboard (Fig. 3.1) is so large that any horizontal movement of the upper and lower liners can be prevented. This assumption is supported by what is actually observed during the tests. Loads are applied on the finite element model as shown in Fig. 3.10. To apply uniform compressive loads, vertical displacement loads are applied on the top liner of the corrugated board. It is noted that this displacement will be divided into a series of displacement load increments for performing the geometric, material and changing-status nonlinearity analysis in this model. To apply the boundary condition, the top liner is constrained in all direction except the vertical directions, while the bottom liner of corrugated cardboard is constrained in all directions. Besides, the symmetry boundary condition is used to model only a quarter of the full size model. Specifically, the two edges of corrugated cardboard are constrained in the horizontal direction due to the symmetry.

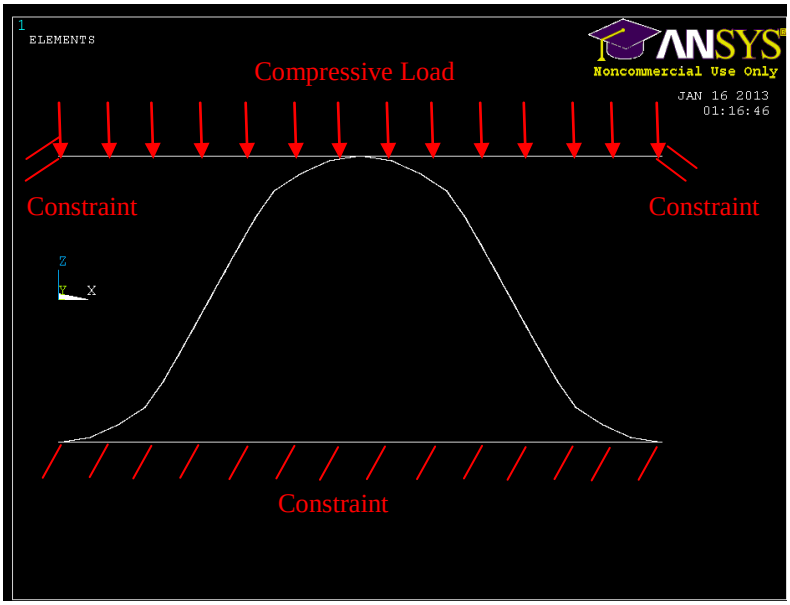

Fig. 3.10 Boundary condition and loads on corrugated cardboard

3.3.7 Nonlinear analysis

The nonlinear analysis is considered for the FE model, which includes geometric nonlinearity, material nonlinearity and changing-status nonlinearity. The geometric nonlinearity is that the stiffness of the structure changes under the loading due to the changes in shape or geometry. For corrugated cardboard, it is found that the geometry of the core changes significantly under the loading, which leads to the change of the stiffness. Thus, the geometric nonlinearity is included and it is performed by use of the 'large displacement analyses option' in the ANSYS software. The material nonlinearity is that the stiffness changes due to the changes of material property. In this FE model, it refers to its plastic material property as mentioned in section 3.2.3. Changing-status nonlinearity is that the stiffness changes due to the changes of status. In this model, it refers to the contact behavior between the liners and the core of corrugated cardboard under the loading as mentioned in section 3.2.6.

3.3.8 Load specification and algorithm selection

To perform the geometric, material and changing-status nonlinearity analysis, Newton-Raphson algorithm is used. In this algorithm, the load is subdivided into a series of load increments.

According to ANSYS (2004), before solution of each load increments, the Newton-Raphson algorithm evaluates the out-of-balance load vector, which is the difference between the restoring forces (the loads corresponding to the element stresses) and the applied loads. It is noted that restoring force is related to the stiffness matrix of the structure, and it is updated according to the change of geometry, material and status for each load increments. The program then performs the solution and checks for convergence. If the convergence criteria are not satisfied, the out-of-balance load vector is re-evaluated, followed by an update of the stiffness matrix to obtain a new solution. This iterative procedure continues until the problem converges. In this finite element model, 100 load increments are found adequate for the accuracy of the analysis. After the above procedure, the solution is initiated and the ANSYS program takes model and load information from the database defined and calculates the results.

3.3.9 Results

The result of the finite element analysis is presented in the format of force VS displacement relation, and the stiffness is calculated based on the relation. Specifically, the displacement refers to the vertical displacement of points at the top liner of the corrugated board, and the force is the sum of the reaction force on the top liner board. The displacement and force were recorded for all displacement loading increments. It is noted that the symmetry model (one quarter of the full size model) is used for the FE analysis in this thesis, thus its force should be multiplied by four to represent the force of the full size model. A typical FE result for a C flute corrugated cardboard with length 30.4 mm and width 30.4 mm is shown in Fig. 3.11, where the horizontal axis is the prescribed displacement and the vertical axis is the force. Upon loading, the specimen responds linearly response up to the first peak load (at 0.8 mm). After the peak load, a decrease of force can be observed from the figure. The slope of the linear part of the force VS displacement relation is calculated as the stiffness.

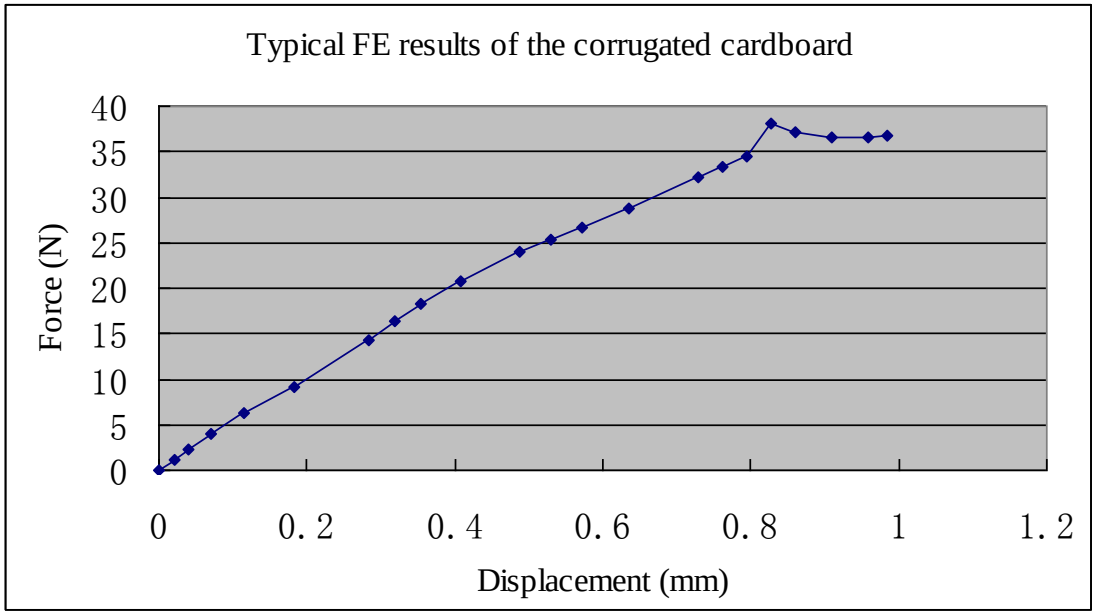

Fig. 3.11 Typical FE model result (30.4 mm × 30.4 mm)

Further, the result of symmetry model of this cardboard was compared with that from the full size model, and good correlation was found between the two results (see Fig. 3.12).

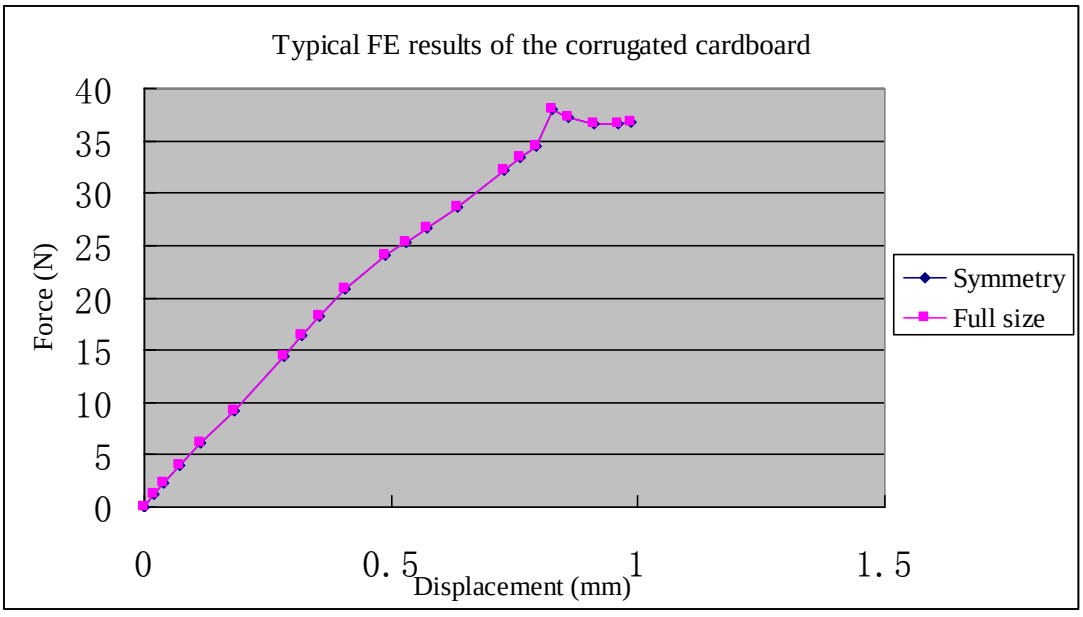

Fig. 3.12 Result of symmetry model and full size model (30.4 mm × 30.4 mm)

3.4 Model Validation

3.4.1 Measurement Test-bed

Fig. 3.12 illustrates the measurement test-bed for the compressive stiffness of corrugated cardboard in its vertical direction. The measurement was conducted according to flat crush test (FCT) method (ASME 1994). The measurement environment was at temperature of 23^{o}C and with the relative humidity of 33%. Referring to Fig. 3.13, the specimen of a corrugated cardboard was placed between a load crosshead and a platen and was subjected to a compressive load from the load crosshead. Specifically, the test specimen was cut with the edges aligned with the machine and cross directions into a rectangle shape. The load was displacement controlled at 1mm/min. The stiffness was calculated based on the prescribed displacement to the specimen and the required load which was recorded.

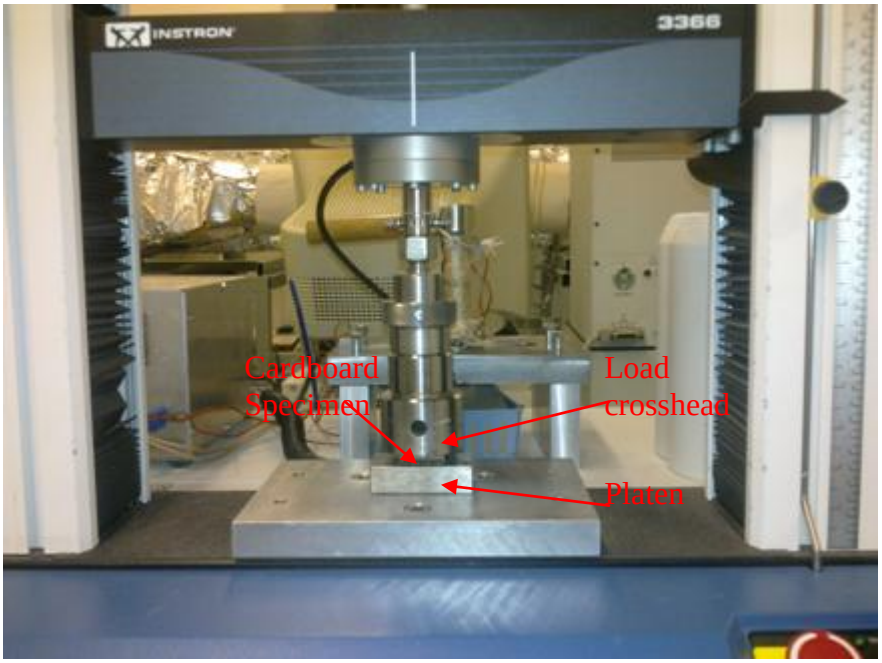

Fig. 3.13 Measurement test-bed for the compressive stiffness of corrugated cardboard in its vertical direction

In order to validate the finite element model as developed before, a “C" flute corrugated cardboard specimen was investigated. The geometry of the specimen was as follows: the flute

length 7.6 mm; length 30.4 mm (4 flute length); width 38 mm; height 3.6 mm and thickness of the liner and core 0.28 mm. Seven new specimens were repeated for the measurement. However, for the FE model, as the symmetry model (one quarter of the full size model) used, its length will change to 15.2 mm (2 flute length) and the width will change to 19 mm, which is shown in Fig. 3.14. It is noted that the force obtained from the symmetry FE model needs to be multiplied by four to be compared with that from the measurement result for the validation.

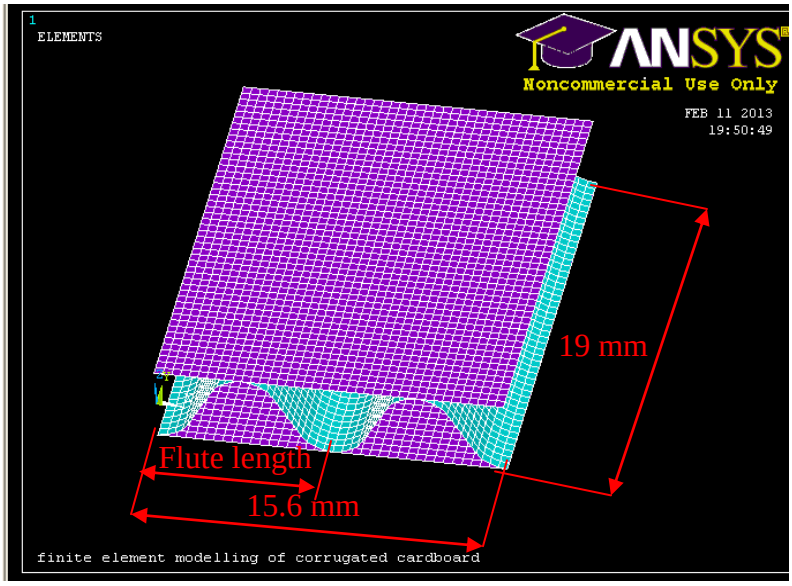

Fig. 3.14 Geometry of FE model for 30.4 mm × 38 mm specimen

3.4.2 Results and validation

A typical force VS displacement curve through the aforementioned measurement is shown in Fig. 3.15. Upon loading, the specimen first shows a nonlinear response until a displacement level (0.2 mm) is reached. This may be attributed to the fact that the liner of cardboard is not flat enough but a bit wavy. Specifically, the initial nonlinear response is largely due to the flattening of these wavy liners. After the initial response, the specimen then responded linearly up to the first peak load at about 185N. Following the peak load, the load required to deform the specimen gradually decreases. This is found to be attributed to the nonlinear plastic material behaviour of corrugated cardboard (Krusper et al., 2007). Seven new specimens were repeated and those results can be found in Fig. 3.16. It can be seen from this figure that the seven specimens responded with a slight variation, which was expected.

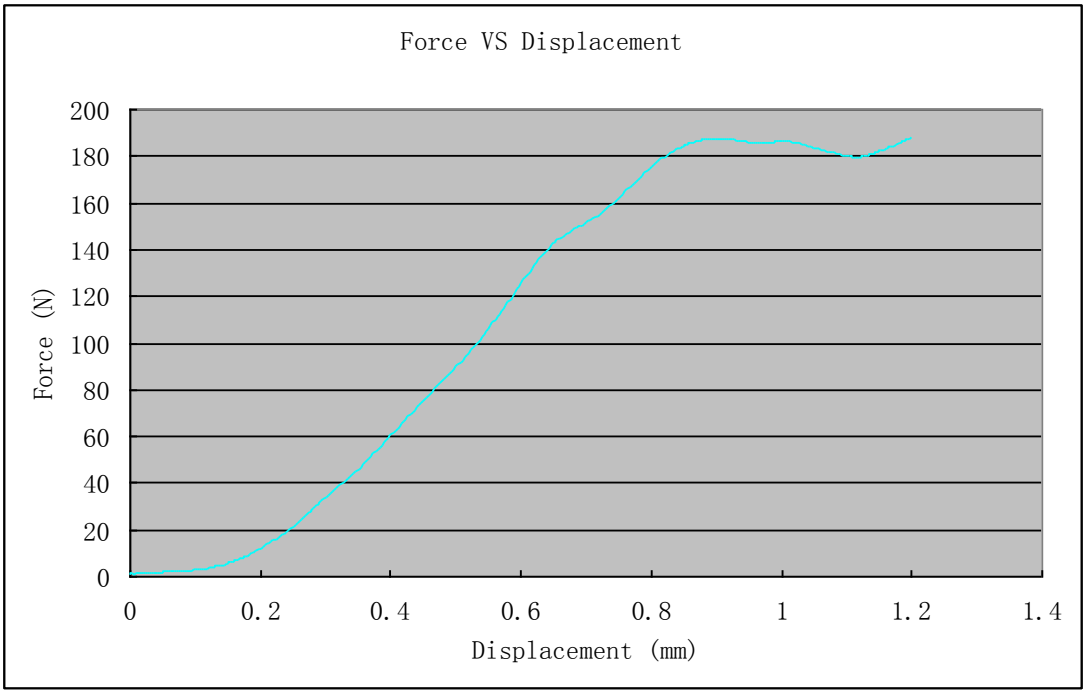

Fig. 3.15 Typical Force VS displacement results (30.4 mm × 38 mm)

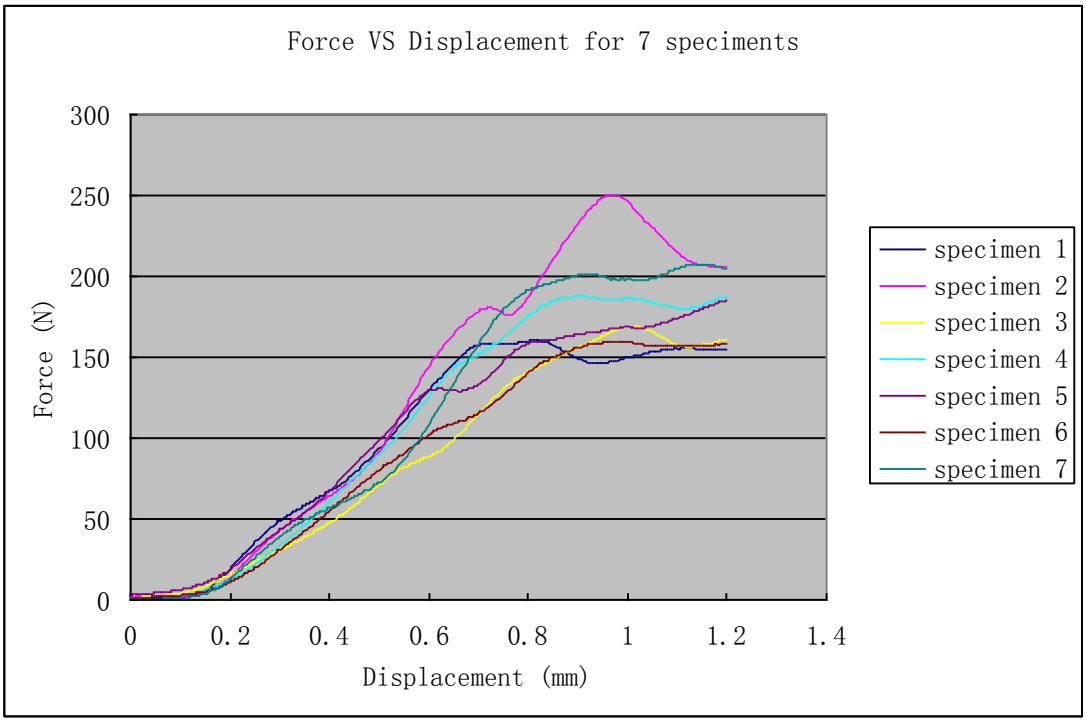

Fig. 3.16 Measurement results of all specimens (30.4 mm × 38 mm)

The measurement results were then used to compare with the finite element analysis results to validate the FE model and analysis. The comparison results are shown in Fig. 3.17. It is found

that the finite element result differs significantly from the measurement result in the initial loading stage, while it is close to the measurement result afterwards. This situation is not surprising because the measured specimen has the wavy liner and it needs to be flattened at the initial stage, while the finite element model assumes that the liner is flat all the time. Thus, the two results are only comparable after the initial stage. The results of the initial stage (up to 30N) are removed from Fig. 3.18.

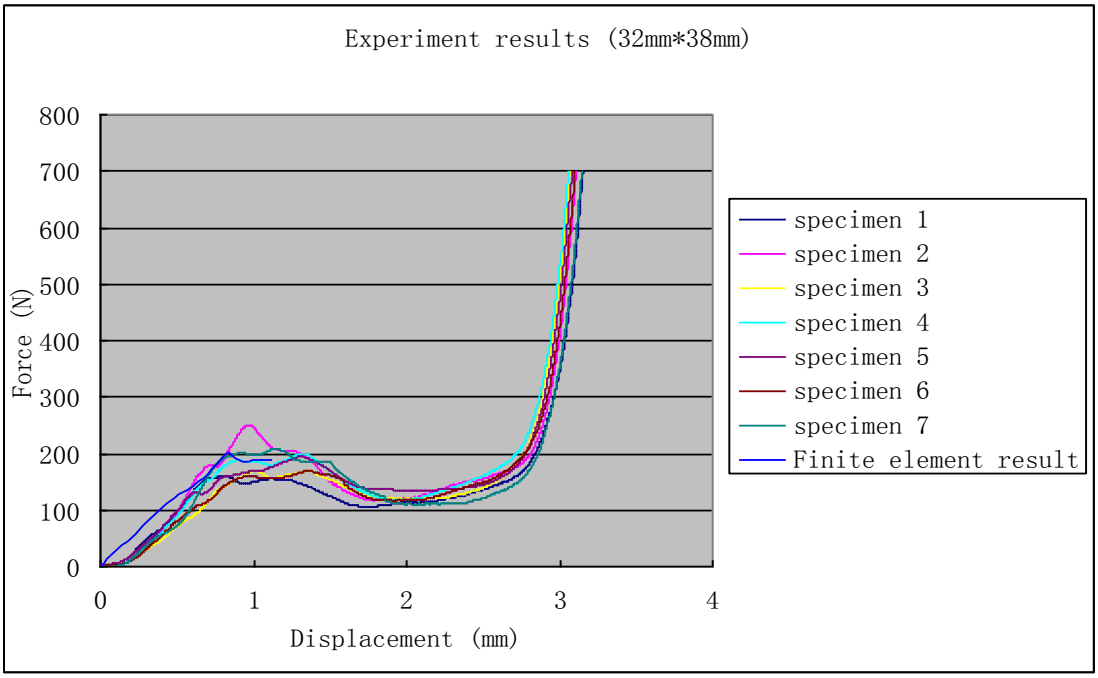

Fig. 3.17 Comparison of the FE results and measurement results (30.4 mm × 38 mm)

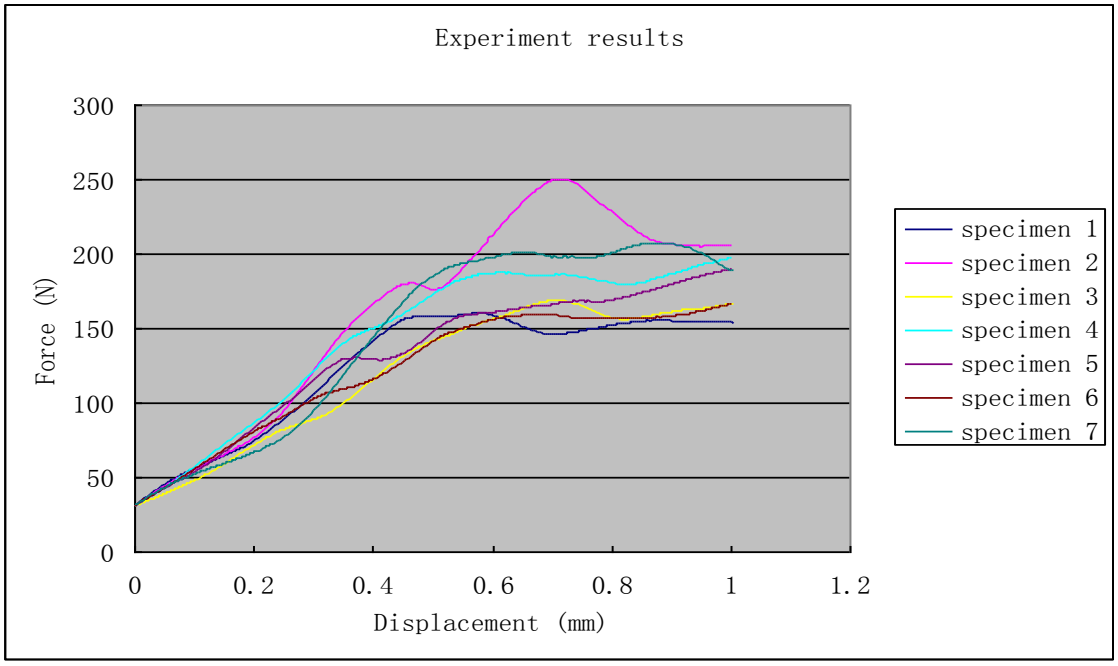

Fig. 3.18 Experiment results for all specimens by removing the initial stage results (30.4 mm × 38 mm)

Variations of cardboard due to manufacturing errors are considered by including the error bar on the measurement results, see Fig. 3.19. The error bar in this case is the standard deviation of the seven specimens.

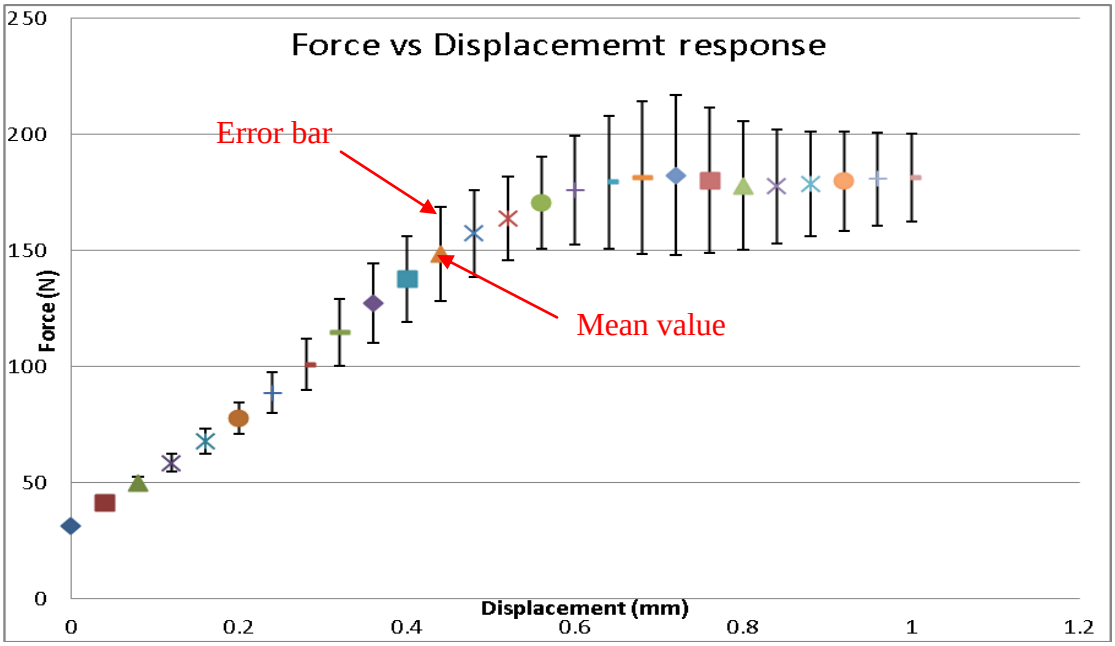

Fig. 3.19 Measurement results with error bars (30.4 mm × 38 mm)

Fig. 3.20 plots the measurement results with error bar and the FEM result. From the figure, it can be seen that the FEM result correlates well with the measurements result. Especially, for both the FEM result and measurement result, the force responds linearly up to a peak value (about 200 N), followed by a decrease of force.

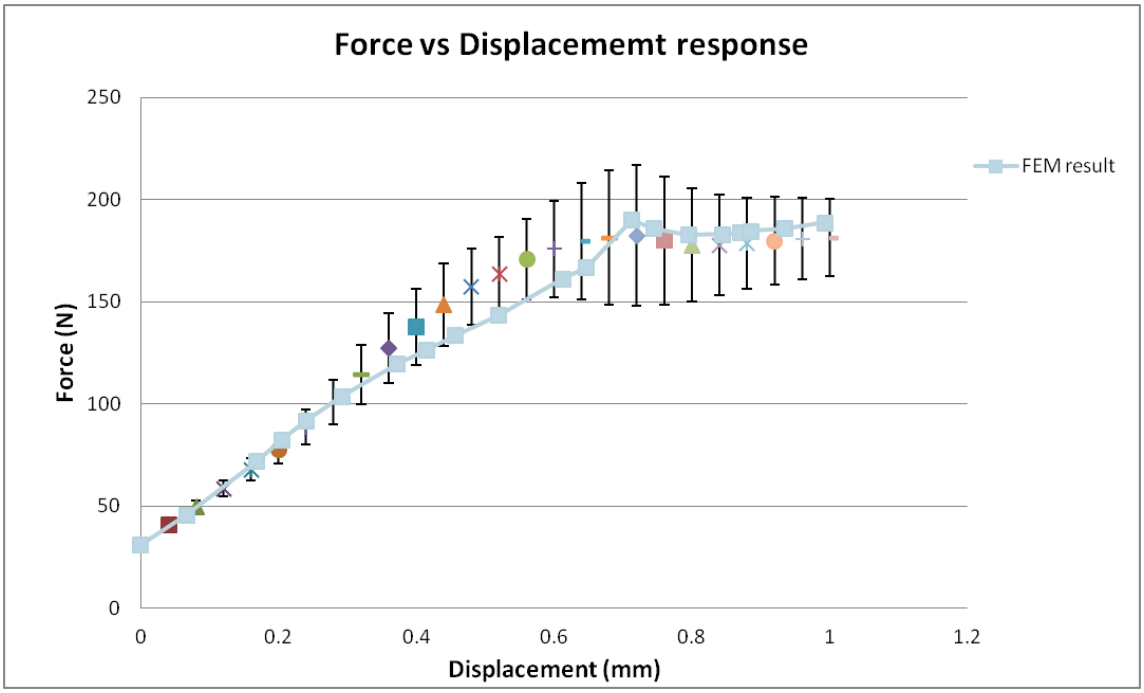

Fig. 3.20 Comparison of measurement results (with error bars) and finite element results (30.4 mm × 38 mm)

Cardboard with another size of length 60.8 mm (8 flute length) and width 38 mm was also studied. However, for the FE model, as the symmetry model (one quarter of the full size model) is used, its length will be 30.4 mm (4 flute length) and width will be 19 mm, which is shown in Fig. 3.21. Fig. 3.22 plots both FEM and measurement results. It can be seen from the figure that the FEM result correlates well with the measurement result up to the displacement of 0.76 mm, followed by a lower value in comparison with the measurement result. This situation may be because the plastic model property was not accurately available. As mentioned before, not all parameters in the model can be readily determined, which is a challenge to modelling.

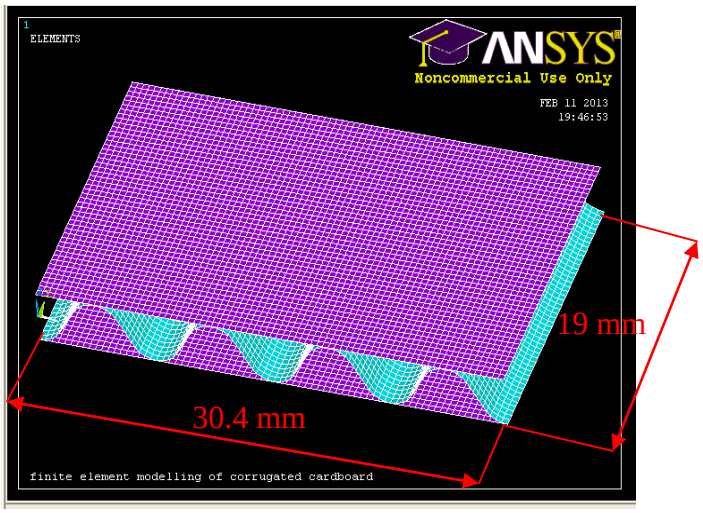

Fig. 3.21 Geometry of FE model for 60.8 mm × 38 mm specimen

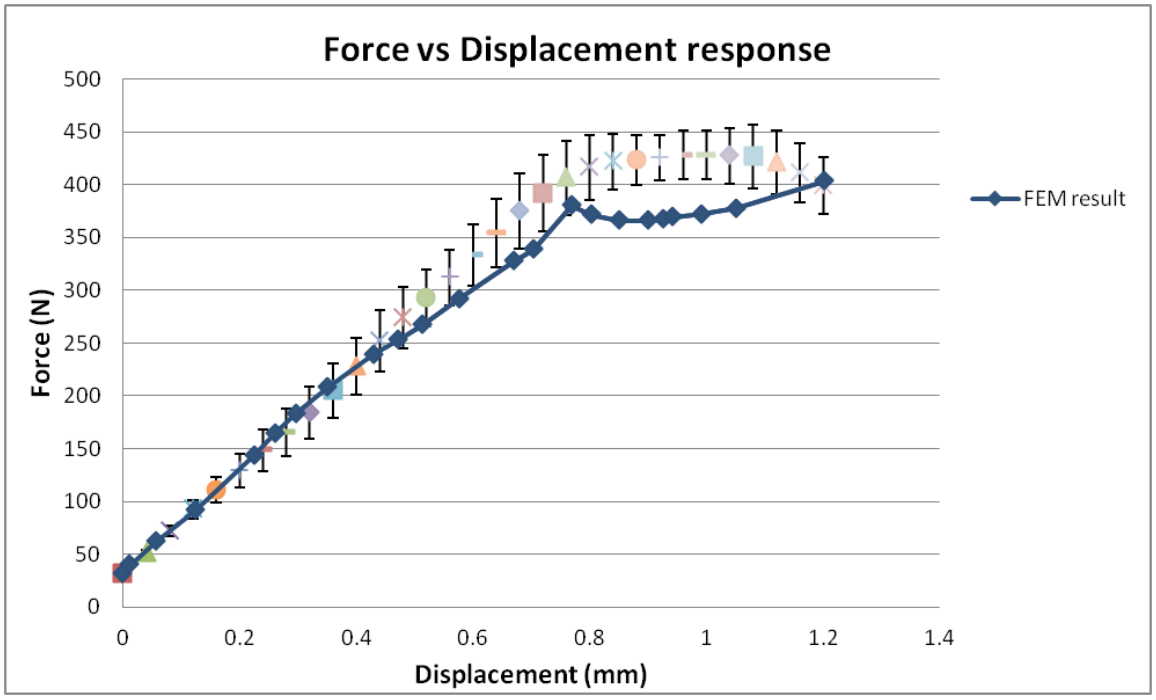

Fig. 3.22 Comparison of the measurement results and FEM results (60.8 mm × 38 mm)

The finite element model by considering the geometry of cardboard as a sine shape has also been investigated, as shown in Fig. 3.23. The results for both cardboards (30.4 mm × 38 mm and 60.8 mm × 38 mm) are shown in Fig. 3.24 and Fig. 3.25, respectively. It can be found from the figure that the results of the sine shape correlates well with both actual shape and the measurement results to the displacement level of 0.4 mm, followed by a lower value in comparison with the

other two results. The discrepancy implies that the difference in the description of the shape of the core may be an important factor for the stiffness of cardboard. There may be an implication from the obtained results that the shape of the core is better to be made as a sine curve to facilitate the manufacturing of cardboard. However, the curve up to the displacement level of 0.4 mm is accurate enough for the prediction of the stiffness.

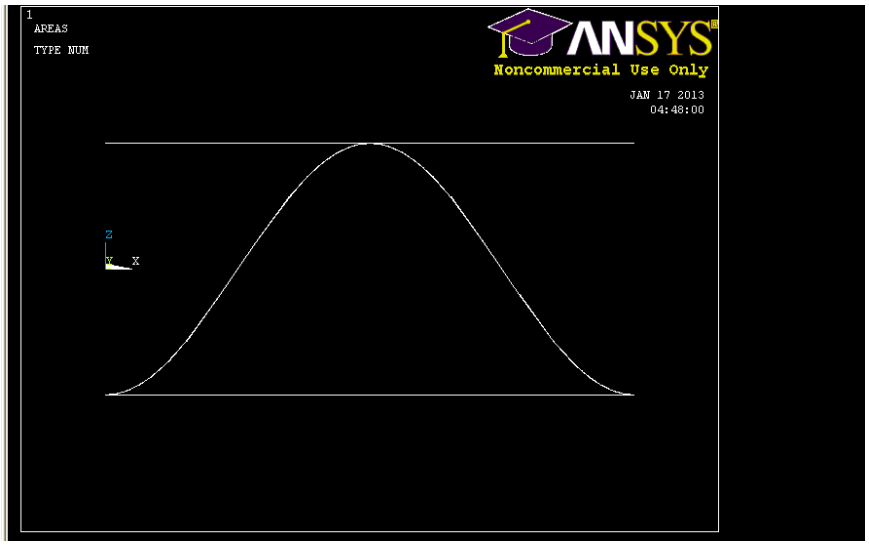

Fig. 3.23 FE model with the sine shape

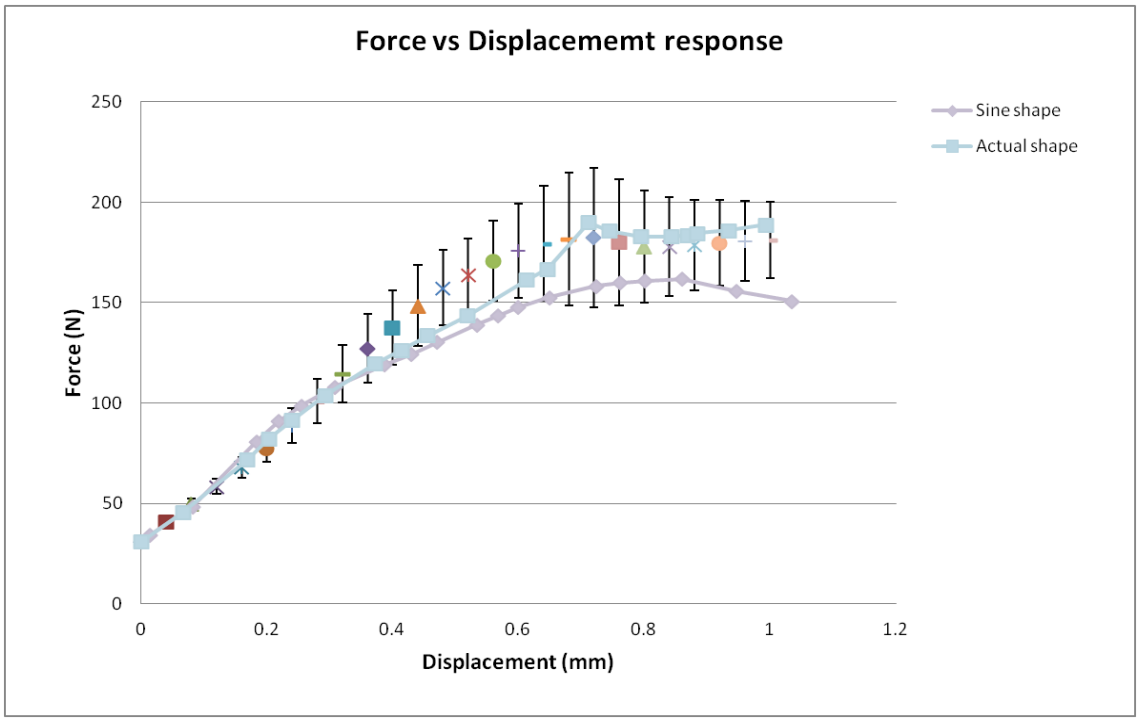

Fig. 3.24 Comparison of the results between sine shape and actual shape (30.4 mm × 38mm)

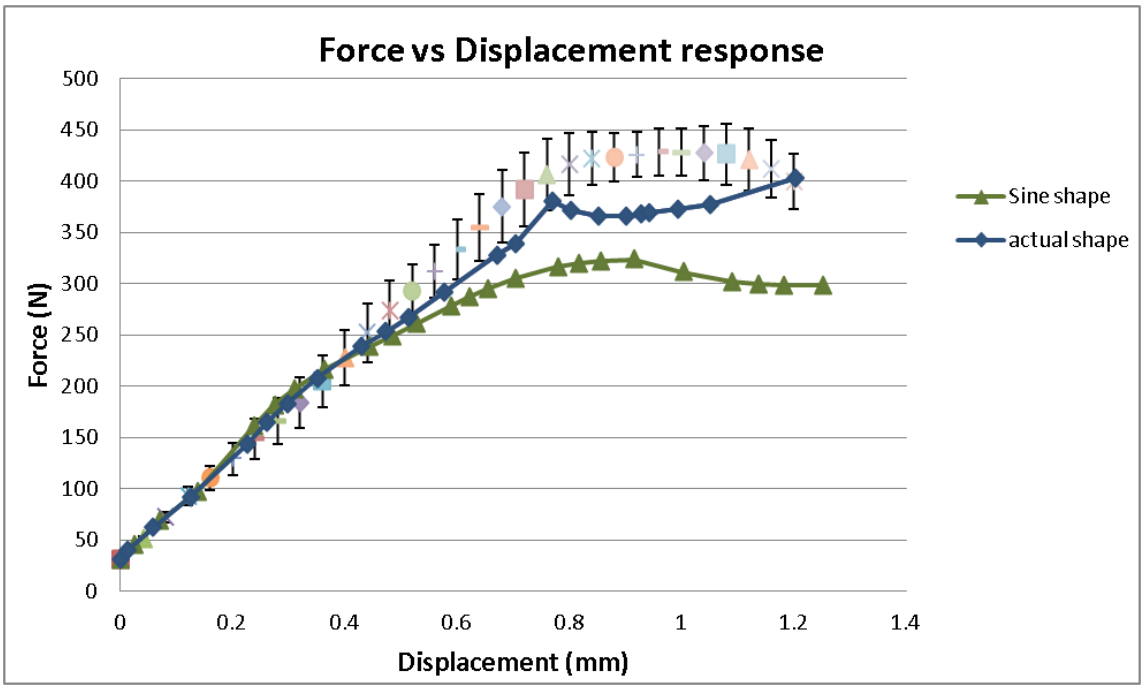

Fig. 3.25 Comparison of results with sine shape and actual shape (60.8 mm × 38 mm)

3.4.3 Discussion

In the literature, Lu et al. (2001) and Krusper et al. (2007) performed a finite element analysis of cardboard. Both Lu's model and Krusper's model are found to be with two disadvantages: (1) The model cannot be applied to cardboard with different widths; (2) The peak load and its following response cannot be predicted. The disadvantage (1) is because the element used in their work is the beam element. The beam element models the geometry such that the length is considerably longer than the width and the thickness. Thus, the beam element is not suitable to model cardboard with the width longer than the length. The disadvantage (2) is due to no consideration of the nonlinear material property of cardboard. It should be noted that the width parameter and peak load are two important variables for the application of cardboard for the vibration isolation. Difference in the width parameter could give rise to significantly different stiffnesses of cardboard. The peak load gives information of how much load cardboard can sustain. If the load from the vibrating machine is larger than the load cardboard can sustain, cardboard cannot provide any stiffness and is useless for vibration isolation. In the finite element

model of this work, a refined FE model with special attention to capture the width parameters and peak load is presented and good validation with the measurement results is achieved.

3.5 Conclusions

The finite element modeling of corrugated cardboard was described in this chapter. This model was used for predicting the stiffness of corrugated cardboard in its vertical direction. When the displacement under compressive loading on corrugated cardboard is prescribed, the associated reaction force can be obtained. The stiffness can then be calculated from the displacement vs reaction force relation. From the comprehensive literature review presented in Chapter 2, it is believed that this model is the most accurate one to predict the stiffness of corrugated cardboard (especially with different width and peak load).

The experiment test bed was established and described in this chapter. The measurement results were compared with the finite element results, and a good correlation between them was achieved for the part of the force-displacement relation up to the peak load, but not in the part after the peak load. The accuracy of this part may be improved with a more accurate acquisition of the nonlinear plastic material property. The finite element model included both an approximated sine shape and an actual shape. The finite element models with both the actual core shape and the approximated sine core shape were effective to predict the stiffness, though the one with actual shape was more accurate than the one with a sine shape especially in predicting the peak load.

CHAPTER 4 APPLICATION – VIBRATION ISOLATION SYSTEM USING CARDBOARDS

4.1 Introduction

This chapter describes the application of the theoretic development in the stiffness and damping of corrugated cardboard to design an isolator for a vacuum pump at the Canadian Light Source (CLS) facility of the University of Saskatchewan. Section 4.2 presents measurement of the damping of cardboard. Section 4.3 presents a lumped model for cardboard system, which is necessary to design a cardboard system. A cardboard system refers to a system that consists of several cardboards in connection. Section 4.4 presents two examples with their designs. Section 4.5 presents validation of the example designs with further discussions. Section 4.6 gives a conclusion.

4.2 Measurement of the Damping of Cardboard

Stiffness and damping of corrugated cardboard are two important properties for a vibration isolator. In Chapter 3, determination of the stiffness was described. In this section, determination of the damping through measurement will be described. Measurement of the damping follows the methods used for that of rubber (Mallik, 1999). The measurement test-bed is shown in Fig. 4.1(a). A vibration exciter, a Brüel & Kjær dynamic signal analyzer, a computer, two accelerometers and three amplifiers were included in the experiment set-up. The analyzer software in the computer first sent a command to the dynamic signal analyzer and it generated a signal to the vibration exciter through amplification from an amplifier. Then, the vibration exciter generated a harmonic excitation on cardboard. Two accelerometers were put on the vibration exciter and the top surface of a steel block; see Fig. 4.2(b), respectively. The

displacements measured from the two accelerometers were recorded in the computer. As illustrated in Fig. 4.2(b), one side of cardboard sticks to the vibration exciter and the other side sticks to the steel block. It is noted that the size of the specimen was selected with the same size as that of the steel block to ensure the load distribution from the block on cardboard is uniform.

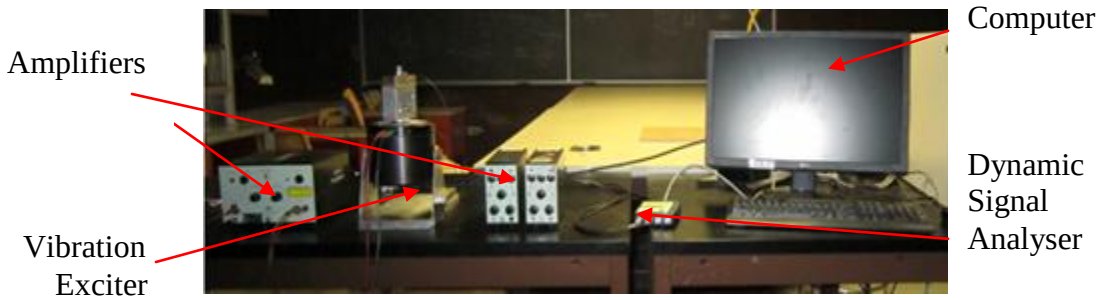

(a)

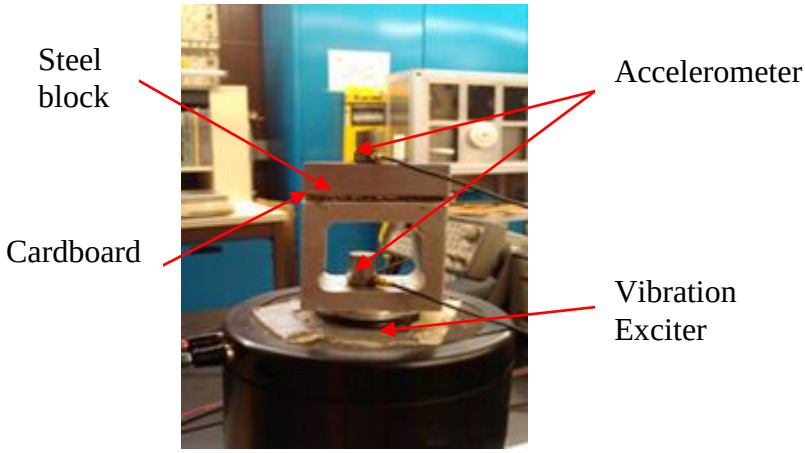

(b)

Fig. 4.1 Measurement test-bed in the laboratory for corrugated cardboard: (a) the instruments and (b) detailed schematic of the vibration exciter

The ratio of the displacement on the top surface of the mass (X_{mass}) to that on the exciter ($X_{exciter}$) is defined as the displacement transmissibility ratio (T_r). This displacement ratio describes the percentage of reduction of vibration by means of cardboard. T_r , which can be found by (Rao, 2003)

$$T_r = \frac{F_T}{F_0} = \left\{ \frac{k^2 + \omega^2 c^2}{(k - m\omega^2)^2 + \omega^2 c^2} \right\}^{1/2} \tag{4.1}$$

where

k : the stiffness of corrugated cardboard,

m : the mass of the steel block,

ω : the frequency from the vibration exciter (unit: rad/s),

c : the damping of corrugated cardboard.

When the resonance ($\omega = \omega_n = \sqrt{\frac{k}{m}}$, where the ω_n is the natural frequency of the whole system) takes place, the damping can be found by (Rao, 2003)

$$c = \sqrt{\frac{km}{T_r^2 - 1}} \tag{4.2}$$

A typical measurement of the displacement transmissibility ratio (T_r) VS the frequency (f) is shown in Fig. 4.2. The frequency (f) in the unit of hertz (Hz) has the relationship with the frequency in rad/s (ω), that is: $\omega = 2\pi f$. The size of cardboard for this measurement is 60.8 mm in length and 38 mm in width (Fig. 4.1), which is the same one used for the determination of the stiffness described in Chapter 3. The stiffness (k) of cardboard is 4.7×10^5 N/m and the mass (m) on cardboard is 400 g. It can be seen from Fig. 4.2 that the resonance takes place at about 119Hz, where the displacement transmissibility ratio $T_r = 7.48$. Based on the measurement of the displacement transmissibility ratio (T_r), damping is calculated to be $c = 58.36 Ns/m$.

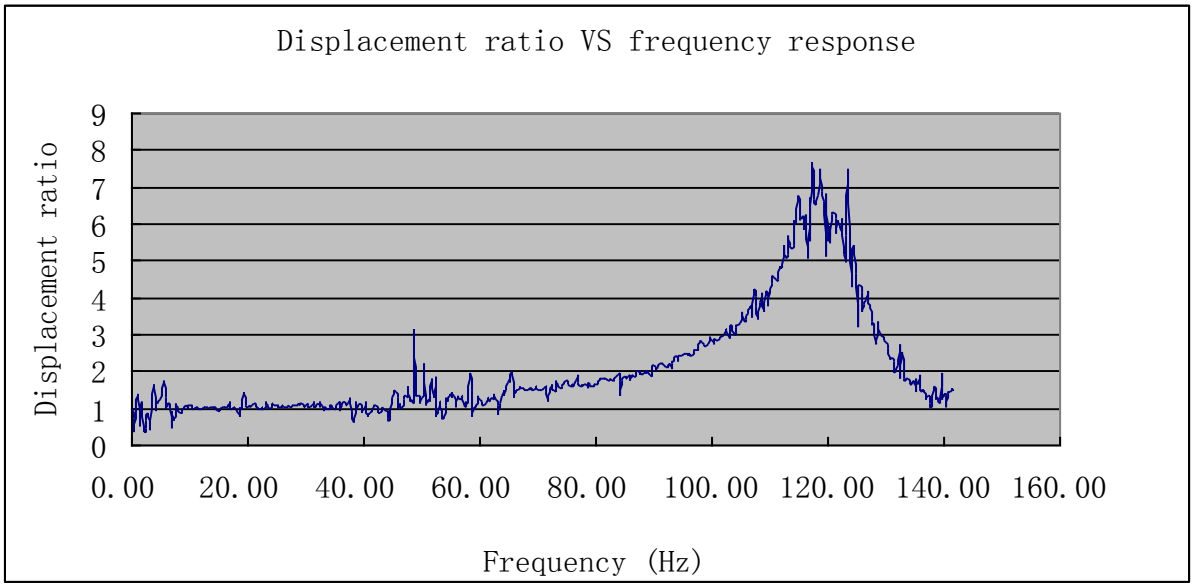

Fig. 4.2 Typical result of displacement ratio VS the frequency

4.3 Lumped Model

At the Canadian Light Source (CLS) Ltd., the vacuum pump is found to be a main vibration source (Li et al., 2010). The pumps transmit vibrations to the ground, causing the ground to vibrate. The ground vibration can then affect other instruments on the ground. In the work presented below, corrugated cardboard is used to reduce the transmission of vibrations generated from the vacuum pump to the ground as shown in Fig. 4.3(a). Fig. 4.3(b) shows a schematic of the system. From Fig. 4.3, it can be seen that the vacuum pump produces a vibrating force which is transmitted to the ground, while corrugated cardboard is put between the pump and ground to reduce this transmission. Corrugated cardboard is thus much like a vibration isolator. It is noted that there may be several cardboards in connection called cardboard system used instead of one cardboard only.

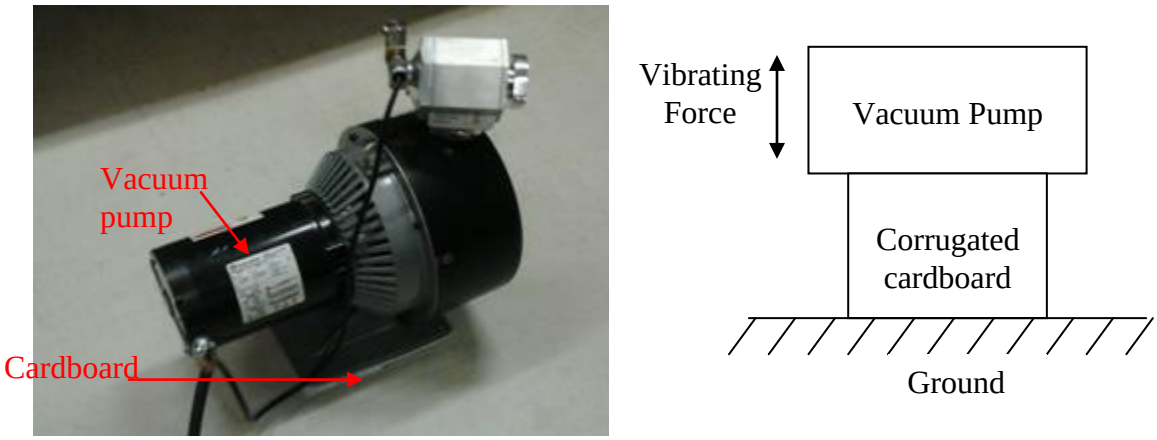

(a) (b)

Fig. 4.3 The vibration isolator system: (a) set-up; (b) schematics

The cardboard system can be represented as a lumped mode, as shown in Fig. 4.4. The lumped model consists of a mass (m), a spring (k) and a damper (c). The mass (m) represents the mass of the pump, while the spring (k) and the damper (c) represent the stiffness and damping of corrugated cardboard, respectively. It is assumed that the vibrating force generated by the vacuum pump is a harmonically varying force, which can be represented by Rao (2003) $F(t) = F_0 \cos \omega t$.

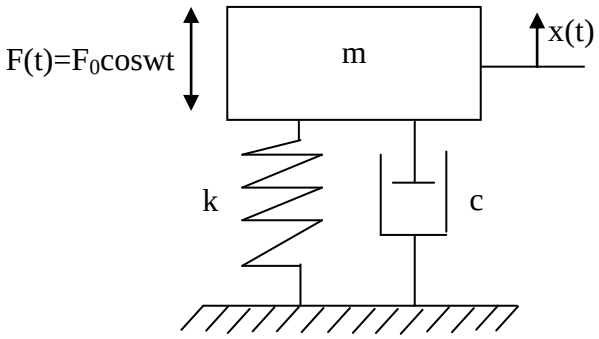

Fig. 4.4 Single-degree-of-freedom lumped model

The equation of motion of the model is (Rao, 2003):

$$m\ddot{x}(t) + c\dot{x}(t) + kx(t) = F_0 \cos \omega t \qquad (4.3)$$

where $x(t)$ is the displacement of the pump and it is further (Rao, 2003):

$$x(t) = X\cos(\omega t - \phi) \tag{4.4}$$

where X is the amplitude of the vibrating displacement, ω is the frequency of the vibrating pump, and ϕ is the phase angle between the vibrating force and vibrating displacement. Substituting Eqn. (4.4) into Eqn. (4.3) leads to the equation which describes the relation of amplitude X and phase angle ϕ; (Rao, 2003):

$$X = \frac{F_0}{[(k - m\omega^2)^2 + \omega^2 c^2]^{1/2}} \tag{4.5}$$

and

$$\phi = \tan^{-1}\left(\frac{\omega c}{k - m\omega^2}\right) \tag{4.6}$$

Further, the force transmitted to the ground via the spring and the damper, $F_t(t)$, is (Rao, 2003):

$$F_t(t) = kx(t) + c\dot{x}(t) = kX\cos(\omega t - \phi) - c\omega X\sin(\omega t - \phi) \tag{4.7}$$

The magnitude of the transmitted force (F_T) is (Rao, 2003):

$$F_T = [(kx)^2 + (c\dot{x})^2]^{1/2} = X\sqrt{k^2 + \omega^2 c^2} = \frac{F_0(k^2 + \omega^2 c^2)^{1/2}}{[(k - m\omega^2)^2 + \omega^2 c^2]^{1/2}} \tag{4.8}$$

The transmission ratio (T_f) of the isolator (i.e. cardboard) is defined as the ratio of the magnitude of the force transmitted to ground (F_T) to that of the vibrating force acting on it (F_0),and it serves as a requirement index for design of vibration isolators, which is given by (Rao, 2003)

$$T_f = \frac{F_T}{F_0} = \left\{\frac{k^2 + \omega^2 c^2}{(k - m\omega^2)^2 + \omega^2 c^2}\right\}^{1/2} \tag{4.9}$$

In order to achieve isolation, the force transmitted to ground (F_T) needs to be less than the vibrating force acting on it (F_0), which is equivalent to $T_f < 1$.

4.4 Examples and Illustrations

Two design examples are described below to illustrate the design process for corrugated cardboard system as a vibration isolator for the vacuum pump in the context of CLS.

4.4.1 Example 1

The procedure to conduct the design is as follows:

Step 1: Define design requirement

The design requirement for the vibration isolator is the transmission ratio T_f <0.8. The requirement can be further represented through Eqn. (4.9) to determine the stiffness and damping for the design, which is given by

$$T_f = \frac{F_T}{F_0} = \left\{ \frac{k^2 + \omega^2 c^2}{(k - m\omega^2)^2 + \omega^2 c^2} \right\}^{1/2} = \left\{ \frac{k^2 + 183.69^2 c^2}{(k - 34 \times 183.69^2)^2 + 183.69^2 c^2} \right\}^{1/2} < 0.8 \quad (4.10)$$

where $m = 34kg$ and $\omega = 183.69 rad/s$ (Pump manual, 2010), while the k and c are variables to be determined. Thus, it can be seen from Eqn. (4.10) that with a given transmission ratio, there are two variables to be determined. This results in many possible combinations of the two variables k and c. In this thesis study, a simplified equation with no consideration of damping c was used for the design, which is given by (Rao, 2003)

$$T_f = \frac{F_T}{F_0} = \frac{k}{m\omega^2 - k} \quad (4.11)$$

Eqn. (4.10) was used for two reasons: (1) For $T_f < 1$, the damping has a very small effect (Rao, 2003) and (2) The simplified equation is more conservative for the design. For the reason (2), the real system with damping can reduce more vibration. From Eqn. (4.11), the requirement for reduction in vibration in terms of amplitude can be represented by

$$T_f = \frac{F_T}{F_0} = \frac{k}{m\omega^2 - k} = \frac{k}{34 \times 183.69^2 - k} < 0.8 \quad (4.12)$$

The stiffness is then calculated to be: $k < 5.10 \times 10^5$ N/m.

Step 2: Design the cardboard system

A number of corrugated cardboards were designed to meet the requirement of stiffness $k < 5.1 \times 10^5$ N/m. A "C flute" cardboard with the size (length 158 mm and width 210 mm) was used in this case, which is shown in Fig. 4.5. The size of cardboard is close to that of the platform of the vacuum pump (Fig. 4.6). Note that the size of cardboard is determined for having a good stability of the vacuum pump (i.e. avoiding rotation).

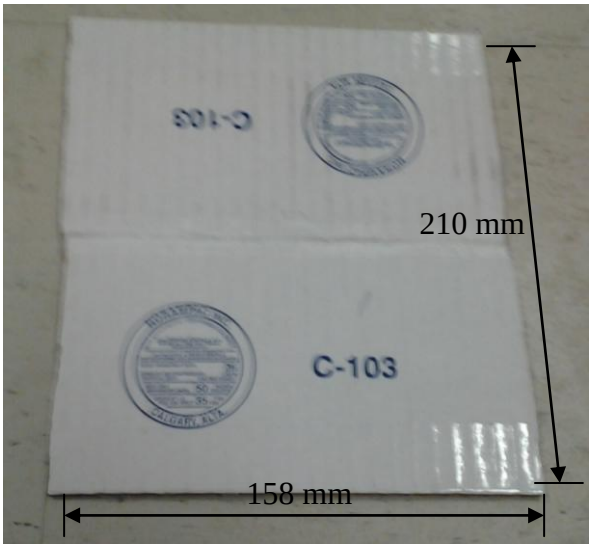

Fig. 4.5 Size of corrugated cardboard for the design

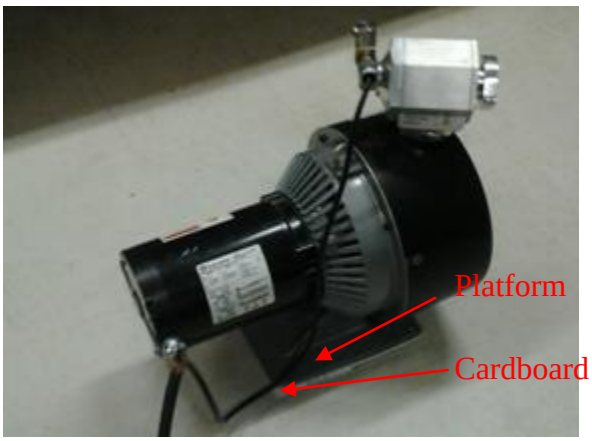

Fig. 4.6 The platform and corrugated cardboard

The stiffness of cardboard employed in cardboard system was then calculated by the finite element model described in Chapter 3. Fig. 4.7 shows the relation between force and displacement found from the finite element model.

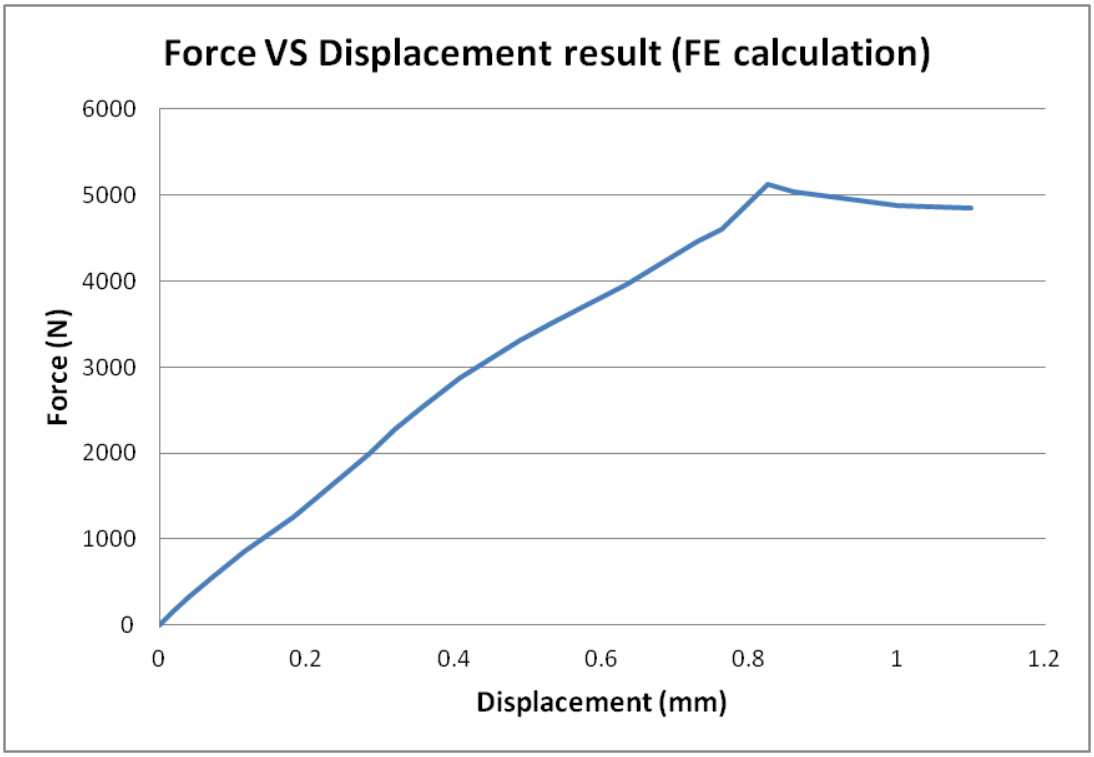

Fig. 4.7 Finite element result (158 mm × 210 mm)

From Fig. 4.7, the stiffness of cardboard is calculated to be 7.11×10^6 N/m, which is much higher than the requirement: $k < 5.10 \times 10^5$ N/m. In order to meet the requirement, a cardboard system was designed, where several cardboards were taken in a serial connection, as shown in Fig. 4.8. The cardboard system was modelled as shown in Fig. 4.9, where m is the mass of the pump, k_1 to k_n is the stiffness of the first cardboard to the stiffness of the *n-th* cardboard in the cardboard system. The design was then to determine the number of cardboards (n).

Fig. 4.8 Cardboard system - cardboards in a serial connection

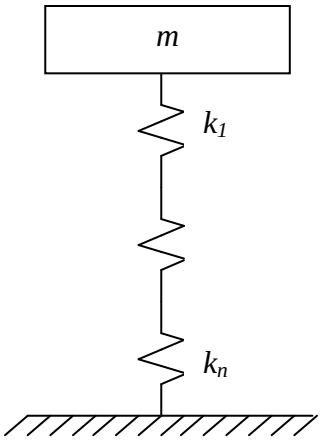

Fig. 4.9 Model of the cardboard system (without damping)

The equivalent stiffness (k_{eqv}) of the cardboard system is calculated by (Rao, 2003)

$$\frac{1}{k_{eqv}} = \frac{1}{k_1} + \frac{1}{k_2} + \cdots + \frac{1}{k_n} \tag{4.13}$$

where

k_{eqv} : The equivalent stiffness of the cardboard system, and

k_1 : The stiffness of cardboard for the first cardboard.

k_n : The stiffness of cardboard for the nth cardboard.

In the case here, as the stiffness of each cardboard is the same ($k_1 = k_2 = \cdots = k_n$), the equivalent stiffness (k_{eqv}) of the multi-layer cardboards is further given by (Rao, 2003)

$$k_{eqv} = \frac{k_1}{n} \tag{4.14}$$

With the equivalent stiffness (the same as the required stiffness) $k_{eqv} < 5.10 \times 10^5$ N/m and the stiffness of each cardboard $k_1 = 7.11 \times 10^6$ N/m, the n is calculated to be larger than 13.9. Thus, 14 cardboards were used in this cardboard system as a vibration isolator. The equivalent stiffness of the 14 cardboards is $k_{eqv} = k_1$ /14= 5.08×10^5 N/m which is less than the required stiffness, so it meets the requirement for the isolator in this case.

Step 3: Calculate the actual response

The actual response (transmissibility ratio) from the designed cardboard system (14 cardboards in a serial connection) is shown below. It is noted that the design process above is simplified with no consideration of the damping, while the damping should play a role in vibration isolation. Fig. 4.10 shows the lumped model including the stiffness and damping.

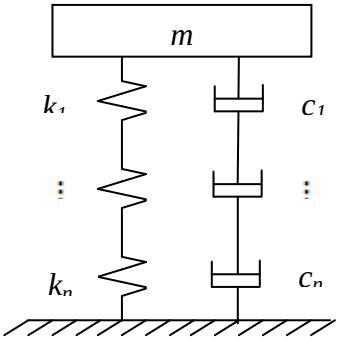

Fig. 4.10 Model of the cardboard system (with damping)

Similar to the stiffness, the damping is also connected in a serial connection. The equivalent damping of the cardboard system can be found by (Rao, 2003)

$$c_{eqv} = c_1 / n \tag{4.15}$$

The determination of the damping of each cardboard follows the approach described in Section 4.1. The size of cardboard was supposed to be with the length 158 mm, width 210 mm, and the mass 34 kg, which are the same as described for the pump test. However, the size and the mass

are larger than those the measurement test-bed (see Fig. 4.1) can sustain. In order to take the measurement, an assumption was made that the damping of cardboard changed proportionally to the change of its size and mass load on it. Thus, a proportionally reduced cardboard with the length 60.8 mm, width 38 mm and mass load 1.94 kg were used. The stiffness (k) of cardboard is 4.74 x 10^5 N/m. The measured displacement transmissibility is shown in Fig. 4.11. It can be seen from Fig. 4.11 that the resonance takes place at about 94 Hz, where the displacement transmissibility ratio $T_r = 4.72$. From the value of the displacement transmissibility ratio (T_r), the damping was calculated to be 55.4 N.s/m. Thus, the damping of the full size cardboard (158 mm and width 210 mm) was $c = 861 N.s/m$. Further, the equivalent damping of all the 14 cardboard in series was $c_{eqv} = c/14 = 61.5 N.s/m$.

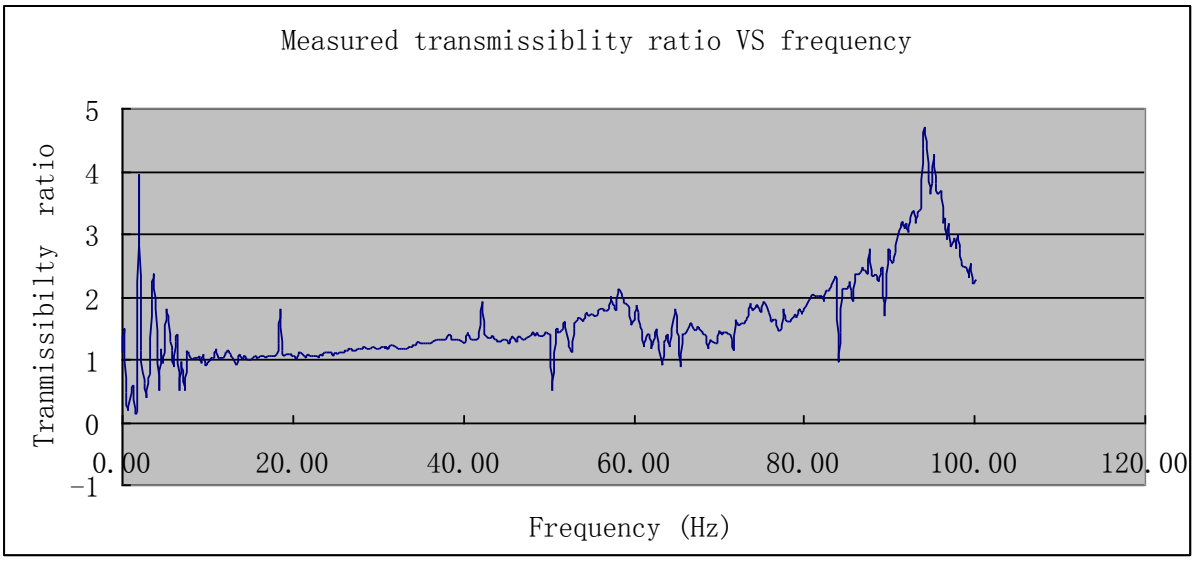

Fig. 4.11 The measured transmissibility ratio VS frequency relation for corrugated cardboard (60.4 mm × 38 mm)

With the equivalent stiffness k_{eqv} =5.08 x 10^5 N/m and equivalent damping c_{eqv} = 61.5 N.s/m. The actual transmissibility ratio (T_f) was calculated to be 0.794 from Eqn. (4.10); see below

$$T_f = \left\{ \frac{k^2 + \omega^2 c^2}{(k - m\omega^2)^2 + \omega^2 c^2} \right\}^{1/2} = \left\{ \frac{507857^2 + 183.69^2 \times 61.5^2}{(507857 - 34 \times 183.69^2)^2 + 183.69^2 \times 61.5^2} \right\}^{1/2} = 0.794 \qquad (4.16)$$

Thus, in the following experimental validation, the experimental result was expected to meet the design requirement (T_f < 0.8), and the actual response was T_f =0.794 in this case.

4.4.2 Example 2

Example 2 follows the same procedure as applied for Example 1.

Step 1: Define design requirement

The design requirement for the vibration isolator was: T_f <0.5. With T_f <0.5, the stiffness required was k<3.82 x 10^5 N/m from Eqn. (4.12). Corrugated cardboards were then designed to meet the requirement of stiffness k<3.82 x 10^5 N/m.

Step 2: Design the cardboard system

The same size of cardboard (length 158 mm and width 210 mm) for Example 1 was used. The stiffness of cardboard was calculated to be 7.11 x 10^6 N/m, which is much larger than the required stiffness at 3.82 x 10^5N/m. Similarly, cardboard was designed with multilayers. With the equivalent stiffness the same as the required stiffness k_{eqv} <3.82 x 10^5 N/m and the stiffness of each cardboard k_1 = 7.11 x 10^6 N/m, the n was calculated from Eqn. (4.11) to be larger than 18.6. Thus, 19 cardboards were used as the cardboard system to meet the requirement. The equivalent stiffness of the 19 cardboards is k_{eqv} =3.74 x 10^5 N/m.

Step 3: Calculate the actual response

The actual response is based on the stiffness and damping of the cardboard system. The cardboard system consists of 19 cardboards in a serial connection. As the damping of one

cardboard (158 mm and width 210 mm) was c=861 N.s/m, the damping of all the 19 cardboard was c=45.3 N.s/m. The actual transmissibility ratio (T_f) was calculated to be 0.484 from Eqn. (4.10); see below

$$T_f = \left\{ \frac{k^2 + \omega^2 c^2}{(k - m\omega^2)^2 + \omega^2 c^2} \right\}^{1/2} = \left\{ \frac{374210^{\,2} + 183.69^2 \times 45.3^2}{(374210 - 34 \times 183.69^2)^2 + 183.69^2 \times 45.3^2} \right\}^{1/2} = 0.484 \quad (4.17)$$

Thus, in the following experimental validation, the experimental result was expected to meet the requirement (T_f < 0.5), and the actual response was T_f =0.484 in this case.

4.5 Results and discussion

4.5.1 Measurement Test-bed

Fig. 4.12 illustrates the measurement test-bed. From the figure, it can be seen that cardboards are put in series under the vacuum pump. Two accelerometers are attached to the ground to measure the acceleration of the vibration on the ground. The measured accelerations are sent to the computer through a Brüel & Kjær dynamic signal analyzer. Both acceleration with cardboards (a_{with}) and acceleration without cardboards ($a_{without}$) are measured (Fig. 4.13).

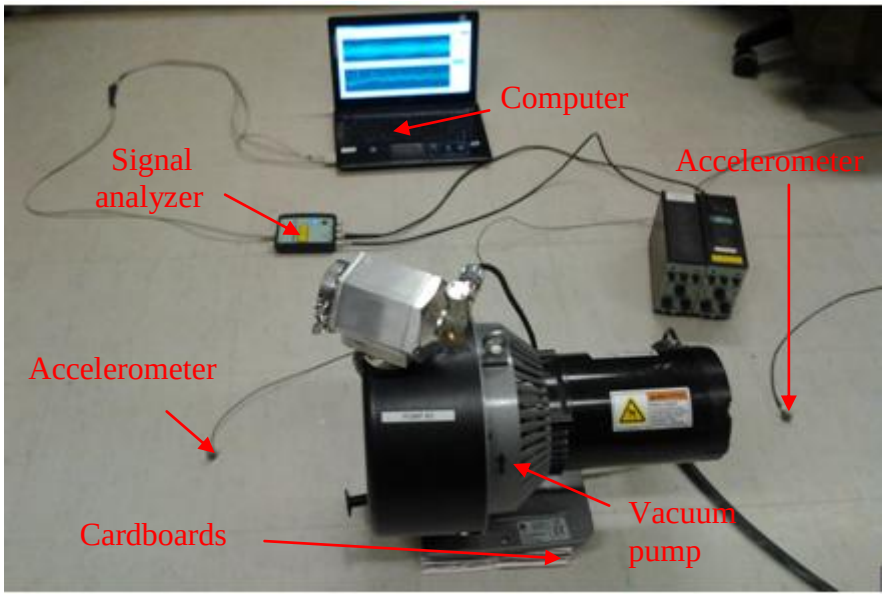

Fig. 4.12 Measurement test-bed for the application

(a) (b)

Fig. 4.13 Measurement (a) with cardboard and (b) without cardboard

The transmissibility ratio is given by

$$T_f = \frac{F_T}{F_0} = \frac{m_{ground} \times a_{with}}{m_{ground} \times a_{without}} = \frac{a_{with}}{a_{wothout}} \tag{4.18}$$

Here, the magnitude of the force that it transmits to ground (F_T) is the product of the mass of the ground m_{ground} times the acceleration on the ground with cardboards (a_{with}), while the magnitude of the vibrating force acting on it (F_0) is the product of the mass of the ground (m_{ground}) times the acceleration on the ground without cardboards ($a_{without}$). Thus, the transmissibility ratio is equal to the ratio of acceleration with cardboards (a_{with}) to that without cardboards ($a_{without}$).

Measurement was conducted on four locations around the vacuum pump. Fig. 4.14 shows the four locations, which are the front, back, left and right to the vacuum pump. The measured transmissibility ratio at each location was found to be sensitive to the location within 2.4 meters away from the vacuum pump (i.e. the ratio measured at 1 meter front to the pump is different from that at 2 meters front to the pump), while the ratio remained stable at the location outside the area. This may be attributed to the noise generated from the pump, which influences the measurement results from the accelerometers. Fig. 4.15, Fig. 4.16 and Fig 4.17 illustrate some of the measurement locations, which are 0.5 m, 1 m, 1.5 m away from the vacuum pump, respectively. As the noise has no effects on the measurement result out of 2.4 meters range, the measurements in the test were conducted at four locations, which are 3 meters away from the

vacuum pump. These four locations are called location 1 (front), location 2 (back), location 3 (left) and location 4 (right).

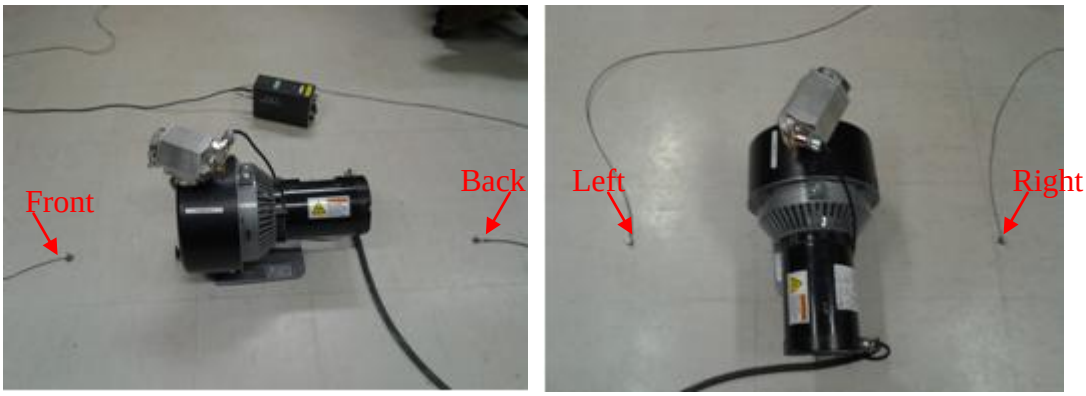

(a) (b)

Fig. 4.14 Measurements on (a) front and back; (b) left and right

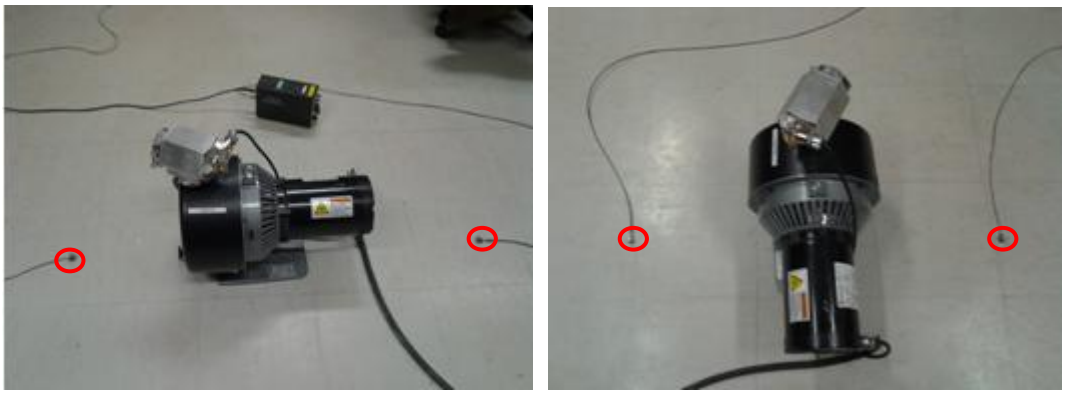

(a) (b)

Fig. 4.15 Locations at 50 cm away from the pump (a) front and back (b); left and right

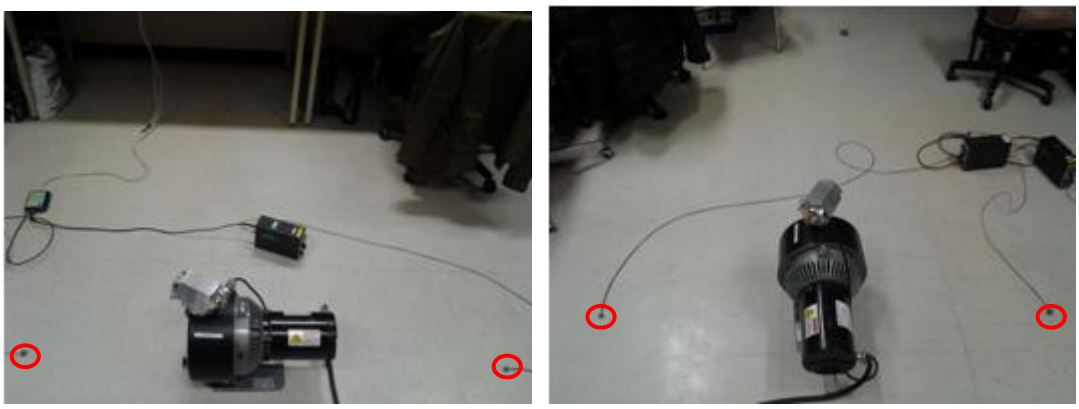

(a) (b)

Fig. 4.16 Locations at 1 m away from the pump (a) front and back; (b) left and right

(a) (b)

Fig. 4.17 locations at 1.5 m away from the pump (a) front and back; (b) left and right

4.5.2 Results and validation

For Example 1, the measured results with and without cardboards (14 cardboards in series) at location 1, location 2, location 3 and location 4 are shown in Fig. 4.18, Fig. 4.19, Fig. 4.20 and Fig. 4.21, respectively. In these figures, the horizontal axis is the frequency and the vertical axis is the acceleration. It is noted that only the acceleration at 29.25 Hz (183.69 rad/s) was recorded as it is the frequency where the pump was operating.

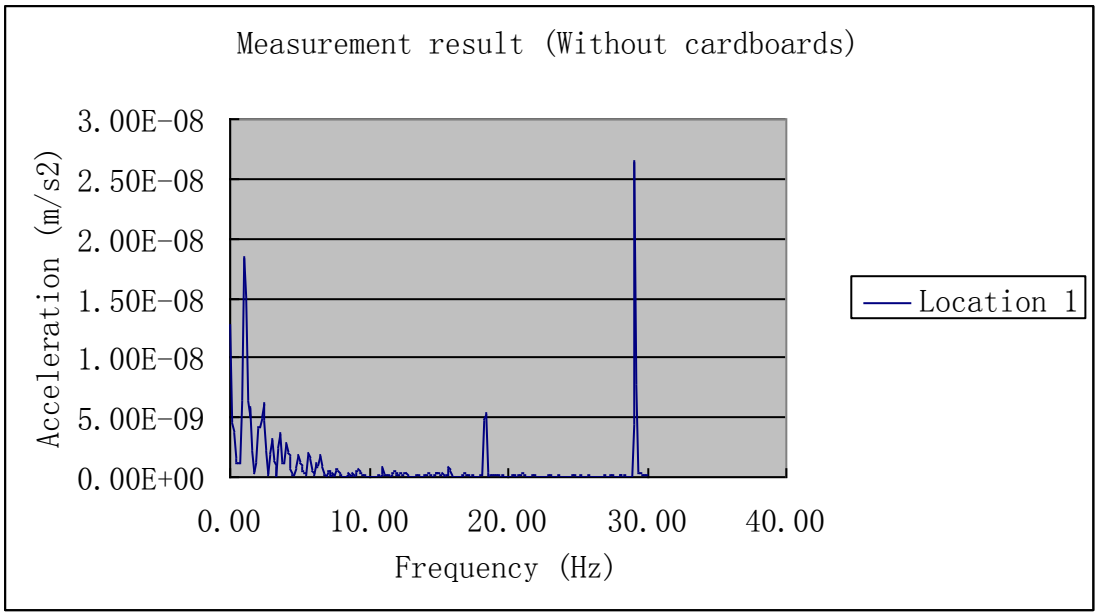

(a)

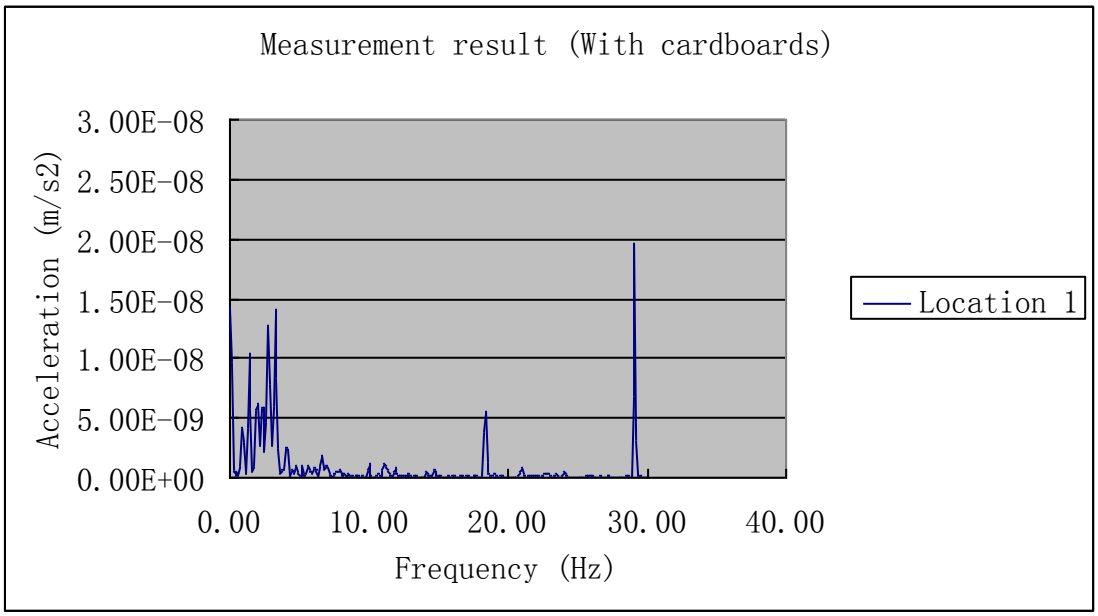

(b)

Fig. 4.18 Measurement results at location 1 (a) without cardboards; (b) with cardboards

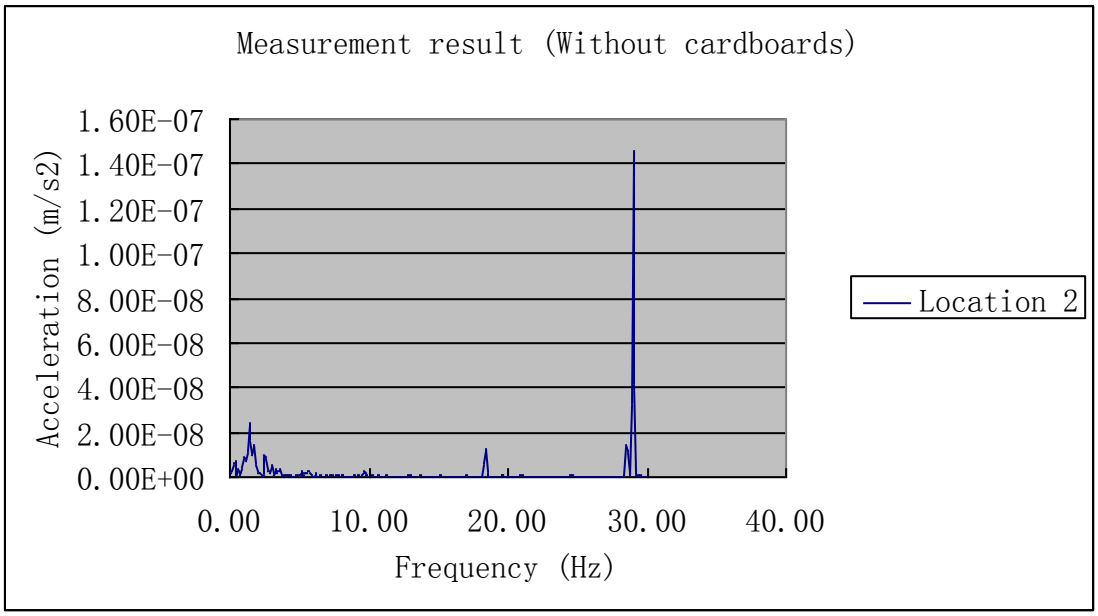

(a)

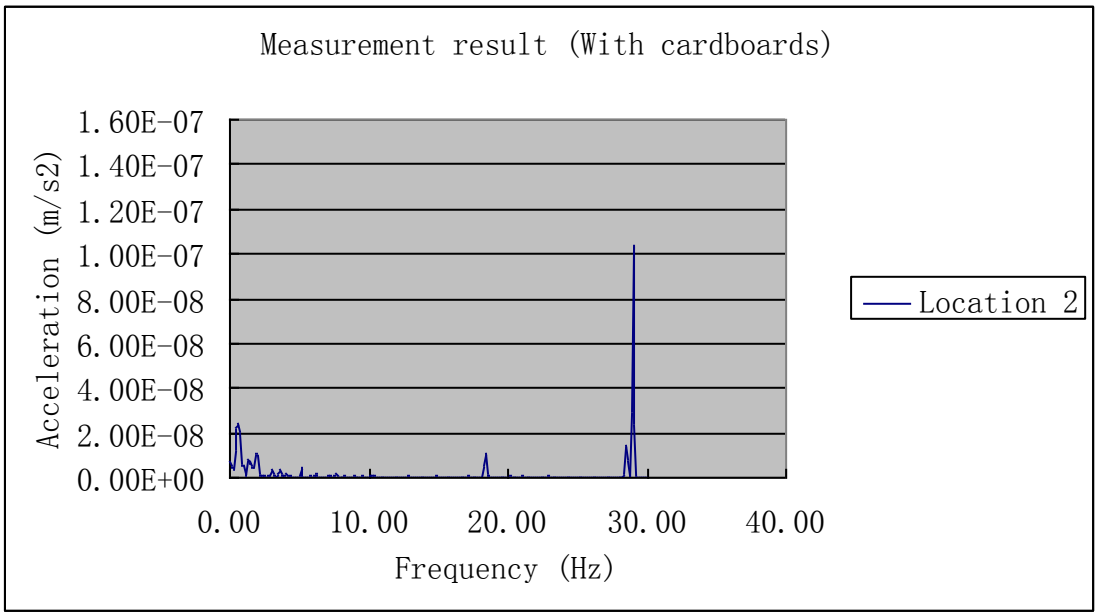

(b)

Fig. 4.19 Measurement results at location 2 (a) without cardboards; (b) with cardboards

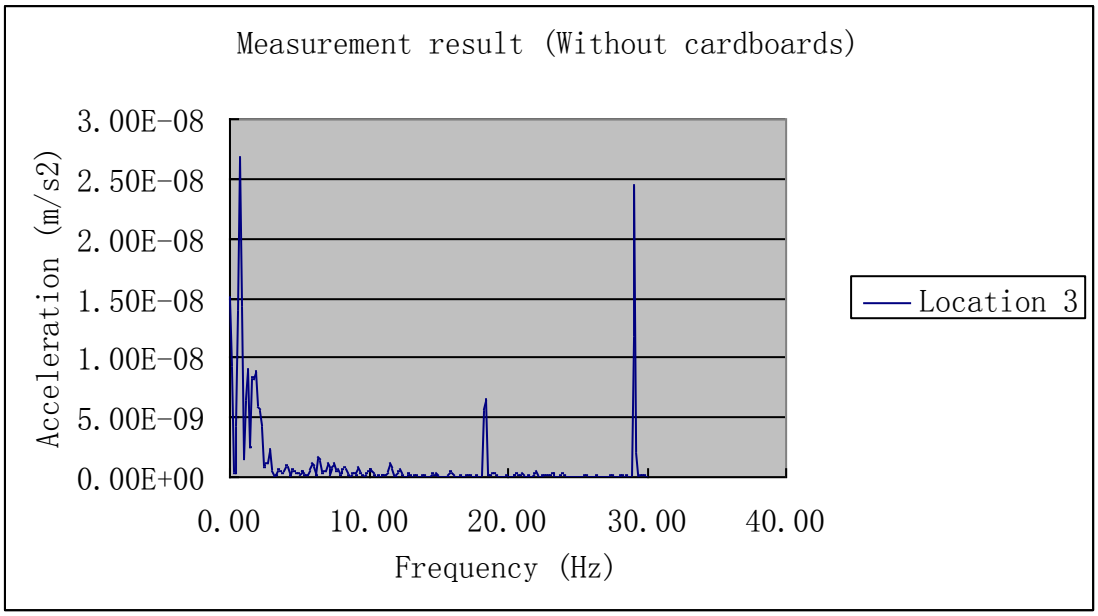

(a)

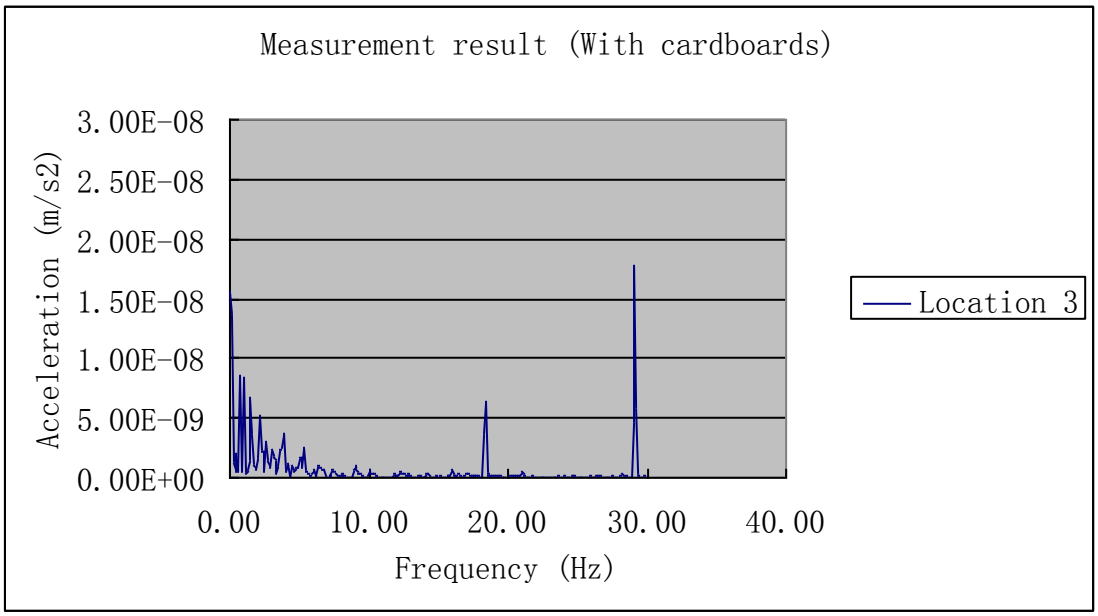

(b)

Fig. 4.20 Measurement results at location 3 (a) without cardboards; (b) with cardboards

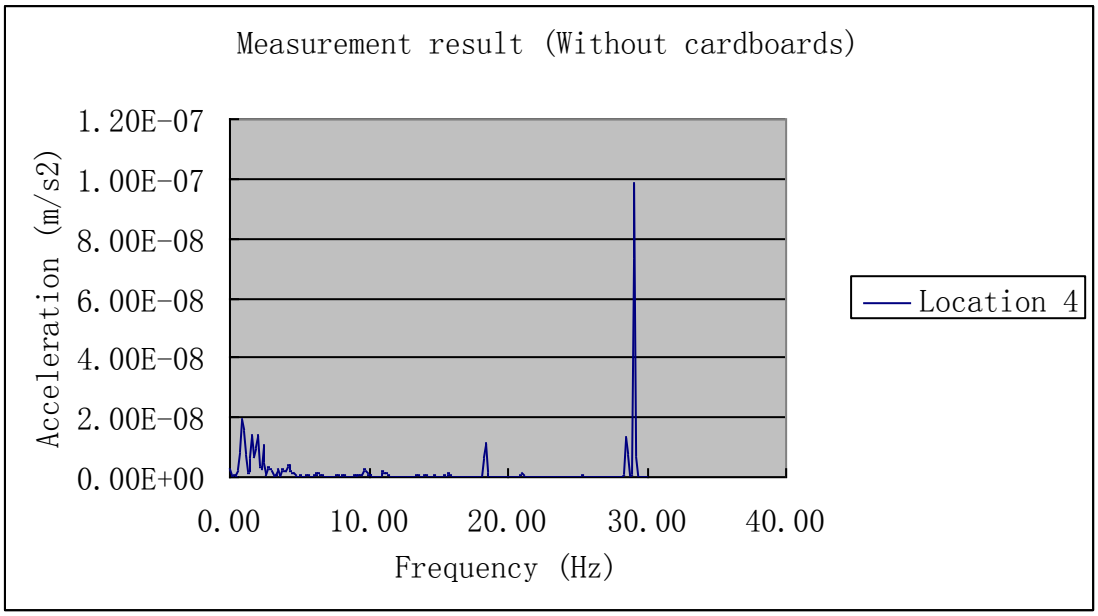

(a)

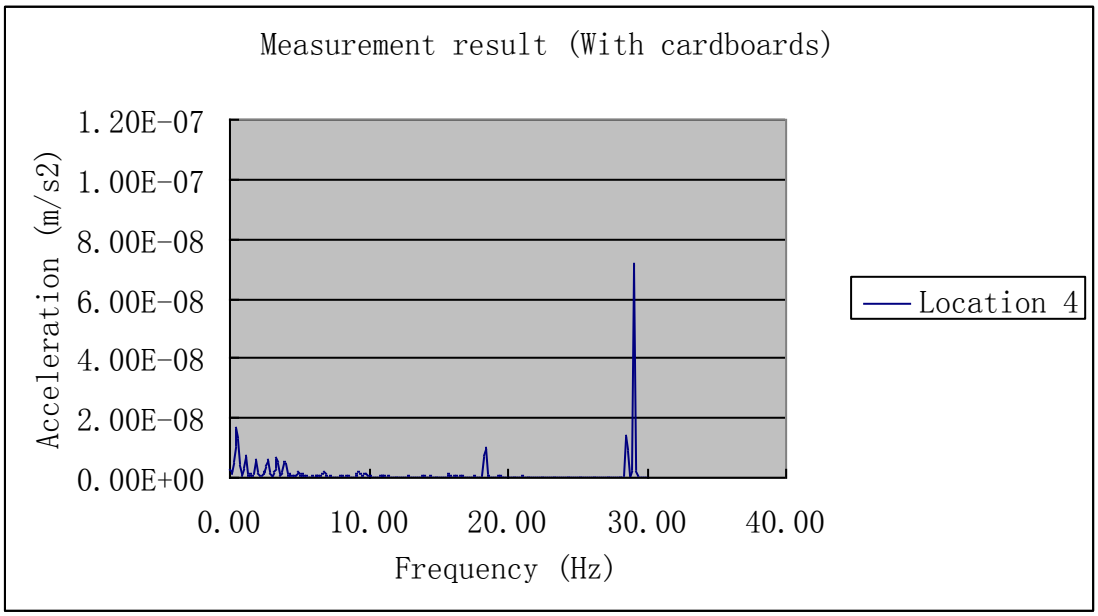

(b)

Fig. 4.21 Measurement results at location 4 (a) without cardboards; (b) with cardboards

The measured results at 29.25 Hz are listed in Table 4.1. The transmissibility ratio is calculated to be 0.739, 0.712, 0.756 and 0.715 for location 1, location 2, location 3 and location 4, respectively. The average of transmissibility ratio is 0.72275.

Table 4.1 Measured results at 29Hz for Example 1

	Location 1	Location 2	Location 3	Location 4
Acceleration without cardboards ($a_{without}$)	2.65e-008	1.46e-007	2.44e-008	9.83e-008
Acceleration with cardboards (a_{with})	1.96e-008	1.04e-007	1.77e-008	7.03e-008
Displacement ratio ($T_f = \frac{a_{with}}{a_{without}}$)	0.739	0.712	0.725	0.715

Thus, it can be seen that the measured transmissibility (T_f =0.72275) meets the requirement (T_f <0.8), while it differs from the actual response (T_f =0.794) with an error of 9.1%.

For Example 2, the measurement results at 29.25Hz with and without cardboards (19 cardboards in series) are listed in Table 4.2. The detailed results over all the frequency range can be found in Appendix B. The transmissibility ratio was calculated to be 0.403, 0.422, 0.431 and 0.414 for location 1, location 2, location 3 and location 4, respectively. The average of transmissibility ratio is 0.4175. Thus, it can be seen that the measured transmissibility (T_f =0.4175) meets the requirement T_f <0.5, while it differs from the actual response (T_f =0.484) with an error of 13.73%.

Table 4.2 Measured results at 29Hz for Example 2

	Location 1	Location 2	Location 3	Location 4
Acceleration without cardboards ($a_{without}$)	2.65e-008	1.46e-007	2.44e-008	9.83e-008
Acceleration with cardboards (a_{with})	1.07e-008	6.16e-008	1.05e-008	4.07e-008
Displacement ratio ($T_f = \frac{a_{with}}{a_{without}}$)	0.404	0.422	0.43	0.414

4.5.3 Discussion

The measured transmissibility ratios of 0.72275 and 0.4175 for the example 1 and example 2 (respectively) meet the design requirements of T_f <0.8 and T_f <0.5, respectively. Further, the

measured transmissibility ratio is compared with the actual response for the validation. Errors of 9.1% and 13.73% are found for example 1 and example 2, respectively. The errors may be attributed to three factors: (1) the horizontal movement of the pump was presented in measurement, while the lumped model assumed no horizontal movement; (2) the difference of stiffness of cardboards in the cardboard system was present due to cardboard manufacturing errors; (3) the error was present in alignment of the cardboards in the cardboard system. Further, the difference in error between the two cases (9.1% to 13.73%) is mainly caused by the factor (2) and factor (3). As with more layers in example 2 than example 1, there are more errors in the stiffness of the cardboard, factor (2), and alignments of cardboards, factor (3), in example 2 than example 1.

4.6 Conclusions

Two examples were used to illustrate the application of the developments in stiffness and damping of corrugated cardboard to design an isolator for a vacuum pump. Both design and experimental validation were conducted. The design was based on the lumped model of the system and the finite element model described in Chapter 3. Specifically, the required stiffness of the cardboard system for the design requirement was first calculated from the lumped model, and then the cardboard system was designed with cardboards in a serial connection to meet the required stiffness. Here, the stiffness of cardboard was calculated from the finite element model described in Chapter 3. The actual response from the designed cardboard system was also presented. The experiments were conducted on four locations, which are 3 meters front, back, left and right to the vacuum pump. The measured results of both examples meet the design requirements, while they differ from the actual response with errors of 9.1% and 13.4% for example 1 and example 2, respectively. The errors may be reduced if the horizontal movement can be taken into account in the lumped model. Overall, the case studies have shown that the stiffness and damping of cardboard determined in this study are adequate for designing corrugated cardboard and its system for vibration isolation.

CHAPTER 5 CONCLUSIONS AND FUTURE WORK

5.1 Overview

This thesis presented a study toward a material system made from corrugated cardboards for vibration isolation. The focus of the study was on understanding and modeling of the mechanical properties of corrugated cardboard under a compressive loading in its vertical direction, and they are stiffness and damping, and they are essentially related to vibration control in general.

In the current literature, finite element methods have been proposed for the stiffness under a compressive loading in its vertical direction. However, these methods are found inaccurate (especially in predicting peak load) for two reasons: (1) no consideration of accurate non-linear properties as well as behaviors, and (2) no consideration of the width of cardboard. It should be noted that the width parameter and peak load are important for the application of the stiffness of cardboard for vibration isolation. Difference in the width parameter could give rise to significantly different stiffnesses of cardboard. The peak load gives information of how much load cardboard can sustain. If the load on cardboard is larger than the peak load, cardboard cannot provide any stiffness for vibration isolation. In the current literature, damping is usually obtained by experiments. However, the experimental approach has not been applied on the damping of corrugated cardboard, to the best of the author's knowledge.

This study was motivated by overcoming these limitations and tailoring the application of cardboard to vibration isolation, which is indeed a new application area. The overall objective of this study was to develop design technologies for cardboard vibration isolator system. The specific objectives were defined for this study.

Objective 1: Develop an accurate finite element model for the stiffness of corrugated cardboard under compressive loading in its vertical direction with special attention to capturing the information of the width parameter and peak load.

Objective 2: Set up a test-bed for measuring the stiffness of cardboard. The measured stiffness will be used to validate the finite element model as developed in Objective 1.

Objective 3: Set up a test-bed and measure the damping of cardboard.

Objective 4: Demonstrate the effectiveness of the stiffness and damping models by designing a vibration isolation system with corrugated cardboards for reduction of vibration of a vacuum pump system.

These objectives have been achieved. The following are the details. A literature review (Chapter 2) was presented to confirm the validity of the proposed objectives. Specifically, it was concluded that the finite element model of corrugated cardboard that can predict stiffness with the width larger than the length and peak load, has not been previously reported in literature, which justifies objective 1 and 2. Measurement on damping of corrugated cardboard has not been reported in the literature, which justifies objective 3. There has never been any design technology for a cardboard system as a vibration isolator in the literature, which justifies the motivation of the whole study as well as objective 4.

In Chapter 3, a finite element model for the stiffness of corrugated cardboard with consideration of the width parameters and peak load was presented. The model was implemented in the ANSYS environment; in particular, a shell element was employed to include different width parameters and nonlinear orthotropic material property was employed to predict the peak load. A test-bed for measuring the stiffness of cardboard was also presented. The measured stiffness was used to validate the stiffness from the finite element model. Finite element model with both an actual core shape and approximated sine core were used to validate the theoretical model with the experiments. Both models were found effective to predict stiffness, though the model with the actual core shape was more accurate.

In Chapter 4, a test bed for measuring the damping of cardboard and two case studies for illustrating the application of the developments in stiffness and damping of the corrugated board to design the isolator for a vacuum pump were presented. The application includes both the design and experimental validation. The validation results have shown that the stiffness and damping of cardboard in this study are adequate, as they are effective in reducing vibrations to the requirement.

5.2 Conclusions

The study presented in this thesis concludes:

(1) The finite element model for corrugated cardboard should take the shell element and consider the nonlinear orthotropic material property for stiffness prediction.

(2) The finite element models with both actual core shape and approximated sine core shape are effective to predict the stiffness, though the one with the actual core shape is more accurate than the one with the sine core shape especially in predicting peak load.

(3) The proposed design procedure for a cardboard system based on the proposed lumped model (in which the stiffness of a single cardboard is computed while the damping of a single cardboard is measured) is effective.

5.3 Contributions

The main contributions of this thesis are described below:

(1) An accurate model of corrugated cardboard for predicting the stiffness of corrugated cardboard (with different widths) and peak load is available to the field of paper-based systems. The way to model the contact behavior between two objects which deform on their own in the model for corrugated cardboard is also useful to similar problems such as gear engagement and follower contact in transmission devices.

(2) A test-bed to measure the damping of cardboard is available for application to vibration isolation. The test-bed is useful to other applications as well.
(3) A complete system for extending the stiffness and damping of a single cardboard to a cardboard system which is composed of a number of cardboards in connection is available for industrial applications in vibration isolation. There is a significant benefit to environment protection and sustainable development. The current study has suggested that rubber isolators can be replaced by cardboard isolators.

5.4 Future Work

Several future endeavors could potentially improve upon this thesis work.

First, the finite element model for corrugated cardboard in this thesis is found inaccurate in predicting the nonlinear force VS deformation relation. This can be improved with a more accurate acquisition of the nonlinear plastic material properties.

Second, the stiffness and damping models developed in this study still have some error for predicting the vibration reduction of the vacuum pump. This error may be reduced if the horizontal movement of the vacuum pump can be taken into account in the stiffness and damping models. That is, a whole cardboard may need to be considered as a multi-degree of freedom system instead of a single degree of freedom system as it was done now.

Finally, fatigue design with consideration of humidity needs to be studied, as the main concern for the paper material is its fatigue failure. Understanding of the fatigue behaviour of cardboard is very important to ensure a reliable industrial system.

REFERENCES

Aboura, Z., Talbi, N., Allaoui, S., 2004, Benzeggagh, M.L., Elastic behaviour of corrugated cardboard: experiments and modelling, *Composite Structure*, vol. 63, pp. 53-62.

Allansson, A., and Svard, B., 2001, Stability and collapse of corrugated board; numerical and experimental analysis, Master's Thesis, Sweden: Division of Structural Mechanics, LTH, Lund University.

ANSYS, 2004. ANSYS Release 8.1 Documentation Preview, Swanson Analysis System, Inc., Houston.

Bandstra, J. P., 1983, Comparison of equivalent viscous damping in discrete and continuous vibrating system, *Transaction of ASME, Journal of Vibration, Acoustics, Stress and Reliability in Design*, vol. 105, pp. 382–392.

Biancolini, M.E., and Brutti, C., 2003, Numerical and experimental investigation of the strength of the corrugated board packages, *Packaging Technology and Science*, vol. 16, no. 2, pp. 47-60.

Beards, C. F. and Williams, J. L., 1977, The damping of structural vibration by rotational slip in structural joint, *Journal of Sound and Vibration*, vol. 53**,** no. 3, pp. 333–340.

Beldie, L., Sandberg, G., Sandberg, L., 2001, Paperboard packages exposed to static loads - finite element modeling and experiments, *Packaging Technology and Science*, vol. 14, pp. 171-178.

Bert, C.W., 1973, Material damping: an introductory review of mathematical models, measure and experimental techniques, *Journal of Sound and Vibration*, vol. 29, no. 2, pp. 129–153.

Bulson, P.S., 1969, The Stability of Flat Plates, American Elsevier Publishing Company, Inc., NY.

Caddell, R. M., Raghava, R. S. and Atkins, A. G., 1973, Yield criterion for anisotropic and pressure dependent solids such as oriented polymers, *Journal of Materials Science*, vol. 8, no. 11, pp. 1641-1646.

Campell, A. C., 2010, The use of A-flute, B-flute, AC flute and BC flute corrugated paperboard as a cushion material, Master's thesis, Clemson University.

Chen, K., 2009, Mechanical dynamics: fundamentals, applications and practices, *Springer*.

Coan, J.M., 1951, Large-Deflection Theory for Plates with Small Initial Curvature Loaded in Edge Compression, *Journal of Applied Mechanics*, vol. 18, pp. 143-151.

Crandall, S. H., 1970, The role of damping in vibration theory, *Journal of Sound and Vibration*, vol. 11, no. 1, pp. 3–18.

Dekker, M., 1999, Stiffness and damping in mechanical design, Technology & Engineering.

Deshpande, V. S., Fleck, N. A. and Ashby, M. F., 2001, Effective properties of the octet-truss lattice material, *Journal of the Mechanics and Physics of Solids*, vol. 49, no. 8, pp. 1747-1769.

Earls, S. W. E., 1966, Theoretical estimation of frictional energy dissipation in a simple lap joint, *Journal of Mechanical Engineering Science*, vol. 8, no. 2, pp. 207–214.

Folie, G.M., 1971, The behaviour and analysis of orthotropic sandwich plates, *Building Science*, vol. 6, pp. 57-67.

Gilchrist, A.C., Suhling, J.C., Urbanik, T.J., 1999, Nonlinear finite element modeling of corrugated board, *Mechanics of Cellulosic Materials*, AMD – vol. 231/MD-vol. 85.

Gooren, L.G.J., 2006, Creasing Behaviour of Corrugated Board – An Experimental and Numerical Approach, Department Mechanical Engineering, Report MT06.06, Eindhoven/The Netherlands.

Hahn, E. K., de Ruvo, A., Westerlind, B. S. & Carlsson, L. A., 1992, Compressive strength of edge-loaded Corrugated Board Panels, *Experimental Mechanics*, vol. 32, pp. 259-58.

Haj-Ali, R., Choi, J., Wei, B.S., Popil, R., Schaepe, M., 2009, Refined nonlinear finite element models of corrugated fiberboards, *Composite structures*, vol. 87, no. 4, pp. 321-333.

Hill, R., 1983, *The Mathematical Theory of Plasticity*. Oxford University Press. New York.

Housner, G. W., Bergman, L. A., 1997, Structural control: past, present and future, *Journal of Engineering Mechanics*, vol. 123, pp. 897-971.

Huang, J.L., Ranier Clement, Sun, Z.H., Wang, J., Zhang, W.J., 2012, Global Stiffness and Natural Frequency Analysis of Compliant Mechanisms with Embedded Actuators with a General-Purpose Finite Element System. *International Journal of Advanced Manufacturing Technology*. DOI 10.1007/s00170-012-4243-8

Johnson, M.W., Jr. and Urbanik, T.J., Analysis of the localized buckling in composite plates structures with application to determining the strength of corrugated fiberboard, *Journal of Composites Technology and Research*, vol. 11, no. 4, pp. 121-127.

Jones, A.L., 1871, Improvement In Paper For Packing, US patent

Krusper, A., Isaksson, P., and Gradin, P., 2007, Modeling of Out-of-Plane Compression Loading of Corrugated Paper Board Structures, *J. Eng. Mech.*, vol. 133, no.11, pp. 1171–1177.

Lapcik, Jr. L., Augustin, P., Pistek, A., Bujnoch, L., 2001, Measurement of the dynamic stiffness of recycled rubber based railway track mats according to the DB-TL 918.071 standard. *Applied Acoustics*, vol. 62, no. 1123-1128.

Li, J.W., Matias, E., Chen, N., Kin, C.-Y., Wang, J., Gorin, J., He, F., Thorpe, P., Lu, Y., Chen, W.F., Grochuski, P., Chen, X.B., and Zhang, W.J., 2011, Investigations of mechanical vibrations for beamlines at the Canadian Light Source, *Journal of Synchrotron Radiation*, vol. 18, pp. 109-116.

Lin, T.R., Farag, N.H., Pan, J., 2004, Evaluation of frequency dependent rubber mount stiffness and damping by impact test, *Applied Acoustics*, vol. 66, pp. 829-844.

Long, O., 1874, Packings For Bottles, Jars, & C., US patent.

Lu, T. J., and Chen, C., 2001, Compressive behaviour of corrugated board panels, *Journal of Composite Materials*, vol. 35, no. 23, pp. 2098–2126.

Luo, S., Suhling, J.C., Laufenberg, T.L., 1995, Bending and twisting tests for measurement of the stiffness of corrugated board, *ASME-Mechanics of Cellulosic Materials*, AMD-vol. 209/MD-vol. 60.

Mallik, A. K., Kher, V., Puri, M., Hatwal, H., 1999, On the modelling of non-linear elastomeric vibration isolators, *Journal of Sound and Vibration*, vol. 219, no. 2, pp. 239-253.

Maltenfort, G.G., 1956, Compression Strength of Corrugated Containers, *Fibre Containers*, vol. 41, no. 7, July.

Mckee, R.C., Gander, J.W., and Wachuta, J.R., 1963, Compression Strength Formula for Corrugated Boxes, *Paperboard packaging*, vol. 48, no. 8, pp. 149-153.

Nadeau, S., Champoux, Y., 2000, Application of the direct complex stiffness method to engine mounts. *Experimental Techniques*, vol. 24, no. 3, pp.21-25.

Nashif, A. D., Jones, D. I. G., and Henderson, J. P., 1985, *Vibration Damping*, John Wiley, New York.

Nordstrand, T., Carlsson, L. A., 1997, Evaluation of transverse shear stiffness of structural core sandwich plates, *Composite Structure*, vol. 37, pp. 145-153.

Nordstrand, T., Carlsson, L.A., and Allen, H.G., 1994, Transverse shear stiffness of structural core sandwich, *Composite Structures*, vol. 27, pp. 317-329.

Peterson, W.S., 1983, Flute/Liner interaction for bending of combined board beams, *Paperboard packaging*, vol. 68, pp. 37-41.

Pommier, J.C., and Poustis, J., 1989, New approach for predicting box stacking strength, *Revue ATIP*., vol. 43, no. 4, pp. 179-181.

Pommier, J.C., and Poustis, J., 1990, Bending stiffness of corrugated board prediction using the finite element method, *Mechanics of Wood and Paper Materials*, ASME AMD, vol. 112, pp. 67-70.

Pommier, J.C., Poustis, J., Fourcade, E., and Morlier, P., 1991, Determination of the Critical Load of a Corrugated Cardboard Box Submitted to Vertical Compression by Finite Elements Methods, Proceddings, *International Paper Physics Conference*, TAPPI. Atlanta, GA, pp. 437-447.

Rahman, A.A., and Abubakr, S. A., Finite element investigation of the role of adhesive in the buckling failure of corrugated fiberboard, *Wood Fiber Science*, vol. 36, pp. 260-268.

Rao, S. S., 2003, Mechanical Vibration, Prentice Hall, fourth edition.

Reddy, J.N., 1994, Energy and variational methods in applied mechanics, *John Wiley*.

Richard, C.M., and Singh, R., 2001, Characterization of rubber isolator nonlinearities in the context of single- and multi-degree-of-freedom experimental systems, *Journal of Sound and Vibration*, vol. 247, no. 5, pp. 807-834.

Romans, T.T.H.J., 2008, Humidity influences on creasing behaviour of corrugated board-an analytical, experimental and numerical approach, Department Mechanical Engineering, Report MT08.29, Eindhoven/The Netherlands.

Shih, C.F., Lee, D., 1978, Further Developments in Anisotropic Plasticity. *Journal of Engineering Materials and Technology*, vol. 100, pp. 294-302.

Talbi, N., Batti, A., Ayad, R., Guo, Y.Q. , 2009, An analytical homogenization model for finite element modeling of corrugated cardboard, *Composite Structure*, vol. 88, no. 2, pp. 280-9.

Thomson, D.J., Van Vliet, W.J., Verheij, J.W., 1998, Developments of the indirect method for measuring the high frequency dynamic stiffness of resilient elements. *Journal of Sound and vibration*, vol. 213, no. 1, pp. 169-188.

Ungar, E. E. and Kerwin, E. M., 1962, Loss factors of viscoelastic systems in terms of energy concepts, *The Journal of the Acoustical Society of America*, vol. 34, no. 7, pp. 954–957.

Urbanik, T.J., 1996, Review of buckling mode and geometry effects on postbuckling strength of corrugated containers, *ASME-PUBLICATIONS-PVP*, vol. 343.

Urbanik, T.J., 1997, Linear and nonlinear material effects on post buckling strength of corrugated containers, *Mech Cellulosic Mater AMD-vol. 221/MD*, vol. 77, pp. 93 – 99.

Urbanik T.J., and Saliklis, E.P., 2002, Finite element corroboration of buckling phenomena observed in corrugated boxes, *Wood and Fiber Science*, vol. 35, pp. 322-333.

Yamaki, N., Post-buckling behaviour of rectangular plates with small initial curvature loaded in edge compression, *Journal of Applied Mechanics*, vol. 26, pp. 407-414.

APPENDIX A

EXPERIMENTAL INDENTIFICATION OF THE MATERIAL CONSTANTS

A.1 Introduction

This Appendix will describe the identification of the material parameters for the liner and core of corrugated cardboard through tensile test. This Appendix is comprised of:

1. Measurement test-bed for tensile test,
2. Identification of material parameters for the liner, and
3. Identification of material parameters for the core.

A.2 Measurement test-bed for tensile test

A tensile test is conducted to obtain the in-plane material constants ($E_x, E_y, \sigma_0, E_t, R_{xx}, R_{yy}$) of cardboard according to ASTM D828-97 standard. The measurement test-bed of the tensile test is shown in Fig. A.1.

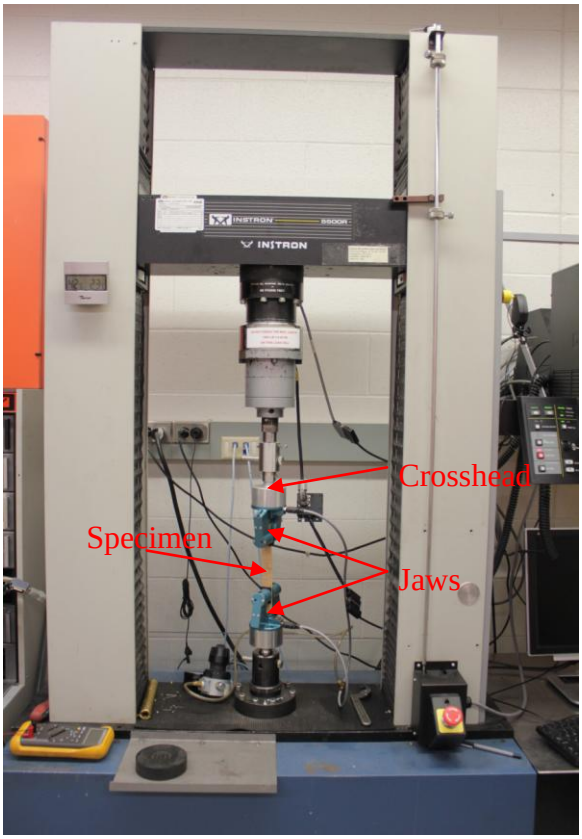

Fig. A.1 The measurement test-bed for the tensile test

The tested specimens were the liner and core of cardboard in both x direction and y direction, which is shown in Fig. A.2. The length, width and thickness of the four types of specimens were all measured to be 270 mm, 24.5 mm, and 2 mm. From Fig. A.1, it can be seen that the specimen is clamped by two jaws and tensile force is applied in the vertical direction by using a crosshead with a sensitive load cell of 500 N. The tensile loading was applied gradually on the specimen with a control of the increment of the resulting displacement at 25.4 mm/min. Both tensile loading and the displacement caused by the tensile loading were recorded. Further, the stress was determined as the tensile load divided by the initial area of the cross section, and strain was determined as the displacement divided by the specimen length. The material property was calculated based on the stress VS strain relation. It is noted that for each type of specimen, four new specimens were repeated.

(a) (b) (c) (d)

Fig. A.2 (a) liner specimen in x direction; (b) liner specimen in y direction; (c) core specimen in x direction; (d) core specimen in y direction

A.2 Identification of material parameters for the liner

Fig. A.3 shows the typical measured stress VS strain response of the liner specimen under the tension in x direction. In the initial loading stage, the specimen shows nonlinear response until an strain level of 0.002 is reached. This is attributed to the fact that the specimen is not flat enough but a bit of wavy. Specifically, the initial nonlinear response was largely due to the flattening of these wavy parts. After the initial stage, all fibers are loaded and the specimen then became flat. However, the response becomes flat until a strain level of 0.003 was reached. This is because that the glue parts of the specimen collapse. The glue parts are the ones which were used to connect the liner and core of cardboard, and the collapse results in the decrease of the strength of the specimen. In other words, the stress required to further deform the specimen decreases. In this case, it decreased to the same stress where the collapse happened and remained until the glue

part had no effect on the strength of the specimen (strain level of 0.003).

After the glue part has no effect, the specimen responded linearly up to yield point at strain level of 0.01. After the yield point, the material responded into the plastic deformation until the failure happens at strain level of 0.014. Referring to Fig. A.3, the elastic modulus E_x is the slope of the linear response, which was calculated to be 3.167 GPa; The reference stress σ_0 was the same as the yield stress in x direction, which is 0.028 GPa; The plastic modulus E_t is the slope of the plastic response, which was calculated to be 2.392 GPa. The R_{xx} is the ratio of the yield stress (0.028Gpa) in x direction to the reference stress (0.028 GPa), which was calculated to be 1.

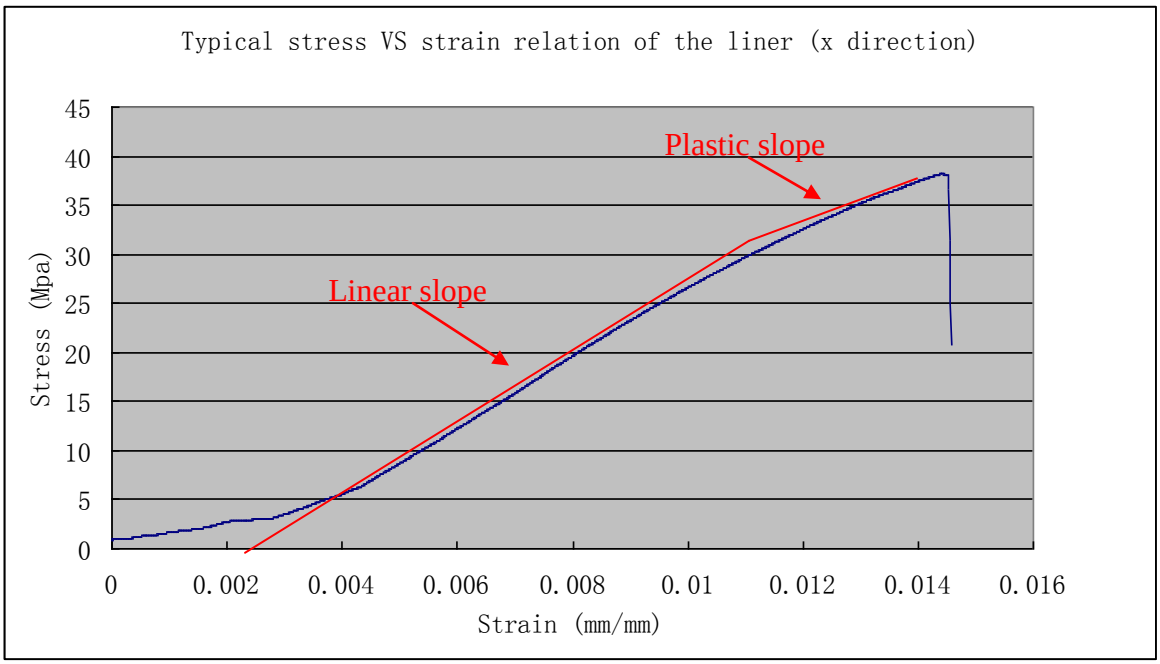

Fig. A.3 Typical stress VS strain relation of the liner in x direction

Fig. A.4 shows the typical measured stress VS strain response of the liner specimen under the tension in y direction. Similarly, in the initial loading stage, the specimen shows nonlinear response due to flattening until a strain level of 0.0025 is reached. Following that, the response becomes flat due to glue effect until a strain level of 0.004 is reached. After that, the specimen responds linearly up to yield point at strain level of 0.008. After the yield point, the material responds into the plastic deformation until the failure happens at strain level of 0.033. Referring

to Fig. A.6, the elastic modulus E_y is calculated to be 1.8 GPa; The yield stress in y direction is found to be 0.011GPa; The R_{yy} is the ratio of the yield stress in y direction (0.011GPa) to the reference stress (0.028GPa), which is 0.4.

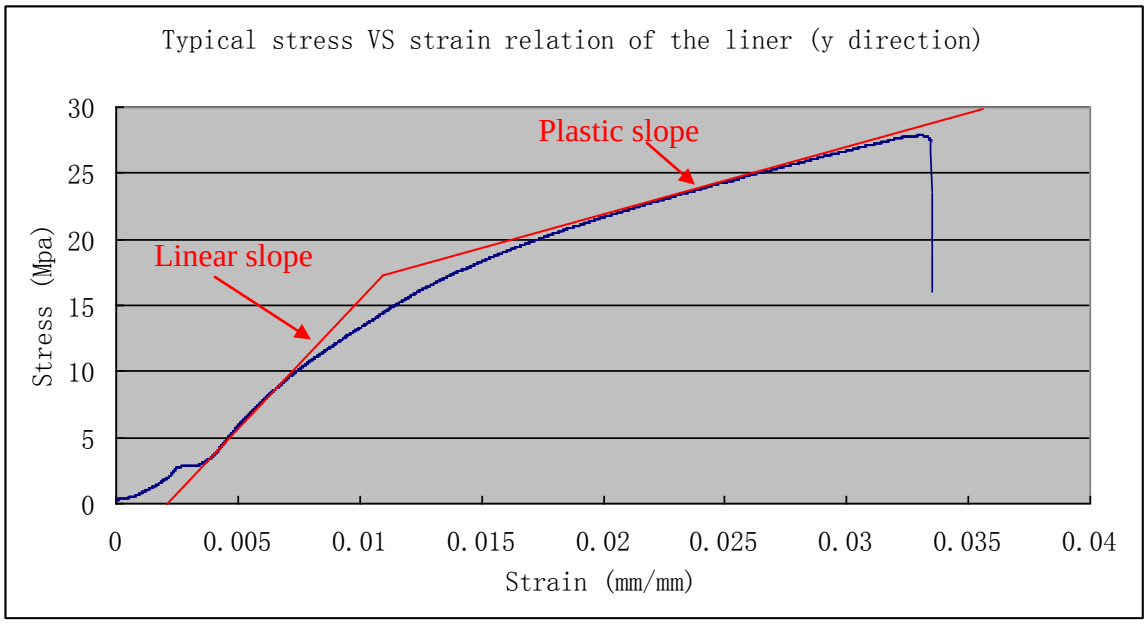

Fig. A.4 Typical stress VS strain relation of the liner in y direction

For both types of specimens, four new specimens were repeated and the results were shown in Fig. A.5. and Fig. A.6, respectively.

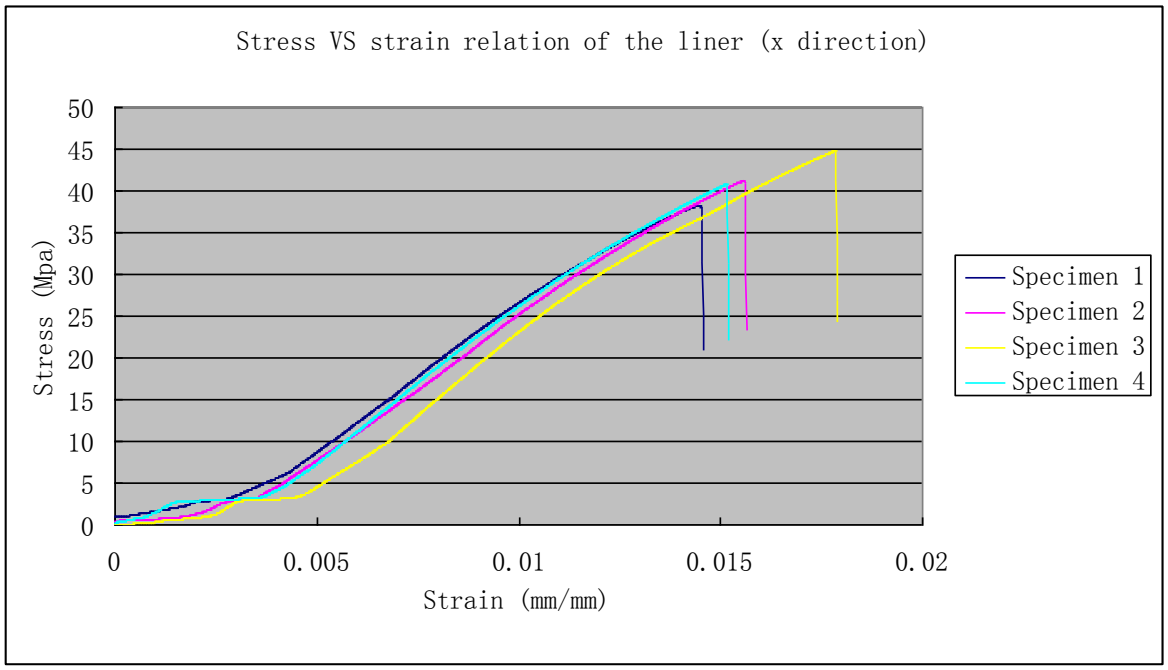

Fig. A.5 Stress VS strain relation of the liner in x direction for all specimens

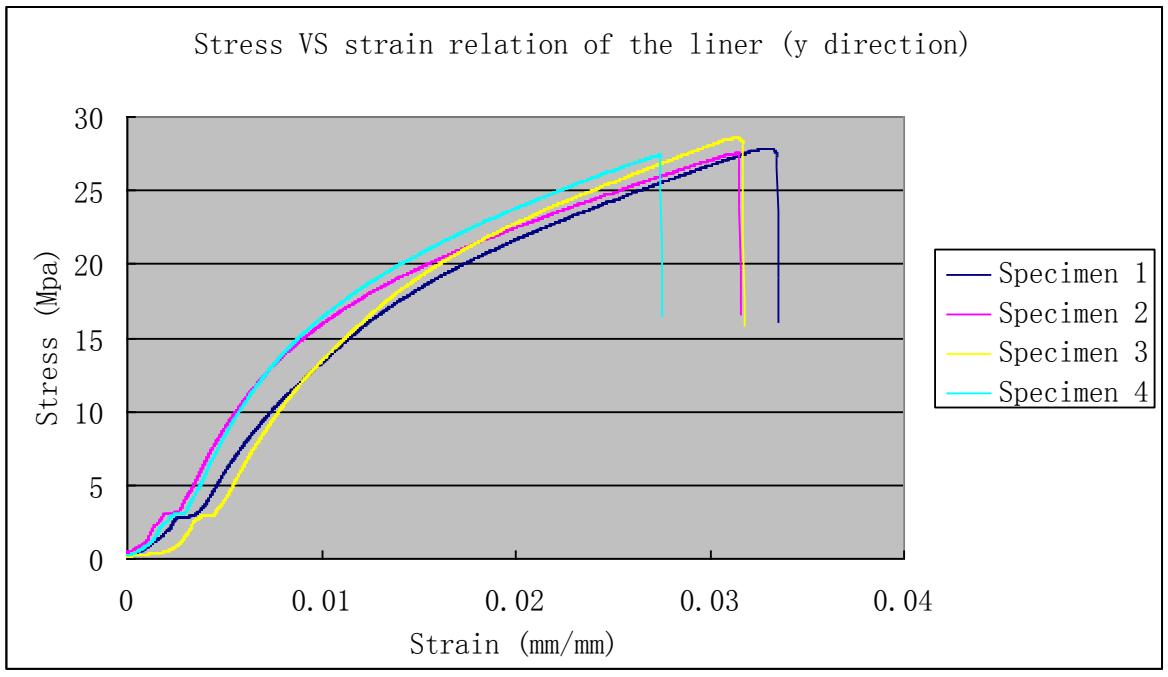

Fig. A.6 Stress VS strain relation of the liner in y direction for all specimens

The average value of the material parameters of the four specimens in both x and y direction are then calculated and listed in table A.1.

Table A.1 Average value of the measured material parameters from four liner specimens

Parameter	Value
E_x (GPa)	3.2
E_y (GPa)	2
σ_0 (GPa)	0.03
E_t (GPa)	2.5
R_{xx}	1
R_{yy}	0.35

Based on the material parameters in Table A.1, the other material parameters are derived according to the empirical equations shown in Section 3.2.3. For the out of plane parameter E_z, it is derived according to Eqn. (3.3) as follows:

$$E_z = E_x / 200 = 3.2GPa / 200 = 0.016GPa \tag{A.1}$$

The shear modulus G_{xy}, G_{xz}, G_{yz} are derived according to Eqn. (3.4), Eqn. (3.5), and Eqn. (3.6), respectively, which is found as

$$G_{xy} = 0.387\sqrt{E_x E_y} = 0.387 \times \sqrt{3.2GPa \times 2GPa} = 1GPa \tag{A.2}$$

$$G_{xz} = E_x / 55 = 3.2GPa / 55 = 0.058GPa \tag{A.3}$$

$$G_{yz} = E_y / 35 = 2GPa / 35 = 0.057GPa \tag{A.4}$$

The value of ν_{xy}, ν_{xz} and ν_{yz} are set according to (Nordstand, 1995), which is 0.34, 0.01 and 0.01, respectively. The value of $R_{zz}, R_{xy}, R_{yz}, R_{xz}$ are related to the value of $\sigma_{zz}^y, \sigma_{xy}^y, \sigma_{yz}^y, \sigma_{xz}^y$, respectively, which are the yield stress in z, xy, yz and xz direction. According to (Gooren, 2006), σ_{zz}^y is about 0.003-0.007GPa, while $\sigma_{xy}^y, \sigma_{yz}^y, \sigma_{xz}^y$ are about 0.003 to 0.011GPa. In this work, σ_{zz}^y is set to be 0.007GPa, and $\sigma_{xy}^y, \sigma_{yz}^y, \sigma_{xz}^y$ are all set to be 0.011 for the first estimate. Further, the

$R_{zz}, R_{xy}, R_{yz}, R_{xz}$ are determined according to Eqn. (3.18), Eqn. (3.19), Eqn. (3.20), and eqn. (3.21), respectively, which are found as below:

$$R_{zz} = \frac{\sigma_{zz}^{y}}{\sigma_0} = \frac{0.007GPa}{0.03GPa} = 0.23 \tag{A.5}$$

$$R_{xy} = \sqrt{3}\frac{\sigma_{xy}^{y}}{\sigma_0} = \sqrt{3} \times \frac{0.011GPa}{0.03GPa} = 0.635 \tag{A.6}$$

$$R_{yz} = \sqrt{3}\frac{\sigma_{yz}^{y}}{\sigma_0} = \sqrt{3} \times \frac{0.011GPa}{0.03GPa} = 0.635 \tag{A.7}$$

$$R_{xz} = \sqrt{3}\frac{\sigma_{xz}^{y}}{\sigma_0} = \sqrt{3} \times \frac{0.011GPa}{0.03GPa} = 0.635 \tag{A.8}$$

Thus, all the material parameters are identified and are listed in Table A.2. A trial and error procedure is performed and the parameters in table A.2 are found accurate for the model.

Table A.2 Material parameters for the liner

Parameter	Value	Parameter	Value
E_x (GPa)	3.2	σ_0 (GPa)	0.03
E_y (GPa)	2	E_t (GPa)	2.5
E_z (GPa)	0.016	R_{xx}	1
v_{xy}	0.34	R_{yy}	0.35
v_{yz}	0.01	R_{zz}	0.23
v_{yz}	0.01	R_{xy}	0.635
G_{xy} (GPa)	1	R_{yz}	0.635
G_{yz} (GPa)	0.057	R_{xz}	0.635
G_{xz} (GPa)	0.058		

A.3 Identification of material parameters for the core

Fig. A.7 shows the typical measured stress VS strain response of the core specimen under the

tension in x direction. Similarly, in the initial loading stage, the specimen shows nonlinear response due to flattening until a strain level of 0.0067 is reached. After that, the specimen responds linearly up to yield point at strain level of 0.0077. After the yield point, the material responds into the plastic deformation until the failure happens at strain level of 0.008. Referring to Fig. A.6, the elastic modulus E_x is calculated to be 0.62 GPa; The reference stress σ_0 is the same as the yield stress in x direction, which is 0.011 MPa; The plastic modulus E_t is the slope of the plastic response, which is 0.56 GPa. The R_{xx} is the ratio of the yield stress in x direction (0.011 GPa) to the reference stress (0.011 GPa), which is 1.

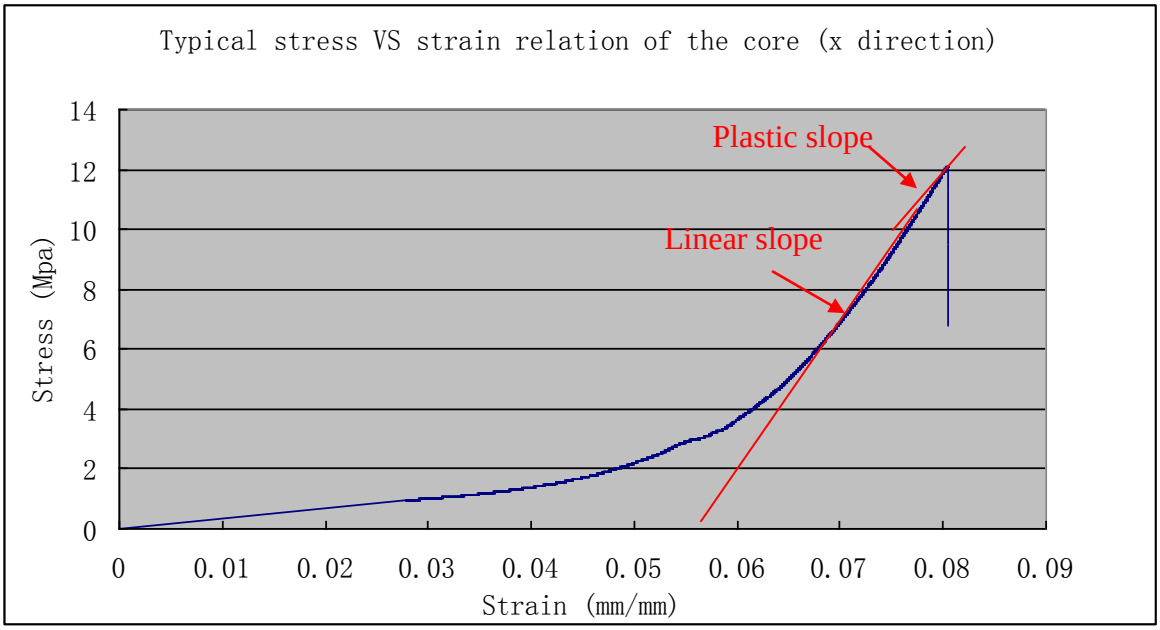

Fig. A.7 Typical stress VS strain relation of the core in x direction

Fig. A.8 shows the typical measured stress VS strain response of the core specimen under the tension in y direction. Similarly, in the initial loading stage, the specimen shows nonlinear response due to flattening until a strain level of 0.00285 is reached. Following that, the response becomes flat due to glue effect until a strain level of 0.0035 is reached. After that, the specimen responds linearly up to yield point at strain level of 0.0088. After the yield point, the material responds into the plastic deformation until the failure happens at strain level of 0.011. Referring to Fig. A.6, the elastic modulus E_y is calculated to be 1.125 GPa; The yield stress in y direction,

is 0.009 GPa; The R_{yy} is the ratio of the yield stress in y direction (0.009 GPa) to the reference stress (0.011 GPa), which is calculated to be 0.8.

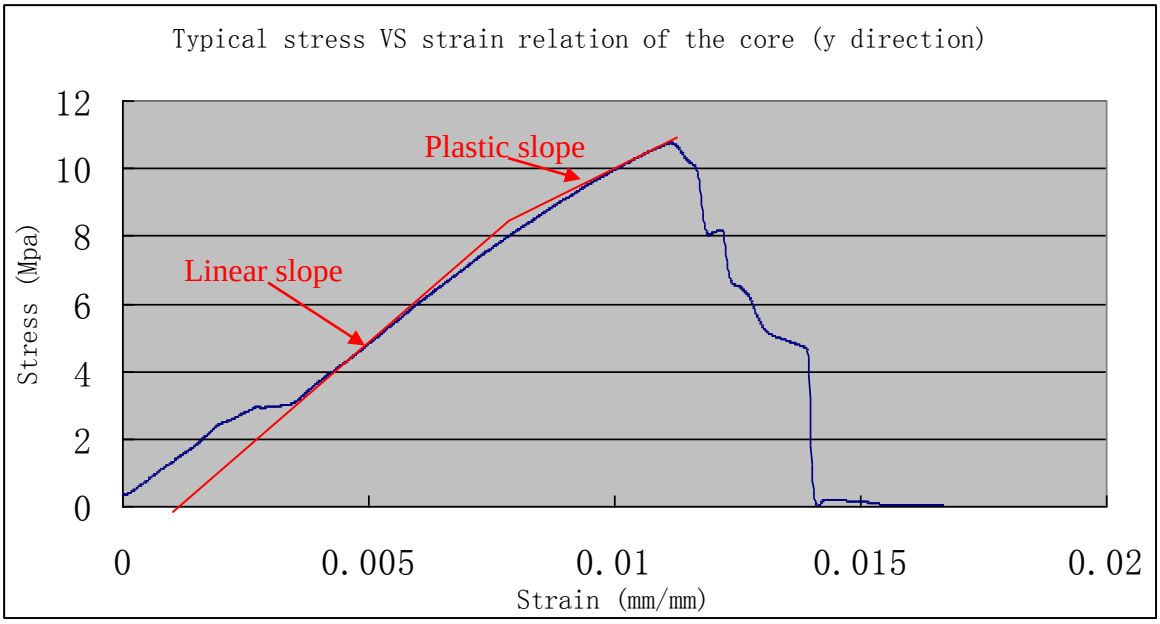

Fig. A.8 Typical stress VS strain relation of the core in y direction

For both types of specimens, four new specimens were repeated and the results were shown in Fig. A.9 and Fig. A.10, respectively.

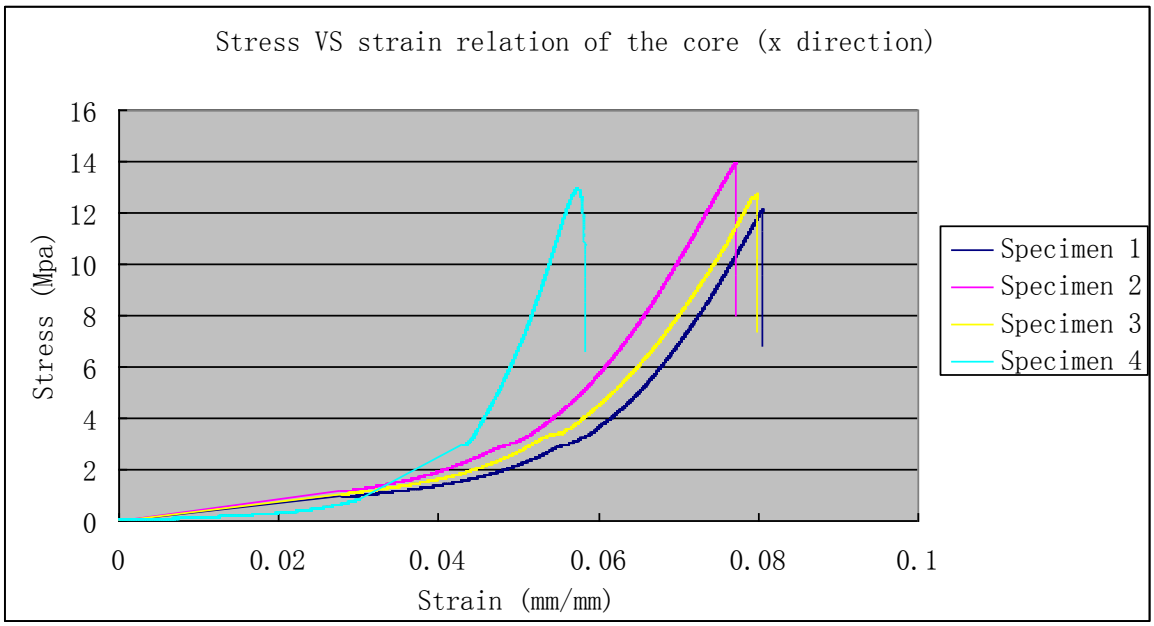

Fig. A.9 Stress VS strain relation of the core in x direction for all specimens

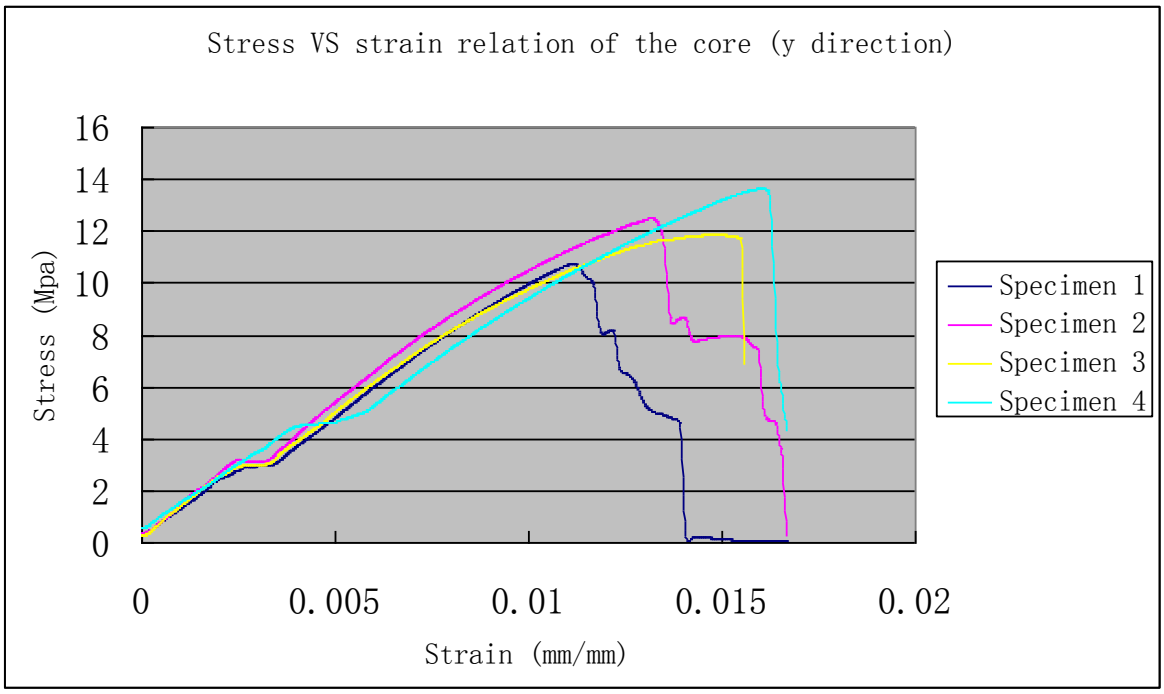

Fig. A.10 Stress VS strain relation of the core in y direction for all specimens

The average value of the material parameters of the four specimens are then calculated and listed in table A. 3.

Table A.3 Average value of the measured material parameters from four core specimens

Parameter	Value
E_x (GPa)	0.8
E_y (GPa)	1.3
σ_0 (GPa)	0.011
E_t (GPa)	0.3
R_{xx}	1
R_{yy}	0.7

Based on the material parameters in Table A.3, the other material parameters are derived according to the empirical equations shown in Section 3.2.3. For the out of plane parameter E_z, it is derived according to Eqn. (3.3) as follows

$$E_z = E_x / 200 = 0.8GPa / 200 = 0.004GPa \tag{A.9}$$

The shear modulus G_{xy}, G_{xz}, G_{yz} are derived according to Eqn. (3.4), Eqn. (3.5), and Eqn. (3.6), respectively, which is found as

$$G_{xy} = 0.387\sqrt{E_x E_y} = 0.387 \times \sqrt{0.8GPa \times 1.3GPa} = 0.394GPa \tag{A.10}$$

$$G_{xz} = E_x / 55 = 0.8GPa / 55 = 0.015GPa \tag{A.11}$$

$$G_{yz} = E_y / 35 = 1.3GPa / 35 = 0.037GPa \tag{A.12}$$

The value of ν_{xy}, ν_{xz} and ν_{yz} are set according to (Nordstand, 1995), which is 0.34, 0.01 and 0.01, respectively. According to (Gooren, 2006), σ_{zz}^{y} is set to be 0.004GPa, and $\sigma_{xy}^{y}, \sigma_{yz}^{y}, \sigma_{xz}^{y}$ are all set to be 0.004 for the first estimate. Further, the $R_{zz}, R_{xy}, R_{yz}, R_{xz}$ are determined according to Eqn. (3.18), Eqn. (3.19), Eqn. (3.20), and Eqn. (3.21), respectively, which are found as below:

$$R_{zz} = \frac{\sigma_{zz}^{y}}{\sigma_0} = \frac{0.004GPa}{0.011GPa} = 0.36 \tag{A.13}$$

$$R_{xy} = \sqrt{3}\frac{\sigma_{xy}^{y}}{\sigma_0} = \sqrt{3} \times \frac{0.04GPa}{0.011GPa} = 0.63 \tag{A.14}$$

$$R_{yz} = \sqrt{3}\frac{\sigma_{yz}^{y}}{\sigma_0} = \sqrt{3} \times \frac{0.004GPa}{0.011GPa} = 0.63 \tag{A.15}$$

$$R_{xz} = \sqrt{3}\frac{\sigma_{xz}^{y}}{\sigma_0} = \sqrt{3} \times \frac{0.004GPa}{0.011GPa} = 0.63 \tag{A.16}$$

Thus, all the material parameters are identified and are listed in Table A.4. A trial and error procedure is performed and the parameters are found not accurate for the model. The parameters are then refined to get the results as close as possible to that of the experiments. The refined parameters are listed in Table A.5.

Table A.4 Material parameters for the core

Parameter	Value	Parameter	Value
E_x (GPa)	0.8	σ_0 (GPa)	0.011
E_y (GPa)	1.3	E_t (GPa)	0.3
E_z (GPa)	0.004	R_{xx}	1
ν_{xy}	0.34	R_{yy}	0.7
ν_{yz}	0.01	R_{zz}	0.36
ν_{yz}	0.01	R_{xy}	0.63
G_{xy} (GPa)	0.394	R_{yz}	0.63
G_{yz} (GPa)	0.037	R_{xz}	0.63
G_{xz} (GPa)	0.015		

Table A.5 Refined material parameters for the core

Parameter	Value	Parameter	Value
E_x (GPa)	5	σ_0 (GPa)	0.011
E_y (GPa)	1.3	E_t (GPa)	0.01
E_z (GPa)	0.025	R_{xx}	1
v_{xy}	0.34	R_{yy}	0.3
v_{yz}	0.01	R_{zz}	0.3
v_{yz}	0.01	R_{xy}	0.63
G_{xy} (GPa)	1	R_{yz}	0.63
G_{yz} (GPa)	0.05	R_{xz}	0.63
G_{xz} (GPa)	0.005		

APPENDIX B

MEASUREMENT RESULTS FOR EXAMPLE 2

B.1 Introduction

This Appendix will show the measurement results for Example 2.

B.2 Measurement results

For Example 2, the measured results with and without cardboards (19 cardboards in series) at location 1, location 2, location 3 and location 4 are shown in Fig. B.1, Fig. B.2, Fig. B.3 and Fig. B.4, respectively. In these figures, the horizontal axis is the frequency and the vertical axis is the acceleration. It is noted that only the acceleration at 29.25 Hz (183.69 rad/s) was recorded as it is the frequency where the pump is operating.

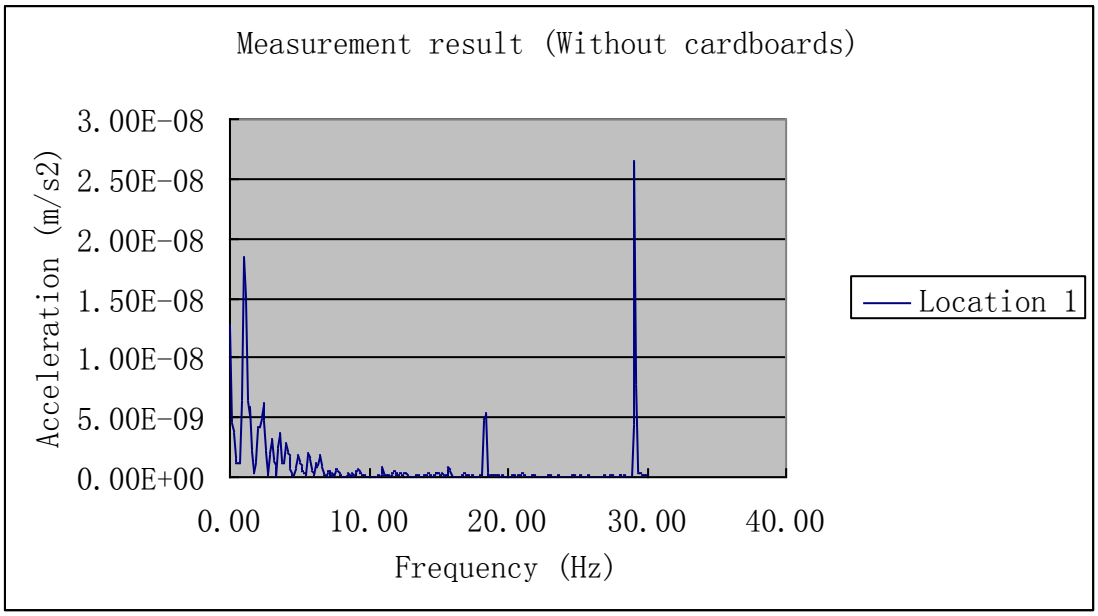

(a)

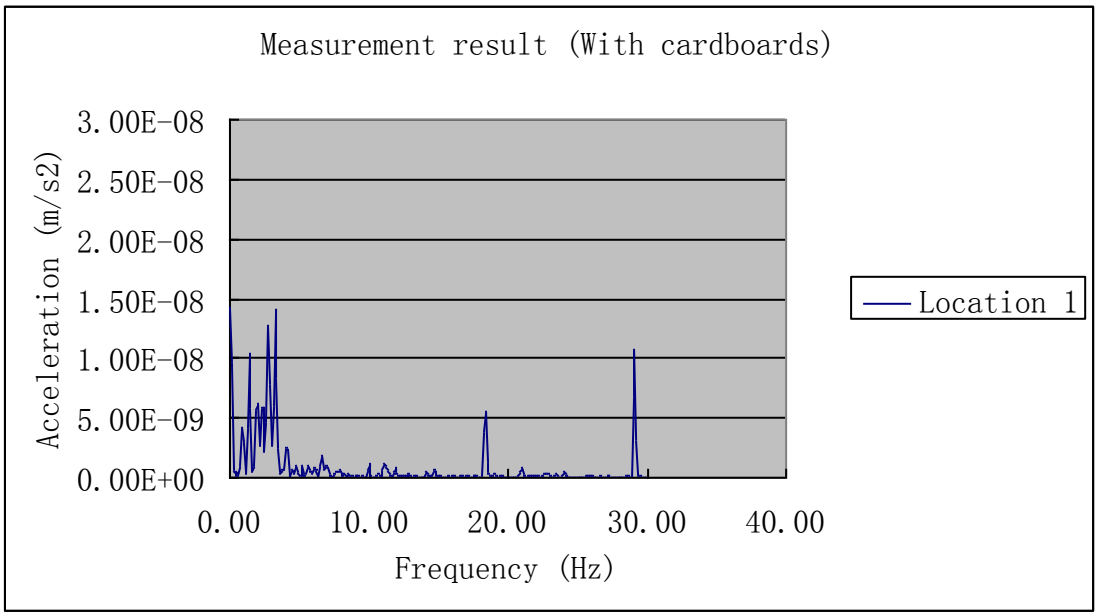

(b)

Fig. B.1 Measurement results for Example 2 at location 1 (a) without cardboards; (b) with cardboards

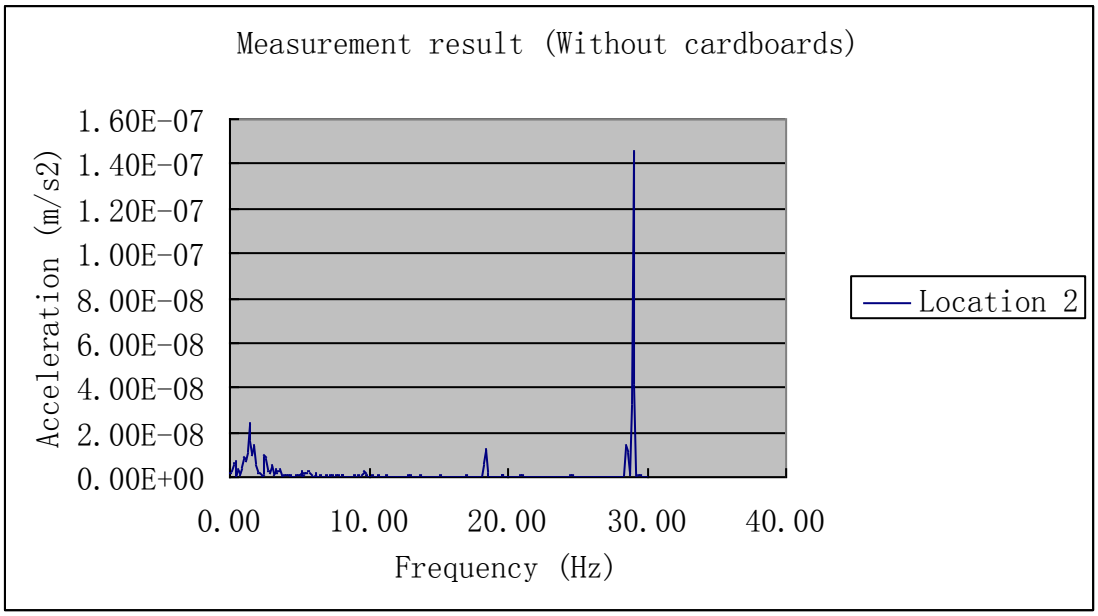

(a)

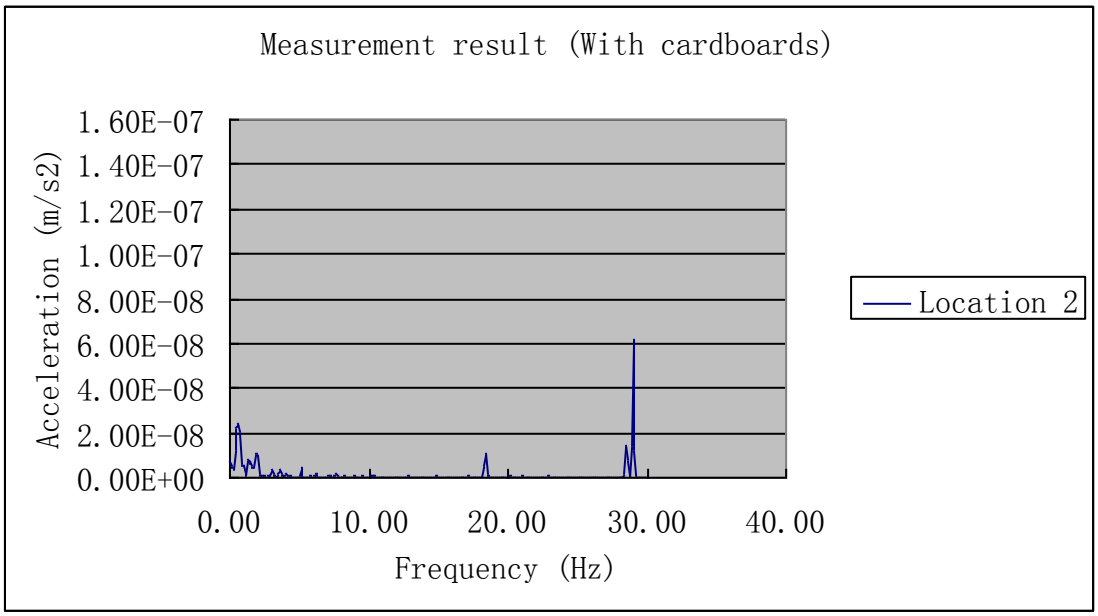

(b)

Fig. B.2 Measurement results for Example 2 at location 2 (a) without cardboards; (b) with cardboards

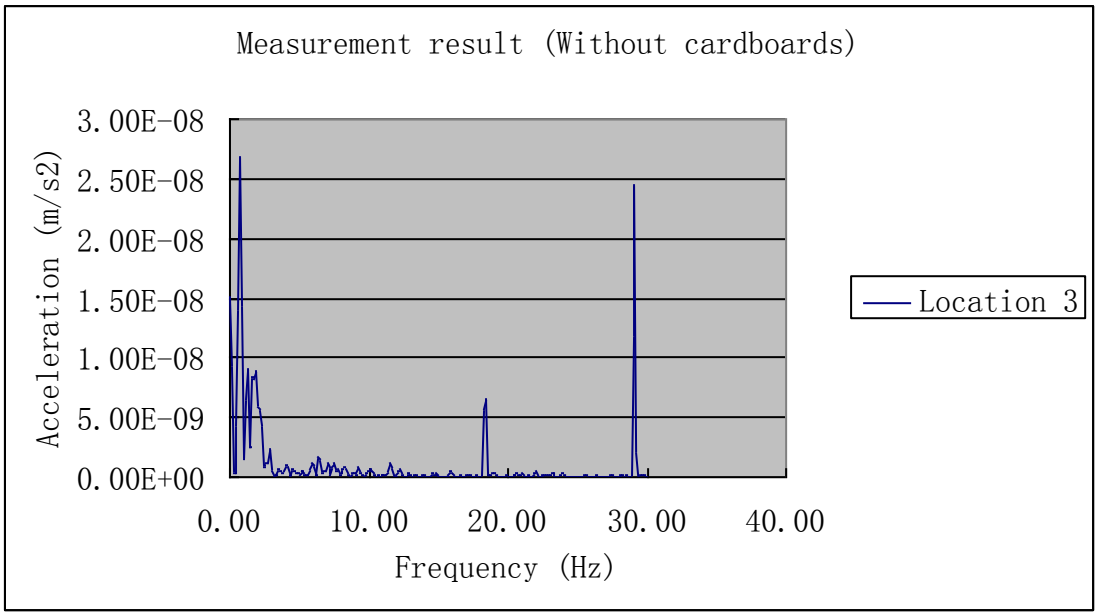

(a)

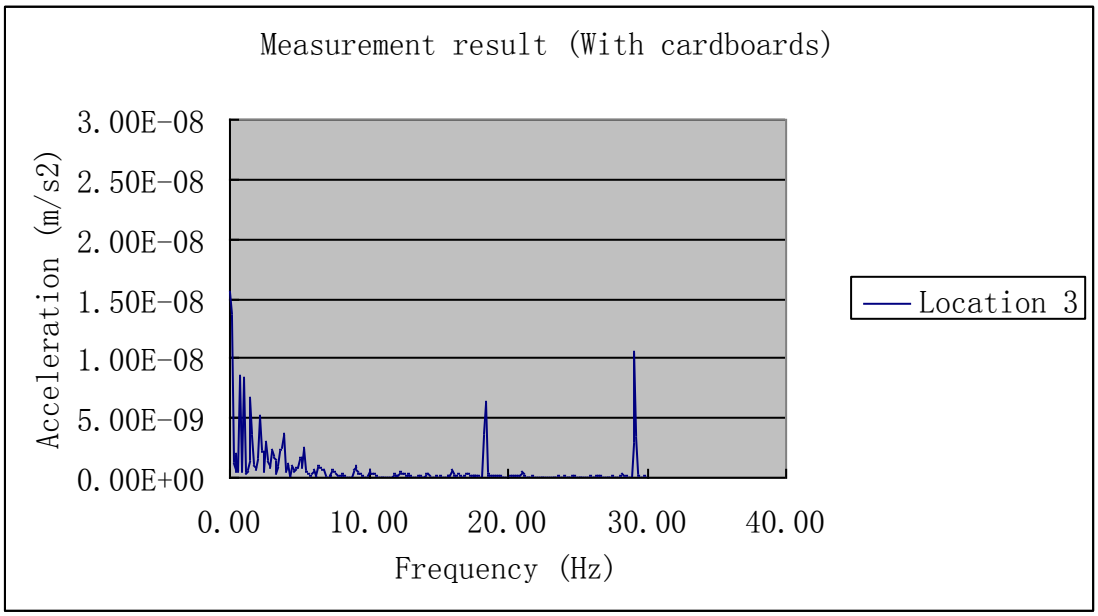

(b)

Fig. B.3 Measurement results for Example 2 at location 3 (a) without cardboards; (b) with cardboards

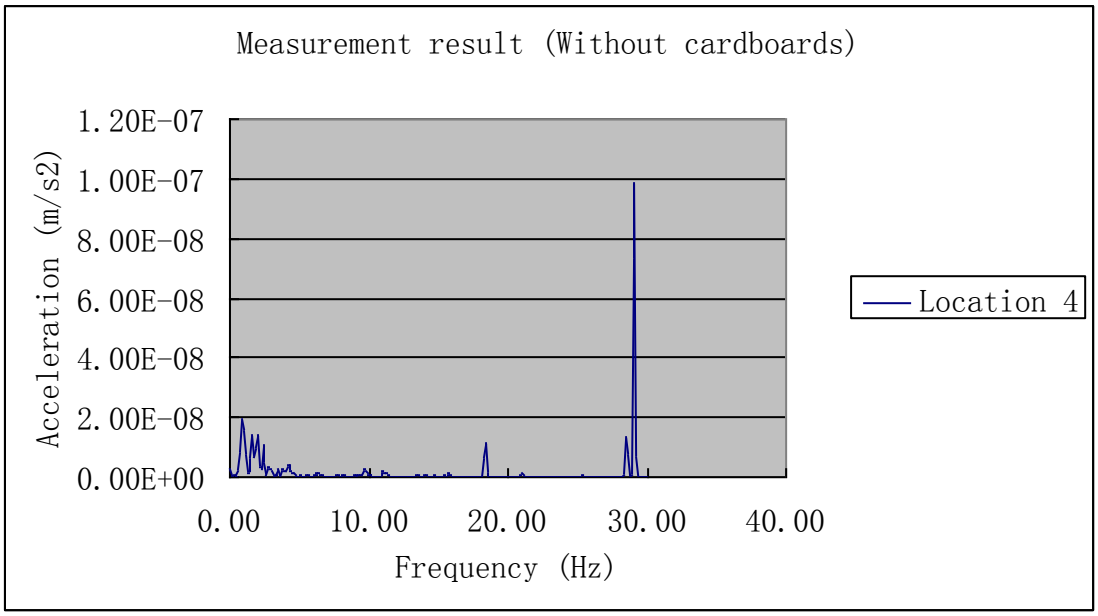

(a)

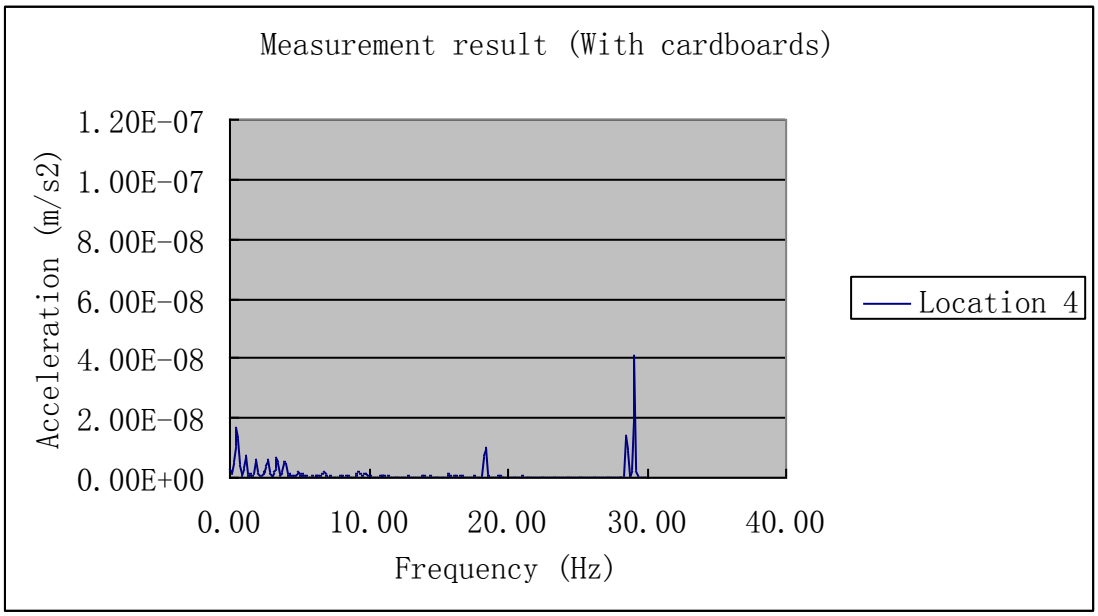

(b)

Fig. B.4 Measurement results for Example 2 at location 4 (a) without cardboards; (b) with cardboards